

LIQUID PHASE ION MOBILITY SPECTROMETRY

By
MAGGIE TAM

A dissertation submitted in partial fulfillment of
the requirements for the degree of

DOCTOR OF PHILOSOPHY

WASHINGTON STATE UNIVERSITY
Department of Chemistry

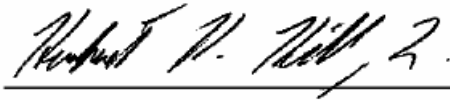
DECEMBER 2006

© Copyright by MAGGIE TAM, 2006
All Rights Reserved

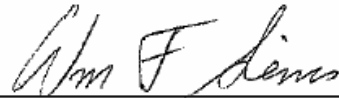
© Copyright by MAGGIE TAM, 2006
All Rights Reserved

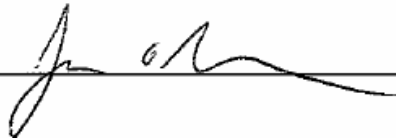
To the Faculty of Washington State University:

The members of the Committee appointed to examine the dissertation of MAGGIE TAM find it satisfactory and recommend that it be accepted.



Chair





Acknowledgement

I would like to thank Dr. Herbert H. Hill, Jr. for his continuous motivation and support throughout my graduate study, and for his teachings and inspiration. He provided me with opportunities to present at international conferences and to work on interesting projects.

I would like to thank my committee: Dr. William F. Siems and Dr. James O. Schenk for their guidance over the years. I would like to thank Dr. Siems for offering me the valuable opportunity to work in the mass spectrometry core facilities, and for teaching me the art and logic of troubleshooting. I would like to thank past and present members from the Hill Research Group, especially Dr. Laura M. Matz and Dr. Brian H. Clowers. Most sincere gratitude to Dr. Prabha Dwivedi for helping me through trying times. I would like to thank my colleagues at LBB2 for sharing their knowledge and experiences: Dr. Stephen Halls, Dr. Gerhard Munske, Dr. Xiaoting Tang, Lisa Washburn, and Dr. Si Wu.

I would like to thank the professional staff in the WSU Chemistry Department for their administrative support: Paula Broemmeling, Carrie Giovannini, Debbie Arrasmith, Marie Martin, Nikki Clark, Roger Crawford, and Gary Johnson. I would like to acknowledge the assistance from the staff of WSU Technical Services: George Henry, Lauren Frei, Fred Schuetze, John Rutherford, Duke Beattie, and Steve Watson, for their immense patience, expertise, and help on instrumental and electrical problems. I would like to thank the WSU Research Foundation, especially Dr. Brian Kraft, for the patent application.

I would like to thank our collaborators, Dr. Amy Moll from Boise State University, Dr. Prashanta Dutta from Washington State University, and their students, for broadening my research experiences.

I would like to acknowledge financial support from the National Institute of Health (NIBIB) and the Army Research Office for funding the thesis project, the WSU Chemistry Department and Laboratory for Biotechnology and Bioanalysis, Unit 2, for the TA positions. I would like to show appreciation for the Stacey Research Scholarship, Jim and Lee Ruck Fellowship, and Don Matteson Fellowship, awarded by the WSU Chemistry Department.

I would like to thank my WSU friends for providing me with lots of encouragement, comfort, and laughter, especially Yan Liu, Wei Liao, Geoffrey and Adeline Puzon. Most important of all, I would like to thank my family for their encouragement throughout my student life: the Tam Family and the Chen family, my daughter Audrey for bringing sunshine to my life, and my husband Jack for his confidence, understanding, and support.

LIQUID PHASE ION MOBILITY SPECTROMETRY

Abstract

by Maggie Tam, Ph.D.

Washington State University

December 2006

Chair: Herbert H. Hill, Jr.

Liquid phase ion mobility spectrometry was developed as a novel analytical separation method, by replacing the drift gas with a non-electrolyte containing liquids. Preliminary studies demonstrated that liquid phase ion mobility spectrometry was achievable. A miniaturized liquid phase ion mobility spectrometer obtained a similar resolving power as a gas phase ion mobility spectrometer ten times its size. A new ionization source, called electrodispersion ionization, was introduced. The non-radioactive electrodispersion ionization source produced liquid phase ions in non-electrolytic liquid medium. Visualization of the electrodispersion ionization process showed electrodispersed droplets of aqueous sample. Exploration of the sample flow rate established the pulsing controllability of electrodispersion ionization. Pulsed electrodispersion ionization source was developed and evaluated for liquid phase ion mobility spectrometry. Results demonstrated the capability of pulsed electrodispersion ionization as a multipurpose ionization source for liquid phase ion

mobility spectrometry, merging three important instrumental processes into a single source: sample introduction, sample ionization, and pulsed ion injection.

Table of Contents

Acknowledgement.....	iii
Abstract.....	v
List of Tables.....	xi
List of Figures.....	xii
Chapter One: Introduction	1
History of ion mobility in liquid phase	1
Gas Phase Ion Mobility as an Analytical Separation Tool.....	4
Liquid Phase Ion Mobility as an Analytical Separation Tool.....	9
Specific Aims	12
Attribution	13
References	14
Chapter Two: Electrodispersion Ionization in Liquids.....	18
Abstract	18
Introduction.....	19
Experimental Section.....	22
Results and Discussions	26
Conclusions	32
Acknowledgements	33

References	34
Chapter Three: Liquid Phase Ion Mobility Spectrometry.....	51
Abstract	51
Introduction.....	52
Experimental Section.....	57
Results and Discussions	62
Conclusions	67
Acknowledgements	67
References	68
Chapter Four: Design, Construction, and Evaluation of an Integrated Liquid Phase Ion Mobility Spectrometer	83
Abstract	83
Introduction.....	84
Design and Fabrication of Integrated Liquid Phase Ion Mobility Spectrometer	88
Results and Discussion	92
Acknowledgements	98
References	99
Chapter Five: Evaluation of Pulsed Electrodispersion Ionization Source for Liquid Phase Ion Mobility Spectrometry	109
Abstract	109

Introduction.....	110
Experimental Section.....	112
Results and Discussion	115
Conclusions.....	119
Acknowledgements	120
References	121
Chapter Six: Conclusions	138
Appendix I: Additional Data from Parametric Studies of Electrodispersion Ionization	145
Appendix II: Additional Graphic Representations of Liquid Phase Ion Mobility Spectrometers.....	152
Appendix III: Electric Circuit for Pulsed Electrodispersion Ionization Source	167
Appendix IV: Secondary Electrospray Ionization-Ion Mobility Spectrometry for Explosive Vapor Detection.....	171
Abstract	171
Introduction.....	173
Experimental Section.....	175
Results And Discussion.....	178
Conclusions	186
Acknowledgement	186

References 187

List of Tables

Chapter One: Tables

Table 1: Resolving Power and Dimensions of Miniaturized Gas Phase IMS instrument.....	17
---	----

Chapter Two: Tables

Table 1: Solution pH values and speciation information for arginine, lysine, and serine at concentrations from 10 μ M to 1 mM.	38
---	----

Table 2: Ionization efficiency of electrodispersion ionization, tabulated with the theoretical and experimental current data.	39
--	----

Chapter Four: Tables

Table 1: Properties and dimensions of the previously reported and integrated LPIMS devices.....	101
---	-----

Table 2: Typical Resistivity Values between a Pair of Adjacent Electrodes in an empty PDMS-LPIMS.....	102
---	-----

Table 3: Total ion current obtained from LTCC-LPIMS.	103
---	-----

Chapter Five: Tables

Table 1: Experimental, literature, and expected mobility values of the aqueous analytes.....	129
--	-----

Appendix IV: Tables

Table 1. The experimental and literature reduced mobility values of explosive species.....	190
--	-----

List of Figures

Chapter Two: Figures

Figure 1: Schematic of the electrodispersion ionization apparatus.....	42
Figure 2: Schematic of the second electrodispersion ionization apparatus..	43
Figure 3: Timed photographs of electrodispersion ionization.....	44
Figure 4: Current generated from electrodispersion ionization..	45
Figure 5: Electrodispersed ion current of 10 μ M basic fuchsin.....	46
Figure 6: Photographs of the paper target from electrodispersion ionization.	47
Figure 7a: Electrodispersed current as a function of sample flow rate in the positive mode.....	48
Figure 7b: Electrodispersed current as a function of sample flow rate in the negative mode.	48
Figure 8: Calibration plot for three amino acids: arginine, lysine, and serine, at 0, 10 μ M, 50 μ M, 100 μ M, 500 μ M, and 1 mM, dissolved in water..	50

Chapter Three: Figures

Figure 1: Schematic of the liquid phase resistive glass ion mobility tube.....	75
Figure 2: Schematic of the enclosed stacked-ring liquid phase ion mobility spectrometer.....	76
Figure 3: This plot showed the effect of the electric field of the ion mobility spectrometer on (a) the total ion current and (b) the ionization and ion transport efficiency of ESI in air and EDI in hexane.	77
Figure 4: The effectiveness of (a) Bradbury-Nielsen shutter and (b) Tyndall shutter in stopping ion current in liquid phase ion mobility spectrometry.	78

Figure 5: Ion current of solvent blank, 10 μ M basic fuchsin, and 1 μ M tetraethylammonium bromide.....	79
Figure 6: LPIMS spectra in mineral oil.....	80
Figure 7: LPIMS spectra in mineral oil.....	81
Figure 8: Pulsed electrodispersion ionization-liquid mobility spectrum of 10 μ M basic fuchsin, dissolved in methanol-water (90:10, v/v), drifting in hexane.	82

Chapter Four: Figures

Figure 1: Schematic of the LTCC-LPIMS.....	105
Figure 2: (a) Top-view schematic of the third generation of PDMS-LPIMS prototype. (b) Close-up three-dimensional view and (c) top-view of the sample nozzle..	106
Figure 3: The surface methyl groups of poly(dimethylsiloxane) are oxidized to hydroxyl group by oxygen plasma.....	107
Figure 4: Plot of total ion current being measured at successive electrodes along the PDMS channel in benzene..	108

Chapter Five: Figures

Figure 1: Schematic of liquid phase ion mobility spectrometer (LPIMS) with pulsed electrodispersion ionization (EDI).	132
Figure 2: Pulsed electrodispersion ionization – liquid phase ion mobility spectra of the solvent blank (methanol-water, 90:10 vol/vol) f.	133
Figure 3: Pulsed electrodispersion ionization – liquid phase ion mobility spectra of the solvent blank (methanol-water, 90:10 vol/vol) was obtained over 30 minutes (179 spectra) in the positive mode.....	134

Figure 4a: Pulsed electrodispersion ionization – liquid phase ion mobility spectrum of 100 μM tetramethylammonium bromide in the positive mode.	135
Figure 4b: Pulsed electrodispersion ionization – liquid phase ion mobility spectrum of 100 μM tetrabutylammonium bromide in the positive mode....	142
Figure 4c: Pulsed electrodispersion ionization – liquid phase ion mobility spectrum of 100 μM bradykinin in the positive mode.	143

Appendix I: Figures

Figure 1: Schematic of the electrodispersion ionization apparatus.	147
Figure 2: Plot of total ion current versus electrodispersion ionization voltage for sample of methanol-water and 100 μM ammonium chloride at a flow rate of 0.1 $\mu\text{L}/\text{min}$ in benzene and decane, in the positive mode.	148
Figure 3: Effect of sample flow rate on electrodispersion ionization efficiency for a sample of methanol-water (90:10) in benzene.....	149
Figure 4: Effect of sample flow rate on electrodispersion ionization efficiency for a sample of methanol-water (90:10) and 100 μM ammonium chloride, in benzene and decane..	150
Figure 5: Effect of sample flow rate on electrodispersion ionization efficiency for a sample of methanol-water (90:10) and 100 μM ammonium chloride, in benzene and decane..	151

Appendix II: Figures

Figure 1: Liquid phase ion mobility spectrometer (LPIMS), constructed from a Pyrex culture tube.....	156
Figure 2: Mobility tube of LPIMS, fabricated from low temperature co-fired ceramic (LTCC)..	157

Figure 3: The complete prototype of low temperature co-fired ceramic-liquid phase ion mobility spectrometer (LTCC-LPIMS).....	158
Figure 4: Schematic of the LTCC-LPIMS prototype, showing (A) the internal electrical connections, and (B) the alignment holes and the external electrical connections.....	159
Figure 5: Photograph of the first generation of poly(dimethylsiloxane)-liquid phase ion mobility spectrometer (PDMS-LPIMS).....	160
Figure 6: Photograph of the second generation of poly(dimethylsiloxane)-liquid phase ion mobility spectrometer (PDMS-LPIMS).	161
Figure 7: Three-dimensional schematic of the third generation of PDMS-LPIMS.	162
Figure 8: Top-view schematic of the third generation of PDMS-LPIMS.	163
Figure 9: Photograph of the fourth generation of PDMS-LPIMS prototype, showing the polyethylene capillaries, which carried in the liquid medium and sample, and the electrical connections.	164
Figure 10: Photograph of a resistive glass-LPIMS.....	165
Figure 11: Photograph of the miniaturized Bradbury-Nielsen gate, with a 4.56 mm i.d., 9.30 mm o.d., and a wire spacing of 0.64 mm.....	166

Appendix III: Figures

Figure 1: Schematic of liquid phase ion mobility spectrometer (LPIMS) with pulsed electrodispersion ionization (EDI).	170
--	-----

Appendix IV: Figures

Figure 1: Schematic of secondary electrospray ionization-ion mobility spectrometer.....	193
---	-----

Figure 2: (a) ESI-IMS spectrum of 10 mg L ⁻¹ TNT; (b) SESI-IMS spectrum of 10 mg L ⁻¹ TNT; (c) ⁶³ Ni-IMS spectrum of 100ng TNT with methylene chloride as dopant.....	194
Figure 3: ⁶³ Ni-IMS spectra of 100ng of (a) RDX (b) NG and (c) PETN. Spectra were obtained at 200 °C with methylene chloride as dopant.	195
Figure 4: SESI-IMS spectra of 50 mg L ⁻¹ (a) RDX (b) NG and (c) PETN in methanol-water. All spectra were run at 125 °C.....	196
Figure 5: Effect of non-volatile dopants.....	197
Figure 6: Thermal stability of RDX, NG, and PETN species.	198
Figure 7: Plot of SESI-IMS reduced mobilities of RDX, NG, and PETN species versus drift tube temperature..	199

Chapter One

Introduction

This project proposed to explore ion mobility in liquid phases as a novel analytical separation technique in a miniaturized setting. Liquid phase ion mobility spectrometry (LPIMS) separates analyte ions in an electric field established, not by electrolyte, but by a series of metal electrodes held at decreasing potentials. The development of a miniaturized LPIMS will have broad impact in separation sciences, providing real-time separation of complex mixtures in the liquid phase.

History of ion mobility in liquid phase

Research of ion mobility in liquid phases began in the early 20th century as a series of physical experiments evolving from conductivity studies of dielectric liquids. The liquid media studied were liquid hydrocarbons, insulating oils and liquefied noble gases.

Bialobrzewski and Jaffé conducted the first experiments of mobility measurements in dielectric liquids in the early 20th century. Bialobrzewski [1] worked on the relation

between ion mobility and the viscosity (η) of the dielectric liquid medium and Jaffé [2] performed ion mobility experiments in hexane. In 1937, Adamczewski [3] performed the first systematic ion mobility experiments in a series of liquid saturated hydrocarbons (pentane, hexane, heptane, octane and nonane) and studied the relation of ion mobility to the coefficient of viscosity. Adamczewski concluded that the mobility (μ) of ion was inversely proportional to $\eta^{3/2}$ at constant temperature, known as the Adamczewski's relation:

$$\mu = A\eta^{-3/2} \quad (1)$$

where A is a numerical coefficient characteristic of each type of ions.

In the 1950s, measurements of mobility of helium ions in liquefied helium were done by Williams [4], L. Meyer et al [5], Careri et al [6] and Atkins [7]. In 1964, Gzowski [8] measured mobility of positive and negative ions in pure and mixtures of hydrocarbons. Although the ions were not identified, he concluded that (1) positive ions of different mobilities were present; (2) mobility of negative ions were greater than that of positive ions in all the liquids studied; (3) mobility of negative ions were found to be inversely proportional to viscosity of liquid, known as the Walden's Rule:

$$\mu = A\eta^{-1} \quad (2)$$

and (4) mobility of positive ions were found to be inversely proportional to $\eta^{3/2}$, same as Adamczewski's finding in 1937.

Adamczewski carried out more physical experiments on ion mobility in saturated hydrocarbons [9] and formulated a relation between ion mobility and the number of carbon atoms in the molecules of saturated hydrocarbons C_nH_{2n+2} [10]:

$$\mu = 96e^{(0.45n)} e^{\left\{ \frac{450}{T} \times [n^{1/2} + 2.33(n-1)^{1/2} - 1.25] \right\}} \quad (3)$$

Interests in mobility studies in dielectric liquids continued, mostly used for physical investigations of positive and negative intrinsic ions of the liquids in the study of the breakdown process of dielectric liquids [11-13], the study of ion recombination and diffusion in liquids subjected to high-energy radiation [14;15], and the study of dielectric liquid properties in particle counters and spark chambers [16;17]. Investigations of ions from extrinsic analyte were less studied. Researchers studied the mobilities of sulfur hexafluoride [18], methyl halides [18], tetramethylparaphenylenediamine [19;20], quinones [20;21], porphines [20;21], and fullerenes [20;22], with the samples dissolved in the same dielectric liquid medium where experiments were conducted.

Up to this date, there has been no research performed on using ion mobility spectrometry in liquid phases as an analytical separation technique for aqueous phase analytes.

Gas Phase Ion Mobility as an Analytical Separation Tool

Gas phase ion mobility began from physicists' experiments in the 1890s by Roentgen [23], and Thompson and Rutherford [24]. Roentgen [23] discovered the ability of X-ray to ionize air. In 1897, Thompson and Rutherford [24] measured the velocities of positive ions produced by X-rays and found the relationship between ion velocity (v), mobility (K) and field strength (E):

$$v = KE \tag{4}$$

In the early 1900s, Langevin [25-27] experimented with gas phase ion in weak electric fields and showed that ionized air was composed of various chemical species, using an instrument similar to today's gas phase ion mobility spectrometer. Mason et al [28] developed the Mason-Schamp equation that relates gas phase ion mobility to the charge and size of the ion:

$$K = \frac{3}{16N} \cdot \left(\frac{2\pi}{\mu kT} \right)^{1/2} \cdot \frac{ze}{\Omega_D} \tag{5}$$

where N is the number density of drift gas, μ is the reduced mass, k is Boltzmann's constant, T is temperature of drift gas, z is the charge of the ion, e is the elementary charge, and Ω_D is the collision cross section of the ion. Ion mobility can be determined from the experimental parameters as:

$$K = \frac{v_d}{E} = \frac{L^2}{Vt_d} \quad (6)$$

To account for the dependence on temperature (T) and pressure (P), and to facilitate comparison among different experimental settings, the mobility constant is commonly normalized to 273 K and 760 mm Hg and reported in literature as the reduced mobility (K_0):

$$K_0 = K \cdot \frac{P}{760} \cdot \frac{273}{T} \quad (7)$$

Gas phase ion mobility spectrometry (IMS) is now the method of choice in drug and explosive detection [29]. Analytes in IMS are separated based on the size-to-charge ratio of the ions and the interaction between the ions and the medium. IMS is capable of separating not only isobaric analytes, but also enantiomers through their different stereospecificities. The size-to-charge separation of IMS complements other separation techniques, such as mass spectrometry, chromatography, and differential mobility spectrometry. Tandem instruments with multidimensional separation units are capable of solving complex analytical problems. As a result, research in IMS has expanded literally and figuratively in the past decade through integration with other analytical methods. On another research front, much effort had been spent on miniaturizing IMS to capture its unique benefits of simple instrumentation, milliseconds-fast analysis time, easy operation, and portability.

Portable IMS devices are widely employed by first responders for the rapid detection of explosives and warfare agents.

Separation Efficiency and Resolution. Several expressions are used to describe the separation efficiency of ion mobility spectrometry. These include the peak width at half height ($w_{1/2}$), the resolving power (R_p), and the number of theoretical plates (N). These terms can be expressed in theory and from experimental data. The peak width at half height is the width of a mobility peak at 50% of its height, and it has units of milliseconds. The experimental resolving power of an ion mobility spectrometer is determined by measuring the drift time (t_d) and peak width at half height ($w_{1/2}$) of a single mobility peak:

$$R_p = \frac{t_d}{w_{1/2}} \quad (8)$$

The typical resolving power obtained from a commercial 3.9-cm long ion mobility spectrometer is about 30, and the resolving power obtained from a research grade 20-cm long ion mobility spectrometer is around 100. The resolving power of ion mobility spectrometry is related to the chromatographic theoretical plate numbers (N) by the following equation:

$$N = 5.55(R_p)^2 \quad (9)$$

Therefore, a commercial ion mobility spectrometer has roughly 5000 theoretical plates, whereas a research grade ion mobility spectrometer has approximately 55,000 theoretical plates.

The diffusion limited resolving power can be expressed as:

$$\text{Diffusion Limited } R_p = \left(\frac{Vez}{16kT \ln 2} \right)^{1/2} = \left(\frac{E \cdot L \cdot ez}{16kT \ln 2} \right)^{1/2} \quad (10)$$

While the diffusion limited resolving power estimates the possible separation power of an ion mobility spectrometer, the theoretical resolving power determines its separation power by taking the additional consideration of the actual operation parameters, such as the pulse width of the ion shutter and the operating pressure as:

$$\text{Theoretical } R_p = \frac{\frac{L^2}{V \cdot K_0} \cdot \frac{P}{760} \cdot \frac{273}{T}}{\left(t_g^2 + \left(\frac{16kT \ln 2}{Vez} \right) \cdot \left(\frac{L^2}{V \cdot K_0} \cdot \frac{P}{760} \cdot \frac{273}{T} \right)^2 \right)^{1/2}} \quad (11)$$

The efficiency of an ion mobility spectrometer can be computed by expressing the experimental resolving power as a percentage of the theoretical resolving power as:

$$\text{Efficiency} = \frac{\text{Experimental } R_p}{\text{Theoretical } R_p} \times 100\% \quad (12)$$

Miniaturization at expense of separation efficiency. Improving separation efficiency has been especially challenging in miniaturized IMS, where separation efficiency suffers at the expense of miniaturization of the instrument. Equation 10 showed that resolving power decreases with the square root of the IMS drift length. Table 1 showed the dimensions, operating parameters, and the resolving powers of four miniaturized gas phase IMS instruments. While a resolving power of over 100 is common for today's large scale gas phase IMS, miniaturized gas phase IMS exhibit resolving powers of 30 or less. Although increasing the applied electric field, or voltage, of the instrument alleviates the problem, IMS is ultimately restricted by its low-electric field requirement. The relationship between ion velocity and electric field is only linear under the low-electric field conditions, where the electrical energy gained is negligible in comparison to the thermal energy acquired by the ions through collisions. In other words, ion mobility is only constant when E/N is less than $2 - 4 \text{ Td}$ ($1 \text{ Td} = 10^{-17} \text{ V cm}^2$). The maximum electric field that can be applied in IMS is:

$$E_{\max} = \frac{3}{16} \cdot \left(\frac{2\pi k}{\mu \cdot T} \right)^{1/2} \cdot \frac{P}{760} \cdot \frac{z \cdot 273}{K_o \left(\frac{m}{M} + \frac{M}{m} \right)} \quad (13)$$

Therefore, the maximum diffusion limited resolving power is:

$$\text{Diffusion Limited } R_{P,\max} = \left[\frac{3}{16} \cdot \left(\frac{2\pi}{k} \right)^{1/2} \cdot \frac{P}{760} \cdot 273 \cdot \frac{e}{16 \ln 2} \cdot \frac{z \cdot L}{K_o \mu^{1/2} \left(\frac{m}{M} + \frac{M}{m} \right) T^{3/2}} \right]^{1/2} \quad (14)$$

Consequently, the maximum diffusion limited resolving power is not only proportional to the square root of the drift length, but also proportional to the square root of pressure for a given analyte and drift gas:

$$\text{Diffusion Limited } R_{P,\text{max}} \propto \left(\frac{P \cdot L}{T^{3/2}} \right)^{1/2} \quad (15)$$

From Equation 8, it is apparent that increasing the pressure of the medium would cancel out the negative effect of miniaturization on separation power of IMS. The extreme of increasing the pressure of a gas will drive a phase transition and condense it into a liquid. In the four decades of research in IMS, there was one aspect that remained unchanged – experiments were conducted only in a gaseous drift medium.

Liquid Phase Ion Mobility as an Analytical Separation Tool

Theoretically, LPIMS can be scaled down while maintaining a high resolving power. Because diffusion coefficients in liquid phase are three orders of magnitude smaller than those in gas phase, it is therefore possible to produce miniature LPIMS instrument which would have the same resolving power as a laboratory-size gas phase IMS, and which would be three orders of magnitude smaller than the laboratory-size gas phase IMS.

Nitrate ion will be used here to predict the resolving power and analysis time of a miniaturized LPIMS in comparison with a laboratory-size gas phase IMS. Nitrate ion has a gas phase ion mobility of $2.31 \text{ cm}^2 \text{ V}^{-1} \text{ s}^{-1}$ [30]. It has a drift time of 9.1 ms in a 13-cm long gas phase IMS drift tube operating at an drift voltage of 3860 V, 700 Torr and 250 °C [30]. The diffusion-limited resolving power of this gas phase IMS system is 88. The ion mobility of nitrate ion in water is $7.40 \times 10^{-4} \text{ cm}^2 \text{ V}^{-1} \text{ s}^{-1}$ [31]. Supposed the LPIMS instrument was reduced by a factor of 100 to 1.3 mm, which is on the scale of a chip channel, the nitrate ion would have a drift time of 5.9 ms with the LPIMS drift tube operating at the same drift voltage of 3860 V and at ambient temperature. This LPIMS instrument would have a diffusion-limited resolving power of 116, a better resolving power than the gas phase IMS instrument due to the reduced operating temperature. The high operating temperature was required in gas phase IMS to desolvate solvent molecules from the electrosprayed droplet. The desolvation mechanism in LPIMS would not require high temperature and thus it could be operated at ambient temperature.

The above nitrate calculation demonstrated that scaling down the LPIMS instrument by two orders of magnitude, the LPIMS analysis time remained on the same millisecond scale and LPIMS could realize a better resolving power than gas phase IMS.

Significance of a Miniaturized High-Resolution LPIMS. The development of LPIMS would have broad impact in the separation sciences, providing rapid separations with high resolution. It would be suitable for military application in

detecting chemical and biological warfare agents, for environmental application in detecting water contaminants, for forensic application in detecting illicit drugs and for clinical application in detecting serum proteins. At this small scale, LPIMS could be developed into real-time high-resolution micro sensors. The small scale also means that LPIMS could be mass-produced in a cost-effective way and become an inexpensive and disposable instrument.

Specific Aims

The primary goal of this project was to develop a miniaturized ion mobility spectrometer in the liquid phase. While ion mobility in gases has been developed into a successful analytical separation tool – gas phase ion mobility spectrometry, ion mobility in liquids has never been explored as a separation technique. The specific aims of this research are to:

1. Develop and evaluate a liquid phase ionization source suitable for LPIMS.
2. Design and construct a miniaturized separation device based on LPIMS.
3. Demonstrate the capability of LPIMS as a novel analytical detection method.

Attribution

The LPIMS instruments in Chapter 2, 3, and 5 were built by Tam, assisted by Technical Service, Washington State University. The low temperature co-fired ceramic LPIMS instrument in Chapter 4 was designed jointly by Tam, Donald Plumlee, and Brian Jacques (from Dr. Amy Moll's group, Materials Science and Engineering, Boise State University), and fabricated by Plumlee and Jacques. The poly(dimethylsiloxane) LPIMS microchannels in Chapter 4 were designed jointly by Tam and Nazmul Al-Mamun (from Dr. Prashanta Dutta's group, School of Mechanical and Materials Engineering, Washington State University), and fabricated by Al-Mamun. All the experiments were planned and conducted by Tam, except part of the poly(dimethylsiloxane)-LPIMS experiments in Chapter 4, which was performed by Tam and Al-Mamun. Chapter 2 and 3 were written in the format as required by *Analytical Chemistry*. Chapter 5 was written in the format as required by *Journal of Chromatography*. Chapter 4 was written in the format as required by the *Review of Scientific Instruments*. The LabView-based data acquisition program and IGOR data input macros were written by Brian H. Clowers [32]. Appendix III was prepared in the format required by *Analytical Chemistry* (M. Tam, H. H. Hill, Jr., *Analytical Chemistry*, **2004**, 76, 2741). The experiments and thesis were conducted under the supervision and scientific guidance of Dr. Herbert H. Hill, Jr.

References

1. C. Bialobrzewski, *Le Radium* **8**, p. 1 (1911).
2. G. Jaffé, Die elektrische Leitfähigkeit des reinen Hexans, *Annalen der Physik* **333**, pp. 326-370 (1909).
3. I. Adamczewski, Mobilités des Ions dans la Série des carbures d'Hydrogène Liquides et Leur Rapport avec le Coefficient de Viscosité, *Annls de Physique* **8**, pp. 309-359 (1937).
4. R. L. Williams, Ionic Mobilities in Argon and Helium Liquids, *Canadian Journal of Physics* **35**, p. 134 (1957).
5. L. Meyer and F. Reif, Mobilities of He Ions in Liquid Helium, *Physical Review* **110**, pp. 279-280 (1958).
6. G. Careri, F. Scaramuzzi and J. O. Thomson, Heat Flush and Mobility of Electric Charges in Liquid Helium I. - Non Turbulent Flow, *Nuovo Cimento* **13**, pp. 186-196 (1959).
7. K. R. Atkins, Ions in Liquid Helium, *Physical Review* **116**, pp. 1339-1343 (1959).
8. O. Gzowski, Mobility of Ions in Liquid Dielectrics, *Nature* **194**, p. 173 (1962).
9. I. Adamczewski and J. H. Calderwood, Viscosity and Charge Carrier Mobility in the Saturated Hydrocarbons, *Journal of Physics D: Applied Physics* **8**, pp. 1211-1218 (1975).
10. I. Adamczewski and J. H. Calderwood, The Mobility of Fast Charge Carriers in Liquid Paraffins and its Dependence on Molecular Structure, *Journal of Physics D: Applied Physics* **9**, pp. 2479-2483 (1976).
11. J. A. Kok, *Electrical Breakdown of Insulating Liquids*. Interscience Publishers, New York (1961).
12. M. J. Morant, Photo-Injection of Charge into Dielectric Liquids, *Nature (London)* **187**, pp. 48-49 (1960).
13. A. M. Sletten, Electric Strength and High-Field Conduction Current in n-Hexane, *Nature (London)* **183**, pp. 311-312 (1959).
14. G. Jaffé, Zur Theorie der Ionisation in Kolonnen, *Annalen der Physik* **347**, pp. 303-344 (1913).

15. J. F. Fowler and F. T. Farmer, Conductivity induced in Unplasticized 'Perspex' by X-rays, *Nature (London)* **175**, pp. 516-517 (1955).
16. H. J. Plumley, Conduction of Electricity by Dielectric Liquids at High Field Strengths, *Physical Review* **59**, pp. 200-207 (1941).
17. I. Adamczewski, Liquid-filled Ionization Chambers as Dosimeters, *Colloques Internationaux du Centre National de la Recherche Scientifique* **179**, pp. 21-44 (1970).
18. A. O. Allen, M. P. Haas and A. Hummel, Measurement of Ionic Mobilities in Dielectric Liquids by Means of Concentric Cylindrical Electrodes, *Journal of Chemical Physics* **64**, pp. 2587-2592 (1976).
19. N. Houser and R. C. Jarnagin, Electron Ejection from Triplet State in Fluid Solutions, *Journal of Chemical Physics* **52**, pp. 1069-1078 (1970).
20. S. K. Lim, M. E. Burba and A. C. Albrecht, Mobilities of Radical Cations and Anions, Dimer Radical Anions, and Relative Electron Affinities by Times of Flight in n-hexane, *Journal of Physical Chemistry* **98**, pp. 9665-9675 (1994).
21. K. S. Haber and A. C. Albrecht, Time-of-Flight Technique for Mobility Measurements in the Condensed Phase, *Journal of Physical Chemistry* **88**, pp. 6025-6030 (1984).
22. M. E. Burba, S. K. Lim and A. C. Albrecht, Relative Electron Affinity of C₆₀ and C₇₀ and the Stokes' Law Radius of the C₇₀ Radical Anion in n-Hexane by Time-of-Flight Mobility Measurements, *Journal of Physical Chemistry* **99**, pp. 11839-11843 (1995).
23. W. C. Röntgen, *Science* **3**, pp. 726-729 (1896).
24. J. J. Thomson and G. P. Rutherford, *Conduction of Electricity through Gases*. Dover, New York (1928).
25. P. Langevin, L'ionisation des Gaz, *Ann. de Chim. Phys.* **28**, pp. 289-384 (1903).
26. P. Langevin, Une Formule Fondamentale de Théorie Cinétique, *Ann. de Chim. et de Phys.* **5**, pp. 245-188 (1905).
27. G. A. Eiceman, Advances in Ion Mobility Spectrometry - 1980-1990, *Critical Reviews in Analytical Chemistry* **22**, pp. 17-36 (1991).
28. H. E. Revercomb and E. A. Mason, Theory of Plasma Chromatography/Gaseous Electrophoresis -- A Review, *Analytical Chemistry* **47**, pp. 970-983 (1975).
29. R. Wilson and A. Brittain, *Explosives in the Service of Man*. Royal Society of Chemistry, Cambridge (1997).

30. G. R. Asbury and Jr. H. H. Hill, Negative Ion Electrospray Ionization Ion Mobility Spectrometry, *International Journal for Ion Mobility Spectrometry* **2**, pp. 1-8 (1999).
31. P. W. Atkins, *Physical Chemistry* (5th Edn). W. H. Freeman and Company, USA (1994).
32. B. H. Clowers, Separation of Gas Phase Isomers Using Ion Mobility and Mass Spectrometry, Washington State University, Pullman WA (2005).
33. J. I. Baumbach, S. Sielemann and P. Pilzecker, Coupling of Multi-Capillary Columns with two Different Types of Ion Mobility Spectrometer, *International Journal for Ion Mobility Spectrometry* **3**, pp. 28-37 (2000).
34. A. B. Kanu, P. E. Haigh and Jr. H. H. Hill, Surface Detection of Chemical Warfare Agent Simulants and Degradation Products, *Analytica Chimica Acta* **553**, pp. 148-159 (2005).
35. J. Xu, W. B. Whitten and J. M. Ramsey, Space Charge Effects on Resolution in a Miniature Ion Mobility Spectrometer, *Analytical Chemistry* **72**, pp. 5787-5791 (2000).
36. St. Sielemann, J. I. Baumbach, H. Schmidt and P. Pilzecker, Quantitative Analysis of Benzene, Toluene, and m-Xylene with the Use of a UV-Ion Mobility Spectrometer, *Field Analytical Chemistry and Technology* **4**, pp. 157-169 (2000).
37. K. B. Pfeifer and A. N. Rumpf, Measurement of Ion Swarm Distribution Functions in Miniature Low-Temperature Co-Fired Ceramic Ion Mobility Spectrometer Drift Tubes, *Analytical Chemistry* **77**, pp. 5215-5220 (2005).

Table 1: Resolving Power and Dimensions of Miniaturized Gas Phase IMS instrument.

	Instrument				
	Graseby AVM [33]	GE Itemiser [34]	Oak Ridge National Lab [35]	GAS μ IMS [36]	Sandia National Lab [37]
Drift Length (mm)	39	39	35	61.5	57
Inner Diameter (mm)	12	12.5	1.7	15	12
Electric Field (V/cm)	244	251	143	375	182
Pulse (μ s)	180	200	0.005	1000	500
Operating Temperature ($^{\circ}$ C)	24	205 \pm 5	64	24	23
Operating Pressure (Torr)	760	703-708	n/a	758	n/a
Resolving Power	20 ^a	16	27 ^a	10 ^a	6.5
Theoretical Resolving Power	28 ^b	25 ^b	39 ^c	9 ^b	18 ^{b,c}

^a Estimated from spectrum

^b Calculated from operating parameters as specified in articles

^c Assumed an operating pressure of 750 Torr (for zip code 87185)

n/a Not available

Chapter Two

Electrodispersion Ionization in Liquids

Abstract

A new ionization source, called electrodispersion ionization (EDI), was developed for generating liquid-phase ions. EDI, the liquid-phase analogue of gas-phase electrospray ionization (ESI), produced ions from aqueous samples in a non-electrolyte containing liquid medium. Visualization of the electrodispersed droplets was demonstrated with aqueous solutions of two dyes, basic fuchsin and bromothymol blue. Continuous and stable current from electrodispersion ionization was measured for inorganic and organic ions by a Faraday plate at a distance of 10 mm away from the ionization source. Quantitative ionization of the method was investigated for several amino acids with detection limits measured in the low ppm range. Under certain operation conditions, combinations of applied voltage and sample flow rate can lead to pulsing of the ion current for the EDI source. Control of this pulsing phenomenon may lead to the elimination of the need for an ion gate in such applications as liquid phase ion mobility spectrometry.

Introduction

Mass spectrometry (MS), ion mobility spectrometry (IMS), and field asymmetric waveform ion mobility spectrometry (FAIMS) are important analytical separation techniques sharing a common operational feature – they all require the production of analyte ions. The conversion of the analyte of interest into charged particles allows distinctive ion manipulation, separation, and detection. Because analysis would be impossible should the sample remain neutral, production of ions is a requisite for these analytical methods. In these instruments, an ion can be accelerated and decelerated by the use of electric and/or magnetic fields. A mixture of analyte ions can be separated based on their mass, momentum, charge, size, and interactions with the medium. Any ionizable chemical is capable of being detected as discharge current by Faraday plate, or indirectly as secondary or cascading particles by electron multiplier, photon multiplier, and multichannel plate. Furthermore, the charge count is related to the sample concentration and thus, quantification can be routinely accomplished. In addition, because the ions can be guided from one spectrometer to another, the tandem coupling of these methods provides a powerful separation process that can produce a wealth of multidimensional information. Examples of multidimensional ion separation methods include tandem MS [1-5], tandem IMS [6;7], tandem IMS and MS [6;8-11], tandem FAIMS and MS [12;13], tandem FAIMS, IMS, and MS [14].

Because all of these powerful analytical methods separate charged analyte, a wide variety of ionization methods have been developed. Electron impact ionization,

chemical ionization, fast atom/ion bombardment, electrospray ionization, matrix assisted laser desorption ionization, and desorption electrospray ionization are a few examples of established ionization methods which have been used in combination with MS or IMS [15-25]. Although these ionization sources ionize gas, liquid, and solid samples, they produce only gas-phase ions.

The production of liquid-phase ions have been less investigated. Radioactive ionization, x-ray irradiation, photo-ionization, and field emission are liquid-phase ionization sources that have been used in the studies of electrical properties of dielectric liquids. These sources produce liquid-phase ions of liquid hydrocarbons, insulating oils, liquefied noble gases, and the impurities within. Ionization by radiation generated positive and negative ions of the irradiated dielectric liquids with alpha particles emitted from radioactive substances such as polonium-210 [26-29], bismuth-212 (ThC) and polonium-212 (ThC') [30], and plutonium-239 [31]; gamma particles emitted from bismuth-214 (RaC) [32]; or with a beam of x-ray [33-36]. In photo-ionization, ions were produced by illuminating the photocathode inside the liquid medium with an intense ultraviolet light [37;38]. Field emission in the liquid-phase, where ions were created by applying a high voltage to a thin tungsten wire [39-41], was basically an extension of the gas-phase field ionization techniques devised by Müller [42].

These liquid-phase ionization methods primarily focused on ionizing the liquid medium and thus were incompatible for the analytical purpose of selectively ionizing a sample analyte, and not the liquid medium. Such an ionization source would be advantageous especially for liquid phase ion mobility spectrometry (LPIMS), which is

being developed as a new analytical separation method [43-45]. In liquid phase ion mobility spectrometry, aqueous analytes are ionized in a non-electrolyte containing liquid and moved along the spectrometer by an electric field established, not by electrolytes, but by a series of metal electrodes held at decreasing potentials. Analytes separate based on the difference in mobilities through an electric field in a non-electrolytic liquid medium. Imperative to the progress of LPIMS is the development of an adequate ionization method that is capable of ionizing aqueous solution of analytes in a non- electrolytic liquid environment.

In this paper, a new ionization source, called electrodispersion ionization (EDI), for liquid phase is introduced. Advantages of EDI over existing liquid-phase ionization techniques include the following: (1) EDI ionizes aqueous phase analytes; (2) EDI ionizes the aqueous sample in a non-electrolyte containing liquid phase, eliminating the need to create a window for external irradiation; and (3) EDI is non-radioactive. There are two proposed EDI mechanisms: one mechanism that involves the balance between surface tension and Coulombic repulsion, much like the charge residue model of ESI [23]; and another mechanism that involves the ejection of charges from the dispersed droplet, much like the ion evaporation method of ESI [23]. More comprehensive study and theoretical assessment are required to elucidate the mechanistic properties of the EDI process. The primary purpose of this study, however, was to introduce this novel approach for ion production in non-electrolyte containing liquids and to demonstrate that the ions could be produced and that they could be transferred through a non-electrolyte containing medium and with detection as discharge current by a Faraday plate.

Experimental Section

Instrumentation. *First Ionization Chamber.* A transparent enclosed ionization chamber was constructed from a Pyrex culture tube (13 mm o.d., 100 mm length) (Figure 1), including an EDI source and a Faraday plate. Aqueous sample was injected by a Harvard syringe pump “11” (Harvard Apparatus, Holliston, MA) through two lengths of fused silica capillary that were joined together by a metal union (250 μm bore). Voltage was applied to the metal union. The capillary entered into the Pyrex culture tube via a polytetrafluoroethylene (PTFE)/silicone septum. A stainless steel Faraday plate was inserted through a slit on the culture tube, cut with a rotating blade, and sealed with silicone rubber (Technical Services, Washington State University, Pullman, WA). Total ion current was detected by the Faraday plate, collected and amplified (10^6 gain) by a Keithley 427 current amplifier (Keithley Instruments, Cleveland, OH) and then processed by a LabView (National Instruments, Austin, TX)-based data acquisition system written in-house [46].

Experiments Conducted in the First Ionization Chamber. The first experiment was to electrodisperse an aqueous solution of 0.16 mM bromothymol blue into decanol. Video of the electrodispersion process was captured with a digital camcorder at 24 frames per second and the EDI current was measured concurrently. The bromothymol blue solution was allowed to flow in the sample capillary. When a blue colored drop could be seen at the tip of the capillary, the sample flow was stopped. The digital filming and current detection began. No voltage was applied to the

sample capillary until after 9 s had passed, when -10 kV was applied. The voltage at the sample capillary remained at -10 kV for the remaining of the experimental run.

The effect of sample flow rate on EDI was investigated in the positive and negative modes, with decanol as the liquid medium. Aqueous solutions of 270 μM acetic acid and 640 μM ammonium hydroxide were used as samples. +10 kV or -10 kV was applied to the sample capillary continuously, depending on the polarity of the experiment. The sample flow rates varied from 0.1 to 5.0 $\mu\text{L}/\text{min}$. The culture tube was rinsed with decanol three times between each experimental run. Current was measured continuously for 10 minutes.

Sensitivity of EDI was shown with calibration of three amino acids, arginine, lysine, and serine. The amino acids were dissolved individually in purified water, in concentrations from 10 μM to 1 mM. The amino acids were electrodispersed at +3000V into a liquid medium of decanol and the sample flow rate was maintained at 1 $\mu\text{L}/\text{min}$. Once more, the culture tube was rinsed with decanol three times between each experimental run.

Second Ionization Chamber. A second apparatus was constructed to accommodate the EDI source, a Faraday plate, and a paper target (Figure 2). An aqueous sample of basic fuchsin was introduced via a fused silica capillary (25 μm i.d. and 150 μm o.d.), with a high voltage applied to the solution in the capillary. The current was detected by the Faraday plate, located directly behind a piece of 1" x 2" high gloss laser paper (Hewlett Packard Company, Palo Alto, CA). Both the Faraday plate and the paper target were virtually grounded through the current amplifier. The

microscope slide, used to support the piece of paper and the Faraday plate, was immersed into a 50-mL Pyrex beaker filled with the IMS medium. Inside the beaker, the sample capillary was positioned 10 mm away from a paper target, and perpendicular to the target. The detected current signal was collected and amplified by the current amplifier, and acquired by a LabView-based data acquisition system.

Experiments Conducted in the Second Ionization Chamber. In this part of experiment, a colored sample solution was electrodispersed towards the paper target in a liquid medium, in order to provide simple verification that the electrodispersed sample could travel across the liquid medium and arrive at the detector. The experiment was first conducted in air with electrospray ionization (ESI), and then repeated in hexane and benzene with EDI for comparison between the two similar ionization sources. The beaker was unfilled during the ESI experiment, and filled with hexane or benzene in the EDI experiments. 10 μM of basic fuchsin was delivered at a rate of 0.5 $\mu\text{L}/\text{min}$. Aqueous solution of basic fuchsin had various intensities of pink, depending on the concentration of the solution. The ionization voltage of +2000 V was applied at 15 s after data collection started, for an interval of 100 s, and was terminated at 115 s. A photograph of each piece of paper was immediately taken after each experiment with a digital camera. A fresh piece of paper was used for each experiment.

Chemicals. The liquid media used in the experiments were decanol (Aldrich Chemical, Milwaukee WI), benzene (Fisher Scientific, Fair Lawn NJ), and hexane (J. T. Baker, Phillipsburg NJ). 0.16 mM of bromothymol blue solution was prepared in

methanol-water (50:50, vol/vol) with 0.3% ammonium hydroxide. This was to ensure that bromothymol blue, with a pKa of 7.10 [47] be present dominantly in its anionic form, where over 99.99% of bromothymol blue was present as anions in 0.3% ammonium hydroxide. HPLC grade methanol (JT Baker, Phillipsburg NJ) and 18.1 MΩ water were used. 640 μM of ammonium hydroxide solution was diluted from 30% stock standard (JT Baker, Phillipsburg NJ) in methanol-water (50:50, vol/vol). 270 μM of acetic acid solution was diluted from 37% stock standard (Fisher Scientific, Fair Lawn NJ) in methanol-water (50:50, vol/vol). L-Lysine, L-Arginine, and L-Serine (Sigma Chemical, St. Louis MO) were dissolved individually in water as 100 mM solutions. Additional solutions ranging in concentrations from 10 μM to 10 mM were prepared by diluting from these 100 mM stock solutions. The aqueous solution of 10 μM basic fuchsin, 4-((4-amino-3-methylphenyl)(4-aminophenyl)methylene)cyclohexa-2,5-dieniminium chloride, was prepared in methanol-water (90:10, vol/vol).

Calculations. The pH values and speciation of arginine, lysine and serine solutions in Table 1 were calculated by solving the acid dissociation equilibriums, charge balance, and mass balance [48].

For determining the ionization efficiency of electrodispersion ionization, the experimental current ($I_{\text{Experimental}}$) data was compared with the theoretical current. Theoretical current ($I_{\text{Theoretical}}$) is the amount of current obtained from all of the samples introduced, by considering the sample concentration (c) and the sample flow rate (f):

$$I_{\text{Theoretical}} = c \times f \times F \quad (1)$$

where F is Faraday's constant. The ionization efficiency was defined by expressing the experimental current as a percentage of the theoretical current:

$$\text{Ionization Efficiency} = \frac{I_{\text{Experimental}}}{I_{\text{Theoretical}}} \times 100\% \quad (2)$$

Results and Discussions

Digital Imaging of Electrodispersion Ionization. This experiment was conducted in the apparatus depicted in Figure 1, with decanol as the liquid medium. The photographs in Figure 3 were captured as still frames from the digital film of the electrodispersion process. The time, at which the frames were captured, was labeled underneath each photograph. A drop of bromothymol blue solution was suspended at the end of the capillary, as shown in Figure 3A. There was no sample flow. An EDI voltage of -10 kV was applied from 9.5 s until the end of the run. From the procession of images, the blue drop of bromothymol blue was observed to gradually reduce in size over time, until it was no longer visible. In addition, there was mist of tiny droplets streaming from the end of the sample capillary. The mist was marked with dotted circles on the photographs where it was more noticeable, in Figures 3C-G, and 3P.

The corresponding current signal, measured at the Faraday plate, was plotted against time in Figure 4. There was no current from 0 s to 9 s, when no voltage had been applied to the sample capillary. The related photographs in Figure 3A and 3B, at 0 s and 5 s, showed that the bromothymol blue droplet remained stationary at the end of the capillary. After the -10 kV was applied from 9.5 s, the current rose to 0.7 μA (Figure 3). The bromothymol blue droplet in Figure 3C, at 10 s, was observed to burst away from the capillary and a small mist of droplets was noticed around the end of the capillary. The current gradually decreased from 0.7 μA to 0.48 μA over the next twenty seconds (Figure 4). Figures 3D-P showed the bromothymol blue droplet gradually reduced in size. The bromothymol blue droplet was last visible in Figure 3K at 18 s and the final mist of droplets was visible in Figure 3P at 26 s. The current experienced a sharp decay at 25.4 s, from 0.48 μA to 0.00 μA . The current remained at zero level from 30 s to 60 s (Figure 4) and there was no bromothymol blue drop or mist of droplets observable in Figure 3Q-T. The correlation between the photographic procession and the current signal of the electrodispersion ionization confirmed that the current measured resulted from the electrodispersed aqueous sample. Similar images and corresponding current data from the EDI process were obtained using aqueous solution of 0.3% ammonium hydroxide and methanol-water solvent (50:50, vol/vol) (not shown).

Visual Evidence of Ion Transport through a Non-electrolyte Containing Liquid Medium. While current data of electrodispersive ionization from the previous section proved that aqueous ions were produced in the organic medium and that the ions had traveled a distance to reach the detector, it was uncertain whether the current

originated from the sample or from oxidation of the liquid medium. More direct proof was necessary to eliminate doubts that ions did travel from the ionization source, through the liquid medium, to the detector. The method proposed was to electrodisperse an aqueous solution of a dye into the liquid medium, position a piece of paper at a distance from the ionization source, and watch for a color spot to appear on the piece of paper.

The second ionization chamber (Figure 2) was used for this experiment. EDI in hexane and in benzene was compared with ESI in air. Aqueous sample of 10 μM basic fuchsin was delivered continuously at 0.5 $\mu\text{L}/\text{min}$ and the EDI voltage of +2000V was applied between 15 s and 115 s. It was observed that the total ion current of EDI in hexane and benzene was comparable to that of ESI in air (Figure 5). There was zero current when the ionization voltage was not applied. The current rose after the voltage was switched on at 15 s and the current remained at a steady level until the voltage was switched off at 115 s, after which the current gradually decayed back to the zero current. The time taken for the current to decay to zero after the voltage had terminated was 3.2 s, 6.7 s, and 8.3 s for ESI in air, EDI in hexane, and EDI in benzene, respectively. The apparent current spike at 15 s was due to a ringing resulting from switching on the high voltage power supply. The current level for ESI in air was 0.34 ± 0.02 nA, 0.80 ± 0.01 nA for EDI in hexane, and 1.02 ± 0.02 nA for EDI in benzene.

Photographs of the corresponding pieces of paper showed pink spots of basic fuchsin from electrospray in air, electrodispersion in hexane and benzene (Figure 6).

The diameter of the pink dye was the widest for ESI in air (1.03 mm), followed by that of EDI in hexane (0.52 mm), and of EDI in benzene (0.29 mm). Coulombic repulsion of the ionization spray is much larger in air than in the liquid due to the three orders of magnitude difference in diffusion between the gas phase and the liquid phase. The initial ion plume was speculated to be broader in air than in liquids, and thus resulting in a wider spot on the paper target in air. The difference in size of the pink dye between the two liquid media could be associated with their difference in viscosity. The viscosity of hexane was 0.326 cP and that of benzene was 0.604 cP [49]. The mobility and diffusion of an ion is inversely proportional to the viscosity of the medium [50-52]. Hence, the diffusion of ions is faster in hexane than in benzene, and this resulted in a wider spot on the paper target in hexane.

Effect of Sample Flow Rates. The effect of sample flow rates was investigated in the apparatus depicted in Figure 1. The current detected on the Faraday plate was plotted versus time for the two samples, 270 μM acetic acid (Figure 7a) and 640 μM ammonium hydroxide (Figure 7b) for the range of sample flow rates. A steady ion current was measured for flow rates from 1.5 to 5.0 $\mu\text{L}/\text{min}$, and the current increased with the flow rates from 0.208 to 0.292 μA for acetic acid and from 0.180 to 0.314 μA for ammonium hydroxide, with an average noise of 0.002 μA . However, at sample flow rates of 1.0 $\mu\text{L}/\text{min}$ and below, the ion current was periodic. As the sample flow rate decreased, the period between current lengthened and the current period shortened. For the positive mode, the period decreased from 29 s, 23 s, to 15 s, for 1.0, 0.5, and 0.1 $\mu\text{L}/\text{min}$ of sample flow rate, respectively. For the negative

mode, the interval increased from 7 s, 25 s, to 99 s, for 1.0, 0.5, and 0.1 $\mu\text{L}/\text{min}$ of sample flow rate, respectively.

As the flow rate was reduced, with the EDI voltage maintained at 10 kV, the sample ions were in fact ejected at a faster rate than they were being delivered. Consequently, there existed a period of time when the sample was depleted of analytes and no current was measured. When the flow rate increased, the sample depletion rate decreased, and the period of zero-current was abbreviated. When the flow rate was sufficiently fast, at 1.5 $\mu\text{L}/\text{min}$ and above, analytes were no longer completely depleted from the sample and a continuously stable current was observed. Alternatively, a stable ion current could be achieved at the lower flow rates with a lower EDI voltage, demonstrating that the EDI source could operate in a continuous or pulsed mode, by adjusting the applied voltage in relation to the sample flow rate. The advantage of having a pulsed ionization source is the possible omission of a physical ion shutter, and thus simplifying the process of miniaturizing an ion mobility spectrometer. Moreover, smaller sample volumes would be required for pulsed ionization, as the sample would not be continuously ionized and dispersed.

Calibration of Amino Acids. Figure 8 demonstrates the quantitative response of three amino acids: arginine, lysine, and serine, using the first ionization chamber. The amino acids were dissolved in water, with no additional organic solvents or acids. Concentrations from 10 μM to 1 mM were used, with a sample flow rate of 1 $\mu\text{L}/\text{min}$ and an EDI voltage of +3000V. It was observed that the current increased

with concentration for lysine and arginine, yet the current did not change appreciably with concentration for serine (Figure 8). The calibration slope for arginine was 1.68 mA/ mM and 1.39 mA/ mM for lysine. The detection limit, as defined as three times the noise level, was 31 μ M (5.4 ppm) for arginine and 12 μ M for lysine (1.8 ppm).

The difference in sensitivities among lysine, arginine, and serine may have been related to their pKa values. Table 1 provides the speciation of these amino acids in the unbuffered solution as a function of concentration and pH. Under the conditions used in this experiment, serine existed primarily as the neutral species and thus did not ionize appreciably during the electrodispersion process. On the other hand, lysine with a pKa of 10.3 [53] and arginine with a pKa of 13.2 [53] existed predominantly in the 1+ state (MH^+).

For concentrations between 10 μ M and 1 mM of arginine and lysine, more than 99.5% were present as the singly charged (MH^+), fewer than 0.02% as the doubly charged ($M+2H$)²⁺, fewer than 0.5% as the neutral species, and a negligible amount as the negatively charged ($M-H$)⁻ (Table 1). In contrast, fewer than 0.02% of serine are present as (MH)⁺, more than 99.5% are neutral, and fewer than 0.5% are negatively charged (Table 1). The results showed that when the sample analyte was largely present as its neutral species, there was an insignificant amount of current signal detected. However, when the sample analyte was present mostly in its ionized form, there was ample detectable current. These results suggested electrodispersion ionization was a process capable of transferring ions pre-existing in the aqueous sample solution and dispersing them into the organic liquid medium.

Efficiency of Ionization. The ionization efficiency of electrodispersion ionization, interpreted as a percentage of the theoretical ion output, was determined for the above EDI experiments of basic fuchsin, ammonium hydroxide, acetic acid, arginine, and lysine (Table 2). Data for 10 μM of arginine and lysine were not included as this concentration was below the detection limit for both amino acids. For basic fuchsin, ammonium hydroxide, and acetic acid, the average ionization efficiency was 15%. The average ionization efficiency for arginine and lysine was 86%. It was not apparent on why there were more ions detected than ions injected at 50 and 100 μM of arginine and lysine, although this may have been due to the existence of doubly charged species under these conditions. The EDI data of the ammonium hydroxide and acetic acid showed that the ionization efficiency increased with decreasing sample flow rate, which was also observed with ESI in gas phase IMS [54].

Conclusions

The results demonstrate the viability of a new ionization method suitable for the ionization of analytes from aqueous phase samples in non-electrolyte containing liquids. This ionization method may be especially useful in combination with liquid phase ion mobility spectrometry and other liquid phase separation methods for ions. Electrodispersion ionization is effective in delivering pre-existent positive and negative ions from aqueous sample solution and dispersing them into the organic liquid medium, with its ionization efficiency dependent upon the sample flow rate. Electrodispersion ionization is capable of ionizing aqueous solutions of inorganic and organic analytes in non-aqueous liquid medium. Furthermore, electrodispersion

ionization can operate in continuous and pulsing modes. In addition to its potential use as an ionization method for analytical methods, it may be useful for the creation of ions or the dispersion of reactants into non-aqueous phases for chemical syntheses.

Acknowledgements

This work was supported by the National Institutes of Biomedical Imaging and Bioengineering, National Institutes of Health (Grant R21EB001950).

References

1. A. K. Shukla and J. H. Futrell, Tandem Mass Spectrometry: Dissociation of Ions by Collisional Activation, *Journal of Mass Spectrometry* **35**, pp. 1069-1090 (2000).
2. K. F. Medzihradzky, J. M. Campbell, M. A. Baldwin, A. M. Falick, P. Juhasz, M. L. Vestal and A. L. Burlingame, The Characteristics of Peptide Collision-Induced Dissociation Using a High-Performance MALDI-TOF/TOF Tandem Mass Spectrometer, *Analytical Chemistry* **72**, pp. 552-558 (2000).
3. J. N. Louris, J. S. Brodbeltlusting, R. G. Cooks, G. L. Glish, G. J. Vanberkel and S. A. McLuckey, Ion Isolation and Sequential Stages of Mass-Spectrometry in a Quadrupole Ion Trap Mass-Spectrometer, *International Journal of Mass Spectrometry and Ion Processes* **96**, pp. 117-137 (1990).
4. J. V. Johnson, R. A. Yost, P. E. Kelley and D. C. Bradford, Tandem-in-Space and Tandem-in-Time Mass-Spectrometry - Triple Quadrupoles and Quadrupole Ion Traps, *Analytical Chemistry* **62**, pp. 2162-2172 (1990).
5. F. W. McLafferty, *Tandem Mass Spectrometry*. John Wiley, New York (1983).
6. S. I. Merenbloom, S. L. Koeniger, S. J. Valentine, M. D. Plasencia and D. E. Clemmer, IMS-IMS and IMS-IMS-IMS/MS for Separating Peptide and Protein Fragment Ions, *Analytical Chemistry* **78**, pp. 2802-2809 (2006).
7. S. L. Koeniger, S. I. Merenbloom, S. J. Valentine, M. F. Jarrold, H. R. Udseth, R. D. Smith and D. E. Clemmer, An IMS-IMS Analogue of MS-MS, *Analytical Chemistry* **78**, pp. 4161-4174 (2006).
8. B. K. Bluhm, K. J. Gilig and D. H. Russell, Development of a Fourier-Transform Ion Cyclotron Resonance Mass Spectrometer-Ion Mobility Spectrometer, *Review of Scientific Instruments* **71**, pp. 4078-4086 (2000).
9. F. W. Karasek, S. H. Kim and Jr. H. H. Hill, Mass Identified Mobility Spectra of p-Nitrophenol and Reactant Ions in Plasma Chromatography, *Analytical Chemistry* **48**, pp. 1133-1137 (1976).
10. B. H. Clowers and Jr. H. H. Hill, Mass Analysis of Mobility-Selected Ion Populations Using Dual Gate-Ion Mobility-Quadrupole Ion Trap Mass Spectrometry, *Analytical Chemistry* **77**, pp. 5877-5882 (2005).
11. R. Guevremont, K. W. M. Siu, J. Y. Wang and L. U. Ding, Combined Ion Mobility Time-Of-Flight Mass Spectrometry Study Of Electrospray-Generated Ions, *Analytical Chemistry* **69**, pp. 3959-3965 (1997).

12. R. Guevremont and R. W. Purves, High Field Asymmetric Waveform Ion Mobility Spectrometry-Mass Spectrometry: An Investigation of Leucine Enkephalin Ions Produced by Electrospray Ionization, *Journal of the American Society for Mass Spectrometry* **10**, pp. 492-501 (1999).
13. E. W. Robinson, D. E. Garcia, R. D. Leib and E. R. Williams, Enhanced Mixture Analysis of Poly(Ethylene Glycol) Using High-Field Asymmetric Waveform Ion Mobility Spectrometry Combined with Fourier Transform Ion Cyclotron Resonance Mass Spectrometry, *Analytical Chemistry* **78**, pp. 2190-2198 (2006).
14. K. Q. Tang, F. M. Li, A. A. Shvartsburg, E. F. Strittmatter and R. D. Smith, Two-Dimensional Gas-Phase Separations Coupled to Mass Spectrometry for Analysis of Complex Mixtures, *Analytical Chemistry* **77**, pp. 6381-6388 (2005).
15. M. Barber, Fast Atom Bombardment Mass Spectrometry, *Analytical Chemistry* **54**, pp. A645-657 (1982).
16. C. B. Shumate and Jr. H. H. Hill, Coronaspray Nebulization and Ionization of Liquid Samples for Ion Mobility Spectrometry, *Analytical Chemistry* **61**, pp. 601-606 (1989).
17. S. Lee, T. Wytenbach and M. T. Bowers, Gas Phase Structures of Sodiated Oligosaccharides by Ion Mobility Ion Chromatography Methods, *International Journal of Mass Spectrometry* **167**, pp. 605-614 (1997).
18. S. Myung, J. M. Wiseman, S. J. Valentine, Z. Takats, R. G. Cooks and D. E. Clemmer, Coupling Desorption Electrospray Ionization with Ion Mobility/Mass Spectrometry or Analysis of Protein Structure: Evidence for Desorption of Folded and Denatured States, *Journal of Physical Chemistry B* **110**, pp. 5045-5051 (2006).
19. R. W. Purves and R. Guevremont, Electrospray Ionization High-Field Asymmetric Waveform Ion Mobility Spectrometry-Mass Spectrometry, *Analytical Chemistry* **71**, pp. 2346-2357 (1999).
20. A. O. Nier, A Mass Spectrometer for Isotope and Gas Analysis, *Review of Scientific Instruments* **18**, pp. 398-411 (1947).
21. A. G. Harrison, *Chemical Ionization Mass Spectrometry*. CRC Press, Boca Raton, FL (1983).
22. M. Barber, R. S. Bardoli and R. D. Segwick, Fast Atom Bombardment of Solids (F.A.B.): A New Ion Source for Mass Spectrometry, *Journal of the Chemical Society, Chemical Communications* pp. 325-327 (1981).
23. P. Kebarle, A Brief Overview of the Present Status of the Mechanisms Involved in Electrospray Mass Spectrometry, *Journal of Mass Spectrometry* **35**, pp. 804-817 (2000).

24. Z. Takats, J. M. Wiseman, B. Gologan and R. G. Cooks, Mass Spectrometry Sampling Under Ambient Conditions with Desorption Electrospray Ionization, *Science* **306**, pp. 471-473 (2004).
25. M. Karas, U. Bahr and U. Giessman, Matrix-Assisted Laser Desorption Ionization Mass-Spectrometry, *Mass Spectrometry Reviews* **10**, pp. 335-357 (1991).
26. R. L. Williams, Ionic Mobilities in Argon and Helium Liquids, *Canadian Journal of Physics* **35**, p. 134 (1957).
27. L. Meyer and F. Reif, Mobilities of He Ions in Liquid Helium, *Physical Review* **110**, pp. 279-280 (1958).
28. G. Careri, F. Scaramuzzi and J. O. Thomson, Heat Flush and Mobility of Electric Charges in Liquid Helium I. - Non Turbulent Flow, *Nuovo Cimento* **13**, pp. 186-196 (1959).
29. G. Aniansson, New Method for Measuring the α -Particle Range and Straggling in Liquids, *Physical Review* **98**, pp. 300-302 (1955).
30. M. S. Malkin and H. L. Schultz, Electron Mobilities in Liquid Argon, *Physical Review* **83**, pp. 1051-1052 (1951).
31. D. W. Swan, Electron Attachment Processes in Liquid Argon containing Oxygen or Nitrogen Impurity, *Proceedings of the Physical Society (London)* **82**, pp. 74-84 (1963).
32. G. W. Hutchinson, Ionization in Liquid and Solid Argon, *Nature* **162**, pp. 610-611 (1948).
33. O. Gzowski and J. Terlecki, A Method for Measuring the Mobility of Ions in Dielectric Liquids, *Acta Physica Polonica* **18**, pp. 191-198 (1959).
34. O. Gzowski, Mobility of Ions in Liquid Dielectrics, *Nature* **194**, p. 173 (1962).
35. B. Jachym, Mobility of Ions in Dielectric Liquids of High Viscosity, *Acta Physica Polonica* **24**, pp. 785-790 (1963).
36. B. Jachym, Ion Mobility in Liquid Cyclohexane, *Acta Physica Polonica* **24**, pp. 243-247 (1963).
37. O. H. LeBlanc. Jr., Electron Drift Mobility in Liquid n-Hexane, *Journal of Chemical Physics* **30**, pp. 1443-1447 (1959).
38. J. Terlecki, Measurement of the Mobility of Negative Ions in Saturated Hydrocarbon Liquids with High Electric Fields, *Nature* **194**, pp. 172-173 (1962).
39. B. L. Henson, Mobility of Positive Ions in Liquefied Argon and Nitrogen, *Physical Review* **135**, pp. A1002-1008 (1964).

40. B. Halpern and R. Gomer, Field Ionization in Liquids, *Journal of Chemical Physics* **51**, pp. 1048-1056 (1969).
41. B. Halpern and R. Gomer, Field Emission in Liquids, *Journal of Chemical Physics* **51**, pp. 1031-1047 (1969).
42. E. W. Müller and K. Bahadur, Field Ionization of Gases at a Metal Surface and the Resolution of the Field Ion Microscope, *Physical Review* **102**, pp. 624-631 (1956).
43. H. H. Hill, Jr. and M. Tam. Ion Mobility Spectrometry Method and Apparatus. US Patent. 7,071,465. July 4, 2006.
44. M. Tam and H. H. Hill, Jr. Liquid Phase Ion Mobility Spectrometry. 14th International Symposium on Ion Mobility Spectrometry. Paris, France. 2005.
45. M. Tam and H. H. Hill, Jr. Analytical Detection by Liquid Phase Ion Mobility Spectrometry. 54th American Society for Mass Spectrometry Conference on Mass Spectrometry. Seattle, WA. 2006.
46. B. H. Clowers, Separation of Gas Phase Isomers Using Ion Mobility and Mass Spectrometry, Washington State University, Pullman WA (2005).
47. D. Gupta, *Journal of Pharmaceutical Science* **57**, pp. 2140-2142 (1968).
48. M. M. Benjamin, *Water Chemistry*. McGraw-Hill, New York (2001).
49. D. R. Lide, *CRC Handbook of Chemistry and Physics* (85th Edn). CRC Press, Boca Raton, FL (2004).
50. D. R. Baker, *Capillary Electrophoresis*. John Wiley & Sons, Inc., New York, NY (1995).
51. J. S. Townsend, The Diffusion of Ions into Gases, *Philosophical Transactions of the Royal Society of London* **A193**, pp. 129-158 (1900).
52. W. Nernst, Zur Kinetik der in Lösung befindlichen Körper - I. Theorie der Diffusion, *Zeitschrift fuer Physikalische Chemie* **2**, pp. 613-637 (1888).
53. S. Budavari, *The Merck Index* (12th Edn). Merck Research Laboratories, Whitehouse Station NJ (1996).
54. X. Tang, J. E. Bruce and Jr. H. H. Hill, Characterizing Electrospray Ionization Using Atmospheric Pressure Ion Mobility Spectrometry, *Analytical Chemistry* **78**, pp. 7751-7760 (2006).

Table 1: Solution pH values and speciation information for arginine, lysine, and serine at concentrations from 10 μ M to 1 mM.

Amino Acid	Formal Conc. (mM)	pH	Fractional Dissociation			
			(M+2H) ²⁺	(M+H) ⁺	M	(M-H) ⁻
Arginine	0.01	6.87	0.002%	99.531%	0.467%	0.000%
	0.05	6.65	0.004%	99.715%	0.281%	0.000%
	0.10	6.52	0.005%	99.785%	0.210%	0.000%
	0.50	6.21	0.010%	99.889%	0.101%	0.000%
	1.00	6.07	0.013%	99.912%	0.075%	0.000%
Lysine	0.01	6.82	0.002%	99.578%	0.419%	0.000%
	0.05	6.57	0.004%	99.761%	0.234%	0.000%
	0.10	6.44	0.006%	99.822%	0.172%	0.000%
	0.50	6.11	0.012%	99.906%	0.082%	0.000%
	1.00	5.98	0.017%	99.923%	0.060%	0.000%
Serine	0.01	6.10	n/a	0.012%	99.907%	0.080%
	0.05	6.24	n/a	0.009%	99.882%	0.109%
	0.10	6.55	n/a	0.004%	99.772%	0.223%
	0.50	6.67	n/a	0.003%	99.700%	0.297%
	1.00	6.88	n/a	0.002%	99.517%	0.481%

Table 2: Ionization efficiency of electrodispersion ionization, tabulated with the theoretical and experimental current data.

Sample	Conc. (μM)	Flow Rate ($\mu\text{l}/\text{min}$)	Liquid Medium	Current (μA , unless stated)		Efficiency of Ionization (%)
				Theoretical	Experimental	
Basic	10	0.5	Benzene	8.04 nA	1.02 ± 0.02 nA	12.7
Fuchsin	10	0.5	Hexane	8.04 nA	0.80 ± 0.01 nA	9.95
Ammonium Hydroxide	640	1.5	Decanol	1.544	0.180 ± 0.003	11.7
	640	2.0	Decanol	2.058	0.242 ± 0.002	11.8
	640	3.0	Decanol	3.087	0.301 ± 0.001	9.76
	640	4.0	Decanol	4.117	0.309 ± 0.002	7.51
	640	5.0	Decanol	5.146	0.314 ± 0.004	6.09
Acetic Acid	270	1.5	Decanol	0.651	0.208 ± 0.003	31.9
	270	2.0	Decanol	0.868	0.228 ± 0.002	26.3
	270	3.0	Decanol	1.303	0.260 ± 0.003	20.0
	270	4.0	Decanol	1.737	0.278 ± 0.002	16.0
	270	5.0	Decanol	2.171	0.292 ± 0.002	13.5
Arginine	50	1.0	Decanol	0.080	0.086 ± 0.009	108
	100	1.0	Decanol	0.160	0.19 ± 0.04	121
	500	1.0	Decanol	0.803	0.332 ± 0.006	41.4
	1000	1.0	Decanol	1.607	1.10 ± 0.02	68.6
Lysine	50	1.0	Decanol	0.080	0.113 ± 0.006	141
	100	1.0	Decanol	0.161	0.17 ± 0.02	105
	500	1.0	Decanol	0.803	0.38 ± 0.01	47.9
	1000	1.0	Decanol	1.607	0.84 ± 0.02	52.3

Figure Captions

Figure 1: Schematic of the electrodispersion ionization apparatus. The ionization chamber was built using a Pyrex culture tube (A) closed with an open top screw cap (B) and a polytetrafluoroethylene (PTFE)/silicone septum (C). The aqueous sample was delivered through a fused silica capillary (D), which had a high voltage applied to it via a metal connection. The current was measured at the Faraday plate (E).

Figure 2: Schematic of the second electrodispersion ionization apparatus. The ionization apparatus included a fused silica capillary (A) for delivering aqueous sample, a paper target (B) and a Faraday plate (C) for detection, and a microscope slide (D) for supporting the paper target and the Faraday plate. The ionization apparatus was housed inside a 50-mL Pyrex beaker (E) filled with the appropriate liquid medium.

Figure 3: Timed photographs of electrodispersion ionization. A drop of bromothymol blue solution was introduced into a liquid medium of decanol through a fused silica capillary. The time, at which the photograph was captured, was labeled underneath the individual photograph. There was no applied EDI voltage from 0 s to 9.5 s, after which -10 kV was applied until 60 s.

Figure 4: Current generated from electrodispersion ionization. An aqueous solution of Bromothymol Blue was electrodispersed into a liquid medium of decanol. The signal corresponded to the photographs in Figure 3.

Figure 5: Electrodispersed ion current of 10 μM basic fuchsin (a) by electrospray ionization (ESI) in air, (b) by electrodispersion ionization (EDI) in hexane, and (c) by EDI in benzene. ESI and EDI voltages of +2000V were applied at 15 s and terminated at 115 s.

Figure 6: Photographs of the paper target from electrodispersion ionization. These were the corresponding paper targets from the results shown in Figure 5, of ionizing 10 μM basic fuchsin (a) by electrospray ionization (ESI) in air, (b) by electrodispersion ionization (EDI) in hexane and (c) by EDI in benzene.

Figure 7a: Electrodispersed current as a function of sample flow rate in the positive mode. Current time plots illustrated the effect of sample flow rate on electrodispersion ionization, with 270 μM acetic acid as sample and decanol as liquid medium. The sample flow rate ranged from 0.1 to 5.0 $\mu\text{L}/\text{min}$.

Figure 7b: Electrodispersed current as a function of sample flow rate in the negative mode. Current time plots illustrated the effect of sample flow rate on electrodispersion ionization with 640 μM ammonium hydroxide as sample, and decanol as liquid medium. The sample flow rate ranged from 0.1 to 5.0 $\mu\text{L}/\text{min}$.

Figure 8: Calibration plot for three amino acids: arginine, lysine, and serine, at 0, 10 μM , 50 μM , 100 μM , 500 μM , and 1 mM, dissolved in water. The EDI solvent was decanol and the applied EDI voltage was +3000V.

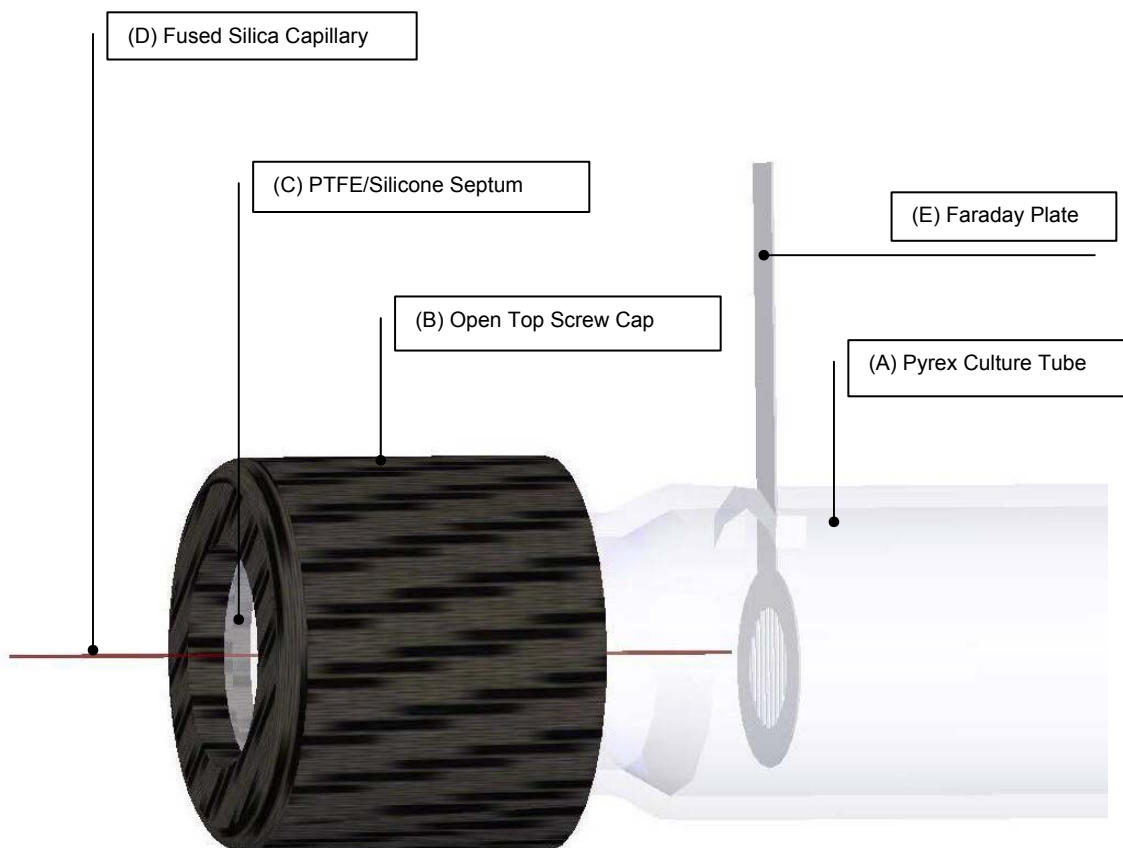


Figure 1: Schematic of the electrodispersion ionization apparatus. The ionization chamber was built using a Pyrex culture tube (A) closed with an open top screw cap (B) and a polytetrafluoroethylene (PTFE)/silicone septum (C). The aqueous sample was delivered through a fused silica capillary (D), which had a high voltage applied to it via a metal connection. The current was measured at the Faraday plate (E).

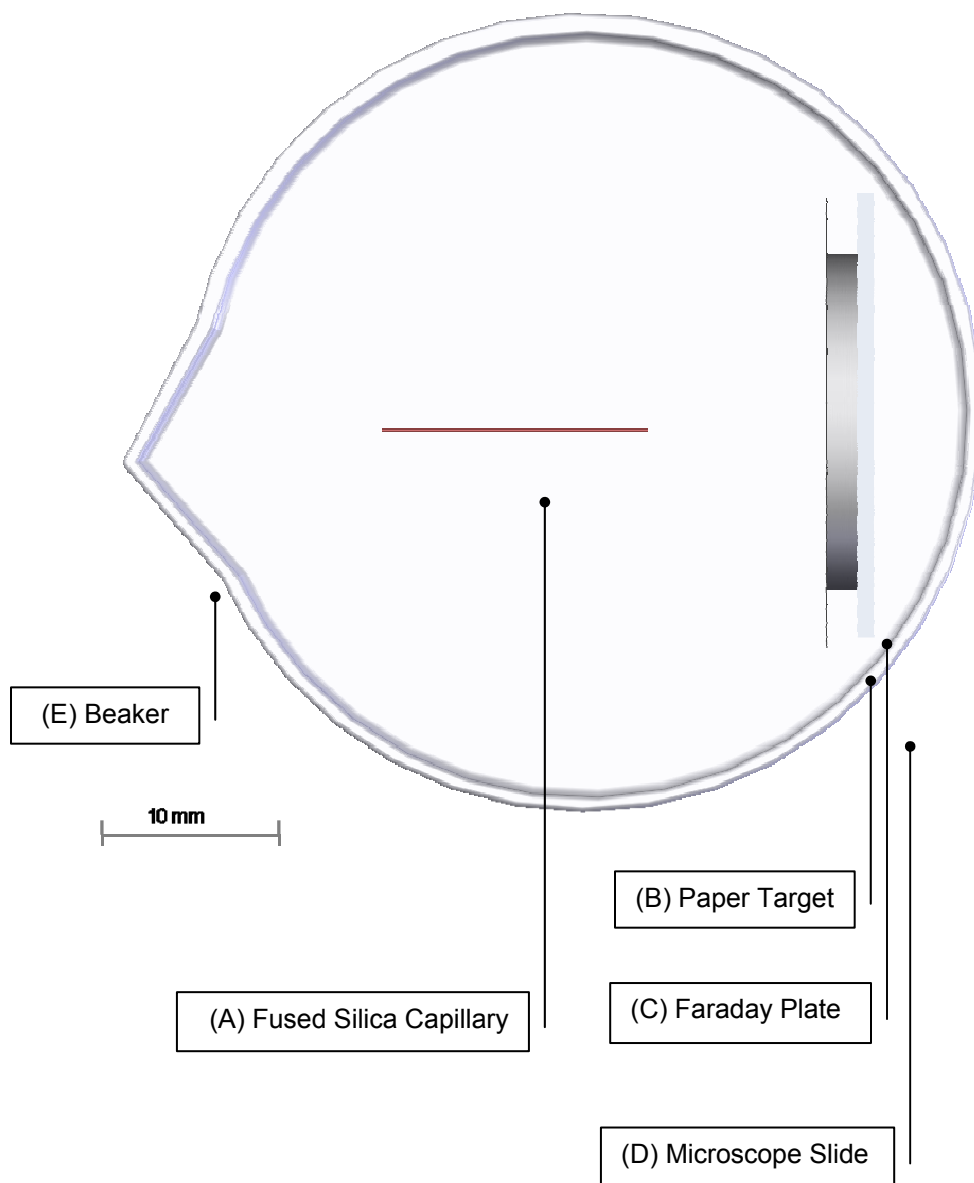


Figure 2: Schematic of the second electrodispersion ionization apparatus. The ionization apparatus included a fused silica capillary (A) for delivering aqueous sample, a paper target (B) and a Faraday plate (C) for detection, and a microscope slide (D) for supporting the paper target and the Faraday plate. The ionization apparatus was housed inside a 50-mL Pyrex beaker (E) filled with the appropriate liquid medium.

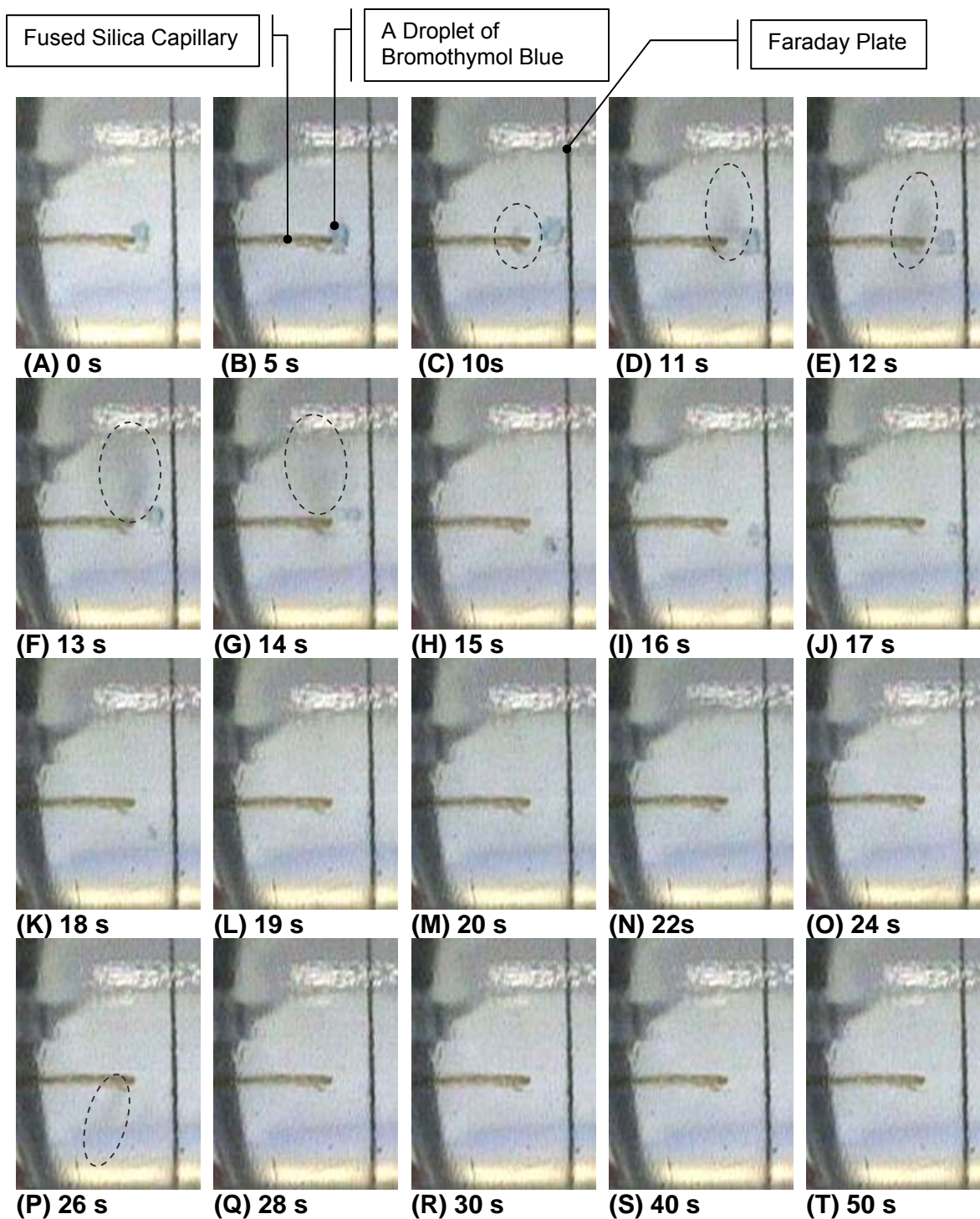


Figure 3: Timed photographs of electrodispersion ionization. A drop of bromothymol blue solution was introduced into a liquid medium of decanol through a fused silica capillary. The time, at which the photograph was captured, was labeled underneath the individual photograph. There was no applied EDI voltage from 0 s to 9.5s, after which -10 kV was applied until 60 s.

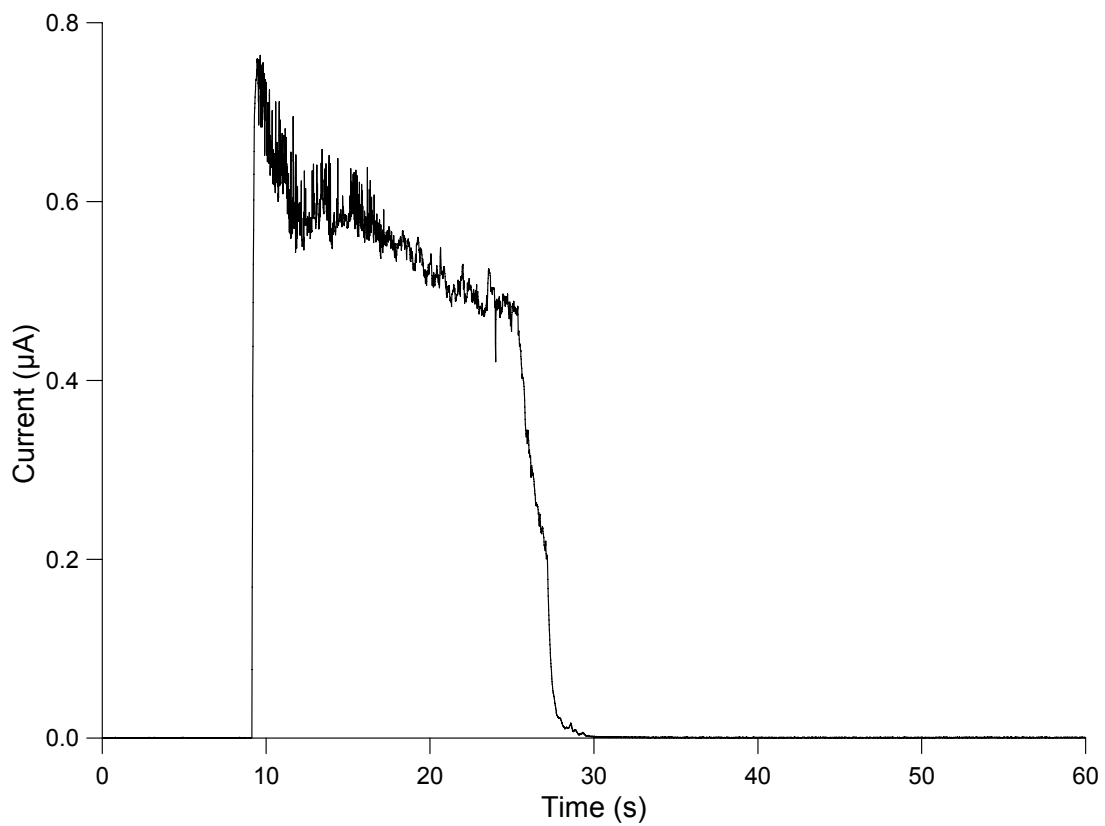


Figure 4: Current generated from electrodispersion ionization. An aqueous solution of Bromothymol Blue was electrodispersed into a liquid medium of decanol. The signal corresponded to the photographs in Figure 3.

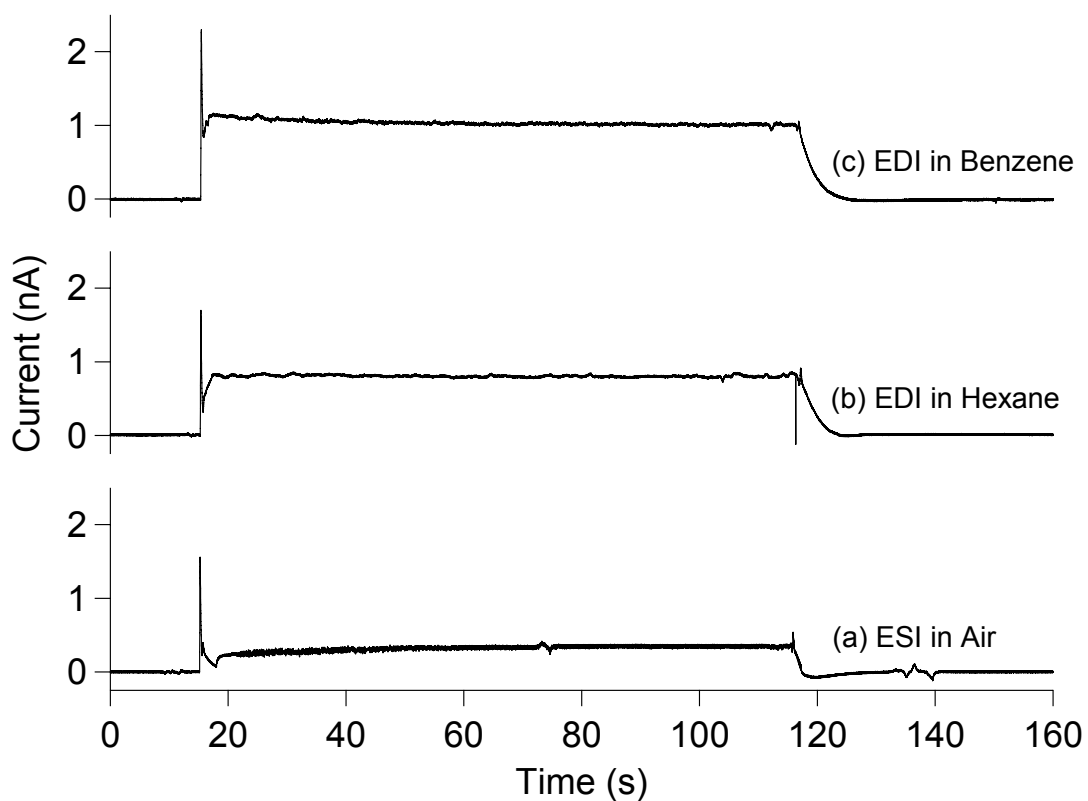


Figure 5: Electrodispersed ion current of 10 μM basic fuchsin (a) by electrospray ionization (ESI) in air, (b) by electrodispersion ionization (EDI) in hexane, and (c) by EDI in benzene. ESI and EDI voltages of +2000V were applied at 15 s and terminated at 115 s.

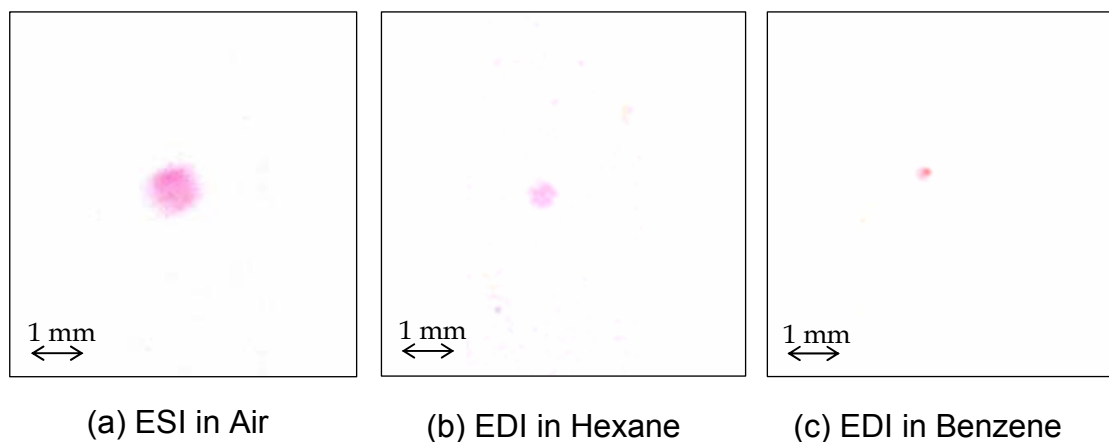


Figure 6: Photographs of the paper target from electrodispersion ionization. These were the corresponding paper targets from the results shown in Figure 5, of ionizing 10 μM basic fuchsin (a) by electrospray ionization (ESI) in air, (b) by electrodispersion ionization (EDI) in hexane and (c) by EDI in benzene.

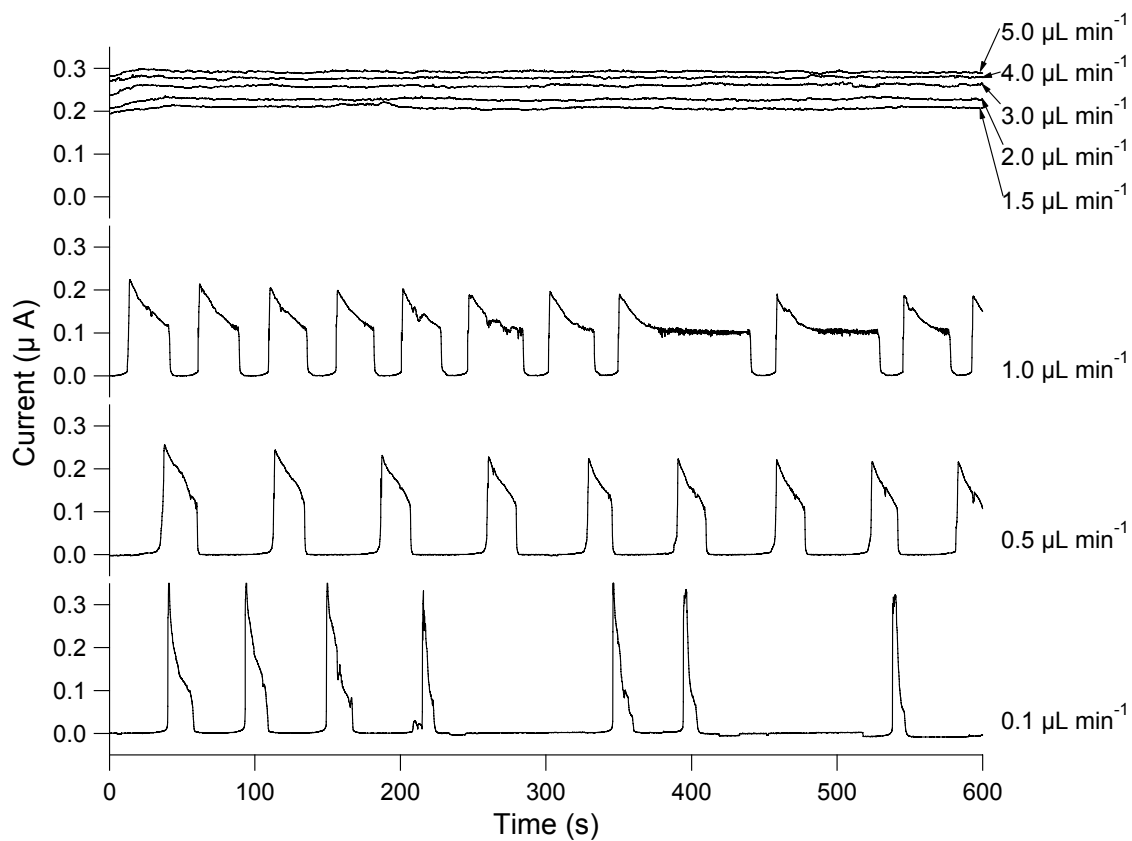


Figure 7a: Electrodispersed current as a function of sample flow rate in the positive mode. Current time plots illustrated the effect of sample flow rate on electrodispersion ionization, with 270 μM acetic acid as sample and decanol as liquid medium. The sample flow rate ranged from 0.1 to 5.0 $\mu\text{L}/\text{min}$.

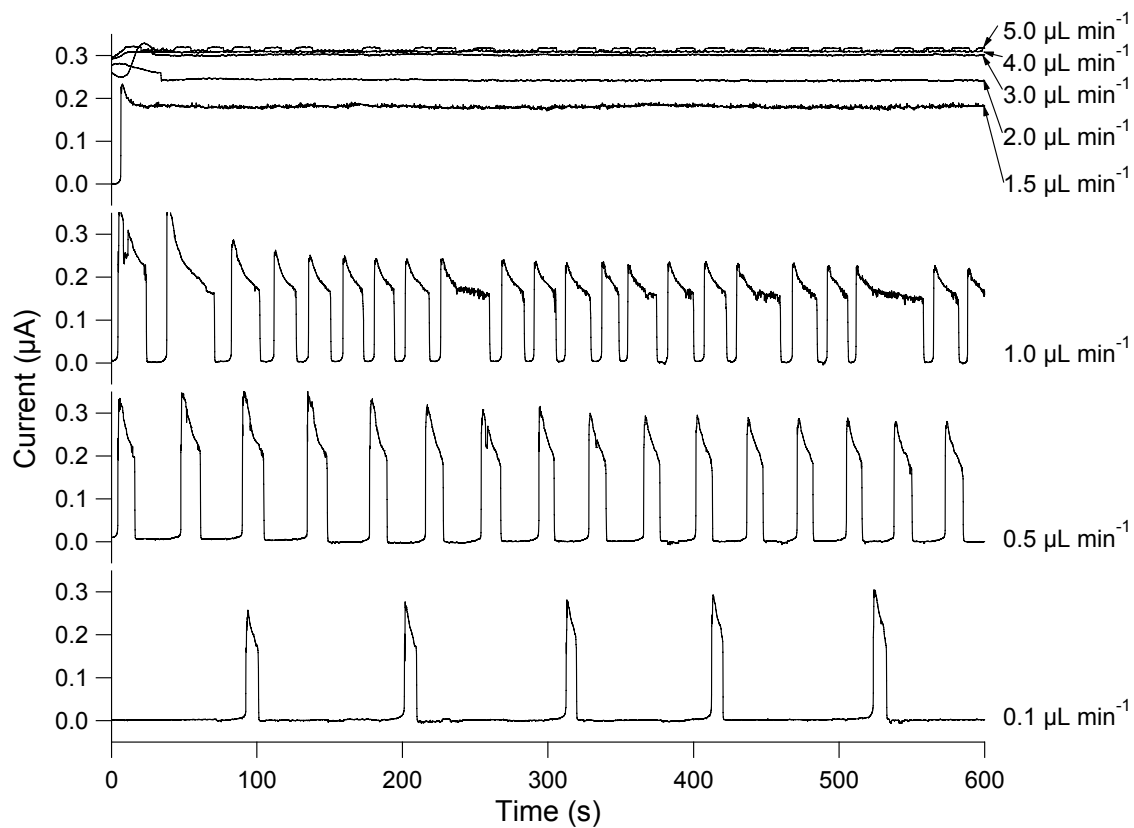


Figure 7b: Electrodispersed current as a function of sample flow rate in the negative mode. Current time plots illustrated the effect of sample flow rate on electrodispersion ionization with 640 µM ammonium hydroxide as sample, and decanol as liquid medium. The sample flow rate ranged from 0.1 to 5.0 µL/min.

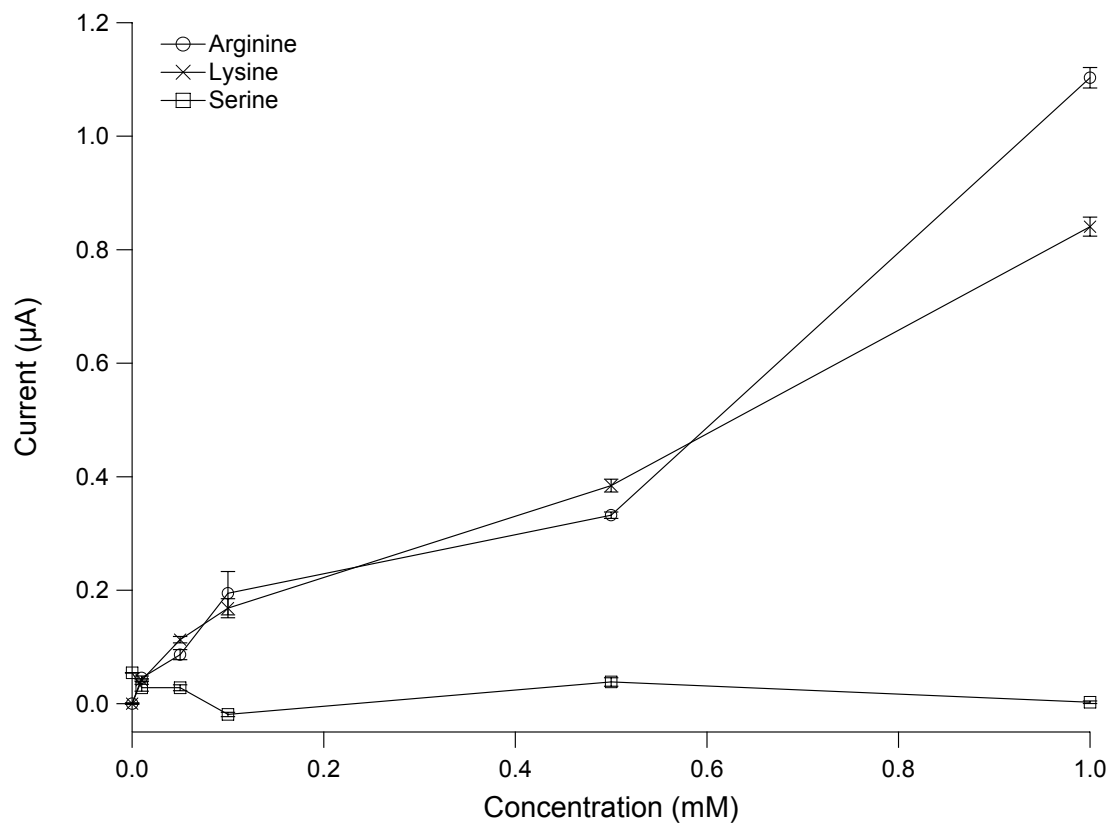


Figure 8: Calibration plot for three amino acids: arginine, lysine, and serine, at 0, 10 μM , 50 μM , 100 μM , 500 μM , and 1 mM, dissolved in water. The EDI solvent was decanol and the applied EDI voltage was +3000V.

Chapter Three

Liquid Phase Ion Mobility Spectrometry

Abstract

Aqueous phase analyte ions were extracted into and transported through a non-electrolyte containing liquid to produce a novel analytical method, called liquid phase ion mobility spectrometry. The movement of ions was directed by an electric field established by using a series of metal rings connected with resistors. Spectra of ammonium nitrate, sodium chloride, and fuchsin demonstrated liquid phase ion mobility spectrometry. Although complex and inadequately resolved, these spectra revealed that the ions could be transported and separated in an ion mobility spectrometer operating in a liquid phase. Preliminary data with pulsed electrodispersion ionization showed that a 5-mm long miniaturized liquid phase ion mobility spectrometer had a resolving power of 17. By replacing the gas medium in gas phase IMS with a non-electrolyte containing liquid medium, a miniaturized liquid phase ion mobility spectrometer obtained a similar resolving power as a gas phase IMS ten times its size.

Introduction

Interest in ion mobility spectrometry (IMS), first called plasma chromatography and sometimes called ion chromatography or gas phase electrophoresis, expanded exponentially in the last 15 years, as judged by the growth of IMS publications from less than 20 per year in 1990 to over 135 per year in 2005. Ion mobility spectrometry separates compounds based on the differences in mobilities in a weak electric field. Ion mobilities depend on the size and charge of the ion as well as the interaction between the ions and the separation medium. Reports have shown not only the separation of isobaric analytes through their size-to-charge ratios in conventional ion mobility spectrometry [1-5], but also the separation of enantiomers through their different stereospecificities in chiral ion mobility spectrometry [6]. In addition, the size-to-charge separation of IMS complements other separation techniques, such as differential mobility spectrometry, mass spectrometry, and chromatography. Tandem instruments with multidimensional separation modes were integrated for unraveling complex metabolomes [7;8], protein structures [9;10] and carbohydrate identities [1]. The addition of IMS to other instruments can improve instrumental selectivity [11-13]. In an effort to increase the capabilities and separation efficiency of IMS, larger and larger IMS instruments have been constructed. A record 210-cm long IMS drift tube [14] and a tandem IMS-IMS drift tube of 182 cm in total length were introduced recently [10]. The 210-cm long IMS was coupled to a quadrupole time-of-flight mass spectrometer (QTOF MS). Lossless ion transmission from the mega long IMS to the QTOF MS was made possible by an ion funnel whose inner diameter tapered gradually [14]. Characterization of fragment ions were made possible by the two

staged IMS-IMS, where molecular ions underwent collisional activation after the first stage of IMS [10].

In contrast to IMS instrument enlargement, much effort has also been spent on miniaturizing IMS to capture its unique benefits of simple instrumentation and milliseconds-fast analysis time [15-19]. Miniaturized IMS instruments have vast applications, from medical, industrial, environmental, to military interests, as personal chemical sensors for military personnel and first line responders [20;21], building air quality sensors [22-24], and medical diagnostic sensors [25-27]. These applications require compact, lightweight, and inexpensive analytical devices that can also provide selective and sensitive monitoring in real-time. Unfortunately, most miniaturized IMS instruments developed to date have significantly reduced resolving powers relative to their larger counter parts. While resolving powers greater than 100 are common today for most large-scale IMS instruments, miniaturized instruments exhibit resolving powers less than 30.

IMS resolution is not only dependent upon resolving power, but also upon separation. Resolving power is a measure of the sharpness of a peak, while separation is a measure of the difference in the average migration times of the product ions of two analytes. Thus, the resolution (R_S) between two analytes, with reduced mobility values K_{0A} and K_{0B} , increase with the IMS resolving power:

$$R_S = 0.59R_P \left(\frac{K_{0A} - K_{0B}}{K_{0A}} \right) \quad (1)$$

Improving IMS resolution is crucial in the development and improvement of miniaturized IMS. High resolving power (R_P) is necessary for separating compounds with similar reduced mobilities (K_0) and for separating complex mixtures. For example, benzene (K_0 2.27 cm²/V·s) and m-xylene (K_0 2.27 cm²/V·s) were separated in a 12 cm long IMS drift tube, with R_P of 18, but a shorter 6 cm long IMS drift tube, with a lower R_P of 10, was unable to separate the two compounds [19].

Drift gas selection has been explored to improve IMS separation by changing the interaction between the analyte ions and the gas medium. Compounds that were inseparable in nitrogen drift gas, could be separated in helium, carbon dioxide, and chiral drift gases in the laboratory-size IMS instrument [6;28] and in miniaturized gas phase IMS instrument [29]. Adding another separation dimension in tandem with a miniaturized ion mobility spectrometry improves the peak capacity of the instrument. Multicapillary columns, gas chromatographic columns, glass wool and silica gel columns have been coupled at the front end of miniaturized ion mobility spectrometers to pre-separate otherwise co-migrating mobility peaks [19;30-32].

For a given analyte and drift gas under low-field condition, where the relationship between ion velocity and electric field is linear and where mobility is constant, the maximum diffusion limited resolving power is proportional to the square root of both the drift length and pressure:

$$\text{Diffusion Limited } R_{p,\max} \propto \left[\frac{P \cdot L}{T^{3/2}} \right]^{1/2} \quad (2)$$

Voltage and electric field do not play a role in the maximum diffusion limited resolving power derivation because it is based on the notion that the highest electric field under the low-field condition is used. It is apparent from equation (2) that increasing the pressure of the medium would cancel out the negative effect of miniaturization on separation efficiency of IMS. The extreme of increasing the pressure of a gas will drive a phase transition and condense it into a liquid.

The objective of this project was to investigate the one parameter that had remained consistent in the forty years of research in IMS – to replace the gaseous medium with a liquid medium. Because of the low diffusion rates of analyte ions in liquids, it should be able to miniaturize the instrumentation for liquid phase ion mobility spectrometry (LPIMS) without concomitant loss in resolving power.

Although gas phase IMS has been called gas phase electrophoresis, LPIMS is different from liquid phase electrophoresis. Like electrophoresis, ions in LPIMS migrate under the influence of an electric field. While the electric field in electrophoresis is established by the charged electrolyte in the liquid medium, LPIMS does not require the presence of charged electrolyte. In LPIMS, the spectrometer has decreasing potential with length that establishes an external electric field. Because the liquid media in LPIMS contain no electrolyte, the only ion current is carried by the ions produced in the ionization source. Hence, a universal Faraday plate can be used to detect the ion current from the analyte. Besides the advantage of offering a simple detection method, the lack of electrolyte in the liquid medium permits the use of higher voltage in LPIMS without experiencing degradation of resolving power due to joule heating.

Research of ion mobility in liquid phases began in the early 20th century as a series of physical experiments evolving from conductivity studies of dielectric liquids. The liquid media studied were liquid hydrocarbons, insulating oils and liquefied noble gases. Bialobrzewski and Jaffé conducted the first experiments of mobility measurements in dielectric liquids. Bialobrzewski [33] worked on the relation between ion mobility and the viscosity (η) of the dielectric liquid medium in 1911 and Jaffé [34] performed ion mobility experiments in hexane in 1913. In 1937, Adamczewski [35] performed the first systematic ion mobility experiments in a series of liquid saturated hydrocarbons and studied the relation of ion mobility to the coefficient of viscosity. Adamczewski concluded that the mobility (μ) of ion was inversely proportional to $\eta^{3/2}$ at constant temperature, known as the Adamczewski's relation. In the 1950s, measurements of mobility of helium ions in liquefied helium were done by Williams [36], L. Meyer et al [37], Careri et al [38] and Atkins [39]. In 1964, Gzowski [40] measured mobility of positive and negative ions in pure and mixtures of hydrocarbons. Although the ions were not identified, he concluded that (1) positive ions of different mobilities were present; (2) mobility of negative ions were greater than that of positive ions in all the liquids studied; (3) mobility of negative ions were found to be inversely proportional to viscosity of liquid, known as the Walden's Rule; and (4) mobility of positive ions were found to be inversely proportional to $\eta^{3/2}$, same as Adamczewski's finding in 1937.

Interests in mobility studies of dielectric liquids persisted. A majority of which consisted of the physical investigations of positive and negative intrinsic ions of the dielectric liquids in the study of the breakdown process of dielectric liquids [41-43],

the study of ion recombination and diffusion in liquids subjected to high-energy radiation [44;45], and the study of dielectric liquid properties in particle counters and spark chambers [46;47]. Investigations of ions from extrinsic analyte were less studied. Examples were the analyses of sulfur hexafluoride [48], methyl halides [48], tetramethylparaphenylenediamine [49;50], quinones [50;51], porphines [50;51], and fullerenes [50;52]. In these instances, the samples were dissolved in the same dielectric liquid medium where experiments were conducted. Up to this date, there has been no research performed on using ion mobility spectrometry in liquid phases as an analytical separation technique for aqueous phase analytes.

For the application of liquid phase ion mobility to analytical chemistry, however, analyte ions, typically in aqueous samples, need to be introduced into the liquid medium and transported through it in order to measure their mobilities. This paper presents the concept of a chemical separation and analysis method based on ion mobility spectrometry using a liquid phase instead of a gas phase as the medium through which analyte ions migrate. LPIMS, on a miniaturized scale, is a novel analytical separation method that is capable of achieving better separation power than a gas phase IMS of the same dimension.

Experimental Section

Instrumentation. *Resistive Glass LPIMS.* The apparatus consisted of an electrodispersion ionization source (EDI), a mobility tube, and a Faraday plate (Figure 1). The apparatus was placed inside a Pyrex dish (10 cm o.d. and 5 cm

height) filled with the liquid medium. The ion mobility tube was a resistive glass tube (Burle Technologies Inc., Lancaster, PA) with a 4.1 mm i.d., 5.4 mm o.d., and 5 mm in length. The internal surface resistance was 10 M Ω and the external surface resistance was discontinued. Electrodes were attached to either ends of the resistive glass tube. Voltage was applied to the front electrode. The end electrode was grounded through a 430-k Ω resistor.

The aqueous sample of 10 μ M basic fuchsin was delivered through a fused silica capillary by a syringe pump (Pump 11 Plus, Harvard Apparatus, Holliston, MA) at 0.5 μ L/min. A polyetheretherketone (PEEK) microelbow junction (Upchurch Scientific In., Oak Harbor, WA) was used to allow a 90° bend of the fused silica capillary. The end of the fused silica capillary was positioned approximately 2 mm in front of the ion mobility tube. The EDI voltage, applied to a metal union, was set at 2000 V above the ion mobility tube voltage. For example, when the voltage applied to the ion mobility tube was 500 V, then the EDI voltage was 2500 V. The aqueous sample was electrodispersed into the liquid medium and transported through the ion mobility tube by the applied electric field. Total ion current was measured on the Faraday plate, located 2.3 mm behind the resistive glass tube. The signal was amplified at 10⁹ volts per ampere by a Keithley 427 current amplifier (Keithley Instruments, Cleveland, OH) and acquired by a LabView (National Instruments, Austin, TX) based data acquisition system. The mobility experiments were carried out in hexane while varying the electric field on the ion mobility tube from 0 to 6000 V/cm. The experiments were repeated with electrospray ionization (ESI) in air for comparison. In order to establish the background current level in the two media, experiments

were also run with voltages applied to the ion mobility tube, but in the absence of sample ionization.

The gating efficiency of Bradbury-Nielsen shutter was examined using an extended variation of the above instrumentation, where the Bradbury-Nielsen shutter was placed between two lengths of resistive glass tube of the same dimension. The Bradbury-Nielsen shutter was constructed from two Macor ceramic rings with 4.56 mm i.d., 9.30 mm o.d., and a thickness of 2.26 mm. Alloy 46 stainless steel wires of 76 μm diameter (California Fine Wire Company, Grover Beach, CA) were wound at 0.64 mm parallel spacing. The shutter wires were sandwiched between the two Macor rings and secured with a ceramic adhesive (Resbond 940, Cotronics Corp., Brooklyn, NY). Alternate wires on the Bradbury-Nielsen shutter were electrically insulated, such that this would create an electrical field, orthogonal to the electric field on the ion mobility spectrometer, when a potential was applied across these alternate wires. The pulsing of the ion shutter was controlled by a Double Pole Single Throw (DPST) two-way switch, constructed by Technical Services of Washington State University.

Stacked-Ring LPIMS. Preliminary LPIMS data was obtained from an enclosed liquid mobility spectrometer constructed at Washington State University (Figure 2). The ion mobility spectrometer was produced by hollowing out half-cylinders from two Teflon blocks. Slits for conducting electrodes were cut into the Teflon block at 1-mm apart. Stainless steel electrodes (Fotofab, Chicago IL) were inserted into each slit. While keeping each of the sixteen electrodes vertically aligned, the two Teflon blocks were

carefully combined and physically sealed by nylon screws at each of the four corners. The ion mobility spectrometer had a 5 mm i.d. and a length of 20 mm. The dimensions of this LPIMS were chosen to be a 1:10 model of the current gas phase IMS in the Hill Research Lab. Liquid medium of mineral oil was pumped into the IMS tube at the entry and exit, labeled as (D) and (E) in Figure 2. Aqueous samples were introduced into the IMS tube through a fused silica capillary with a stainless steel sleeve. The EDI voltage was applied to the stainless steel sleeve. The electrodes were connected externally in series with 1-M Ω resistors. With 1000 V applied to the first electrode, the electric field of the mobility tube was 482 V/cm.

In order to time the arrival of ions at the Faraday plate, a Tyndall ion shutter was used [53]. A photo-etched gate electrode, with parallel wires 0.14 mm wide and 0.46 mm spacing, was positioned at the sixth electrode. To close the shutter, the voltage of the gate electrode was electrically shorted to the eighth electrode to form a potential well that stopped the ions from migrating forward. To open the shutter, the voltage of the gate electrode was switched back to its normal voltage, in line with the resistor series, allowing ions to migrate forward.

For the ammonium nitrate experiment, an aqueous solution of 2.8 mM ammonium nitrate was injected into the LPIMS at 0.25 μ L/min. +3000V was applied to the first electrode with an electric field of +1714 V/cm. The voltage on the gate electrode was +2100 V. The ion shutter pulse width was 5 s. For the sodium chloride experiment, an aqueous solution of 2.2 mM of sodium chloride was delivered at 1 μ L/min. The

EDI voltage was +1000V. The voltage on the gate electrode was measured to be +684 V and the electric field was +558 V/cm. A faster gate pulse of 0.2 s was used.

The effectiveness of the Tyndall shutter was examined in this apparatus with the upper Teflon block removed, due to a leakage problem. The LPIMS was placed inside a Pyrex dish filled with hexane. The spectrometer had a total length of 29.5 mm and an electric field of 1695 V/cm. Methanol-water (90:10, vol/vol), with flow rate of at 0.1 $\mu\text{L}/\text{min}$, was ionized by an EDI voltage of +6000V.

Materials and Reagent. The liquid media used in these experiments were hexane (J. T. Baker, Phillipsburg NJ) and USP grade mineral oil (Penreco, Karns City PA). 10 μM basic fuchsin (4-((4-amino-3-methylphenyl)(4-aminophenyl)methylene)cyclohexa-2,5-dieniminium chloride) and 1 μM tetraethylammonium bromide (Sigma-Aldrich, St. Louis, MO) were both prepared in methanol-water (90:10, vol/vol). 2.8 mM of ammonium nitrate (Fisher Scientific, Fair Lawn NJ) and 2.2 mM of sodium chloride (JT Baker, Phillipsburg NJ) were prepared in methanol-water (50:50, vol/vol). The methanol solvent used was HPLC grade (JT Baker, Phillipsburg NJ). The 18.1 M Ω water used was ultra-purified with a water purification system (Barnstead Int., Dubuque, IA).

Results and Discussions

Ion transmission through non-electrolyte containing liquids. The initial objective was to demonstrate that ions can travel through a non-electrolyte containing liquid under the influence of an electric field. The experiments were conducted in the apparatus shown in Figure 1, with hexane as the liquid medium. Ions were generated in hexane from a 10 μM aqueous solution of fuchsin by placing a high voltage on a capillary in which an aqueous sample was flowing into the hexane at a rate of 0.5 $\mu\text{L}/\text{min}$. In a manner similar to electrospray ionization, small charged droplets of aqueous sample in hexane were generated through Coulombic repulsion. This ionization process has been called electrodispersion ionization (EDI)[54]. Current in the apparatus was measured with the electric field of the mobility tube varied from 0 to 6000 V/cm. For comparison between EDI and its gas phase analogue, electrospray ionization (ESI), the experiments were conducted in air. The same aqueous sample was ionized by ESI for the same range of IMS electric field. The ionized sample traveled through the mobility tube in the respective medium. The experiments were also repeated without sample ionization to establish the background current level.

The background current levels in hexane and air were quite similar. At 5000 V/cm, the background current in hexane was 4 pA, with a noise level of ± 7 pA; and the background current in air was 1 pA, with a noise level of ± 4 pA. While there were arcing between the two electrodes attached to the resistive glass tube at 5000 V/cm

in air, there was no arcing in hexane. However, gas bubbles could be observed at an electric field of 6500 V/cm and above in hexane, possibly due to electrochemical oxidation of impurities in hexane.

Results showed that the electrodispersed ion moved along an ion mobility spectrometer in the non-electrolyte containing hexane under the influence of an electric field. Furthermore, the total ion current increased with the electric field of the mobility tube for both EDI in hexane and for ESI in air (Figure 3a). The total EDI current reached a maximum of 1.4 nA at 6000 V/cm and the ESI current reached a maximum of 1.2 nA at 4500 V/cm. Figure 3b showed that ionization and ion transport efficiency also increased with the electric field. The efficiency leveled off at 15% for an electric field of 4000V/cm and above.

Effectiveness of Ion Shutters in the Liquid Phase. Prior to conducting liquid phase ion mobility experiments. Bradbury-Nielsen shutter and Tyndall shutter were evaluated in the liquid phase. The electric field of the LPIMS was 600 V/cm and 1695 V/cm used in the examination of Bradbury-Nielsen shutter and Tyndall shutter, respectively. Figure 4a and b showed the percentage of the total ion current stopped by the Bradbury-Nielsen shutter and the Tyndall shutter, respectively, in hexane.

The Bradbury-Nielsen shutter was able to stop 90% of the ions at an orthogonal field of 6000 V/cm (10 times the electric field of the LPIMS) and it was able to stop 95% of the ions at an orthogonal field of 11100V/cm (18.5 times the electric field of the LPIMS) (Figure 4a). These results suggested that an effective Bradbury-Nielsen shutter would require an orthogonal field of 19000V/cm (32 times the electric field of

the LPIMS). Unfortunately, at higher orthogonal fields, noise increased and arcing between the gate wires occurred.

The maximum reverse field of obtainable on the Tyndall shutter was 13690 V/cm, which was 8 times greater than the electric field of the LPIMS, stopped 95% of the total ion current (Figure 4b). This suggested that a reverse field of 14260V/cm, or 8.5 times greater than the forward mobility field, would be sufficient in stopping the ions from migrating further.

To further evaluate the effectiveness of the Tyndall shutter, ion current from electrodispersed samples was measured while the shutter was held in the closed position for the first 10 s, and then opened for the following 10 s of the spectrum. The samples analyzed were 10 μ M basic fuchsin, 1 μ M tetraethylammonium bromide, and the methanol-water sample blank. Figure 5 showed that substantial current was registered for the three samples when gate was opened, compared to when gate was close. The current measured for the sample blank was 8.2 ± 0.7 pA, 24.5 ± 0.8 pA for fuchsin, and 27.6 ± 0.9 pA for tetraethylammonium bromide. Gate pulse ringing was registered at 0 s and 10 s when the ion shutter closed and opened. After the ion shutter closed, the current decayed to zero in 5 s. This was the time required for the ions remaining in the spectrometer from the previous experiment to reach the detector. After the ion shutter opened, there was a delay between 1.5 s to 2.0 s before the current rose. This time delay was the time the ions required to travel from the ion shutter to the Faraday plate, or their mobility time.

Gated liquid phase ion mobility spectrometry. LPIMS spectra were obtained by introducing short pulses of ions through the Tyndall ion shutter, using the apparatus depicted in Figure 2, in mineral oil. The ion shutter pulse width was 5 s. The positive LPIMS spectrum of 2.8 mM of ammonium nitrate, at a flow rate of 0.25 $\mu\text{L}/\text{min}$, showed a prominent current signal (Figure 6, black). The complexity of the ammonium nitrate spectrum indicated that the ions had not been completely desolvated. The two most intense peaks, at 10.1 s and 42.9 s, had mobility values of $2.1 \times 10^{-4} \text{ cm}^2/\text{Vs}$ and $5.0 \times 10^{-5} \text{ cm}^2/\text{Vs}$, respectively. The mobility value of ammonium ions in water is $7.6 \times 10^{-4} \text{ cm}^2/\text{Vs}$ [55]. With a viscosity of 57 cP, the mineral oil is about 60 times more viscous than water. The ion mobility is inversely proportional to the viscosity of the medium and hence the ion mobility in mineral oil should be 60 times slower than that in water. The expected mobility of ammonium ion in mineral oil would be $1.3 \times 10^{-5} \text{ cm}^2/\text{Vs}$. The experimental mobility values were 4 and 16 times faster than expected. Although this spectrum was noisy and relatively low resolution, it showed that LPIMS is achievable and possible.

The ion shutter pulse width was shortened to 0.2 s in the subsequent experiment to reduce peak broadening. The background spectrum in the absence of sample was shown in blue (Figure 7). The positive LPIMS spectrum of sodium chloride in Figure 7 (black spectrum) was less complex than the ammonium nitrate spectrum and showed a signal peak at 15.6 s with a mobility of $1.4 \times 10^{-4} \text{ cm}^2/\text{Vs}$. The literature value of ion mobility of sodium ion in water of $5.2 \times 10^{-4} \text{ cm}^2/\text{Vs}$ [55] and the expected mobility of Na^+ in mineral oil is $8.7 \times 10^{-6} \text{ cm}^2/\text{Vs}$. The experimental ion mobility value of $1.4 \times 10^{-4} \text{ cm}^2/\text{Vs}$ was 16 times faster than anticipated.

Preliminary demonstration of pulsed EDI-LPIMS. Electrodispersion ionization source was operated in a pulse mode, using the apparatus depicted in Figure 1. No ion shutter was used. The pulsed injection of ions was controlled by alternating the EDI voltage between a voltage sufficient to induce ionization (+2000V) and a lower voltage (+500V). The EDI voltage was maintained at the upper voltage for 0.5 s, and switched to the lower voltage for the remaining of the experiment.

Figure 8 showed the pulsed EDI-LPIMS spectrum of 10 μM basic fuchsin, at a flow rate of 0.1 $\mu\text{L}/\text{min}$, drifting in hexane at an electric field of 978 V/cm. The spectrum in full scale was displayed, as an insert in Figure 8, to show the voltage ringing from the ionization pulse at 0 s and 0.5 s. The pulsed injection of ions significantly reduced the spectrum complexity in comparison with the gated spectra. Because ions were only introduced during the ionization pulse, there were no additional aqueous analyte injected into the spectrometer while the mobility data was collected. A single peak was observed for basic fuchsin at a drift time of 1.01 s and a mobility of $2.72 \times 10^{-3} \text{ cm}^2/\text{V}\cdot\text{s}$. The peak width was 0.06 s, which was shorter than the 0.5 s ionization pulse. This suggested that at a low sample flow rate, the sample was ejected at a faster rate than it was being delivered. The LPIMS had a resolving power of 17.

This resolving power was better than several gas phase IMS that were 8 to 12 times longer [18;19;56]. The resolving power per unit drift length of miniature gas phase IMS ranged from 1.1 cm^{-1} to 7.7 cm^{-1} [18;19;56-58]. The resolving power per unit drift length of this 5-mm LPIMS was 34 cm^{-1} .

Conclusions

This first demonstration of liquid phase ion mobility spectrometry, with electrodispersion ionization, introduces the concept of a new analytical separation technique on a miniature scale. Aqueous ions are moved along the LPIMS by an electric field, established by conducting electrodes held at decreasing potentials, in a non-electrolyte containing liquid medium. The ion transport efficiency of LPIMS improves linearly with the applied electric field of the spectrometer. The gate injected LPIMS spectra are inadequately resolved, due to the extension of solvation and the inefficiency of the ion shutters. While further approaches are necessary to assist sample desolvation and to improve gating of ions, pulsed EDI-LPIMS data demonstrated LPIMS as a promising novel analytical technique for the liquid phase.

Acknowledgements

This work was supported by the National Institutes of Biomedical Imaging and Bioengineering, National Institutes of Health (Grant R21EB001950).

References

1. B. H. Clowers, B. Bendiak, P. Dwivedi, W. E. Steiner and Jr. H. H. Hill, Separation of Sodiated Isobaric Disaccharides Using Electrospray Ionization-Atmospheric Pressure Ion Mobility-Time of Flight Mass Spectrometry, *Journal of the American Society for Mass Spectrometry* **16** , pp. 660-669 (2005).
2. S. N. Jackson, H. Y. N. Wang and A. S. Woods, Direct Tissue Analysis of Phospholipids in Rat Brain Using MALDI-TOFMS and MALDI-Ion Mobility-TOFMS, *Journal of the American Society for Mass Spectrometry* **16**, pp. 133-138 (2005).
3. C. A. Srebalus, J. W. Li., W. S. Marshall and D. E. Clemmer, Gas Phase Separations of Electrosprayed Peptide Libraries, *Analytical Chemistry* **71**, pp. 3918-3927 (1999).
4. G. R. Asbury and Jr. H. H. Hill, Separation of Amino Acids by Ion Mobility Spectrometry, *Journal of Chromatography A* **902**, pp. 433-437 (2000).
5. C. S. Creaser and J. R. Griffiths, Atmospheric Pressure Ion Mobility Spectrometry Studies of Cyclic and Acyclic Polyethers, *Analytica Chimica Acta* **436**, pp. 273-279 (2001).
6. P. Dwivedi, C. Wu and Jr. H. H. Hill, Gas Phase Chiral Separations by Ion Mobility Spectrometry, *Analytical Chemistry* **ASAP** DOI: 10.1021/ac0608772 (2006).
7. V. Ruzsanyi, J. I. Baumbach, S. I. Sielemann, P. Litterst, M. Westhoff and L. Freitag, Detection of human metabolites using multi-capillary columns coupled to ion mobility spectrometers, *Journal of Chromatography A* **1084**, pp. 145-151 (2005).
8. P. Wu, P. Dwivedi, S. J. Klopsch, G. J. Puzon, L. Xun and Jr. H. H. Hill, Metabolic Profiling by Ion Mobility Mass Spectrometry (IMMS), **Manuscript in Preparation**, (2006).
9. S. I. Merenbloom , S. L. Koeniger, S. J. Valentine, M. D. Plasencia and D. E. Clemmer, IMS-IMS and IMS-IMS-IMS/MS for Separating Peptide and Protein Fragment Ions, *Analytical Chemistry* **78**, pp. 2802-2809 (2006).
10. S. L. Koeniger, S. I. Merenbloom, S. J. Valentine, M. F. Jarrold, H. R. Udseth, R. D. Smith and D. E. Clemmer, An IMS-IMS Analogue of MS-MS, *Analytical Chemistry* **78** , pp. 4161-4174 (2006).
11. D. A. Atkinson, Jr. H. H. Hill and T. D. Shultz, Quantification of Mammalian Lignans in Biological-Fluids Using Gas-Chromatography with Ion Mobility

- Detection, *Journal of Chromatography-Biomedical Applications* **617**, pp. 173-179 (1993).
12. B. T. Ruotolo, G. F. Verbeck, L. M. Thomson, A. S. Woods, K. J. Gillig and D. H. Russell, Distinguishing between Phosphorylated and Nonphosphorylated Peptides with Ion Mobility-Mass Spectrometry, *Journal of Proteome Research* **1**, pp. 303-306 (2002).
 13. L. M. Matz, H. M. Dion and Jr. H. H. Hill, Evaluation of Capillary Liquid Chromatography-Electrospray Ionization Ion Mobility Spectrometry with Mass Spectrometry Detection, *Journal of Chromatography A* **946**, pp. 59-68 (2002).
 14. K. Tang, A. A. Shvartsburg, H-N Lee, D. C. Prior, M. A. Bauschbach, F. Li, A. V. Tolmachev, G. A. Anderson and R. D. Smith, High-Sensitivity Ion Mobility Spectrometry/Mass Spectrometry Using Electrodynamic Ion Funnel Interfaces, *Analytical Chemistry* **77**, pp. 3330-3339 (2005).
 15. J. Xu, W. B. Whitten, T. A. Lewis and J. M. Ramsey, A Miniature Ion Mobility Spectrometer with a Pulsed Corona-Discharge Ion Source, *International Journal for Ion Mobility Spectrometry* **4**, pp. 3-6 (2001).
 16. J. I. Baumbach, D. Berger, J. W. Leonhardt and D. Klockow, Ion Mobility Sensor in Environmental Analytical Chemistry -- Concept and First Results, *Intern. J. Environ. Anal. Chem.* **52**, pp. 189-193 (1993).
 17. J. Xu, W. B. Whitten and J. M. Ramsey, Pulsed-Ionization Miniature Ion Mobility Spectrometer, *Analytical Chemistry* **75**, pp. 4206-4210 (2003).
 18. K. B. Pfeifer and A. N. Rumpf, Measurement of Ion Swarm Distribution Functions in Miniature Low-Temperature Co-Fired Ceramic Ion Mobility Spectrometer Drift Tubes, *Analytical Chemistry* **77**, pp. 5215-5220 (2005).
 19. St. Sielemann, J. I. Baumbach, H. Schmidt and P. Pilzecker, Quantitative Analysis of Benzene, Toluene, and m-Xylene with the Use of a UV-Ion Mobility Spectrometer, *Field Analytical Chemistry and Technology* **4**, pp. 157-169 (2000).
 20. J. P. Carrico, A. W. Davis, D. N. Campbell, J. E. Roehl, G. R. Sima, G. E. Spangler, K. N. Vora and R. J. White, Chemical Detection and Alarm for Hazardous Chemicals Using Ion Mobility Instrumentation, *American Laboratory* **18**, p. 152 (1986).
 21. D. D. Fetterolf and T. D. Clark, Detection of Trace Explosive Evidence by Ion Mobility Spectrometry, *Journal of Forensic Science* **38**, pp. 28-39 (1993).
 22. Z. Karpas, Y. Pollevoy and S. Melloul, Determination of Bromine in Air by Ion Mobility Spectrometry, *Analytica Chimica Acta* **249**, pp. 503-507 (1991).
 23. H. R. Bollan, D. J. West and J. L. Brokenshire, Assessment of Ion Mobility Spectrometry for Monitoring Monoethanolamine in Recycled Atmospheres,

- International Journal for Ion Mobility Spectrometry* **1**, pp. 48-53 (1998).
24. G. Gordon, G. Pacey, B. Bubnis, S. Laszewski and J. Gaines, Safety in the Workplace: Ambient Chlorine Dioxide Measurements in the Presence of Chlorine, *Chemical Oxidation* **4**, pp. 23-30 (1997).
 25. J. P. Dworzanski, W. H. McClennen, P. A. Cole, S. N. Thorton, H. L. C. Meuzelaar, N. S. Arnold and A. P. Snyder, Field-Portable, Automated Pyrolysis-GC/IMS System for Rapid Biomarker Detection in Aerosols: a Feasibility Study, *Field Analytical Chemistry and Technology* **1**, pp. 295-305 (1997).
 26. V. Ruzsanyi, S. Sielemann and J. I. Baumbach, Determination of VOCs in Human Breath Using IMS, *International Journal for Ion Mobility Spectrometry* **5**, pp. 45-48 (2002).
 27. Z. Karpas, W. Chaim, B. Tilman, R. Gdalevsky and A. Lorber, A Diagnosis of Vaginal Infections by Ion Mobility Spectrometry, *International Journal for Ion Mobility Spectrometry* **5**, pp. 49-54 (2002).
 28. L. M. Matz and Jr. H. H. Hill, Investigation of Drift Gas Selectivity in High Resolution Ion Mobility Spectrometry with Mass Spectrometry Detection, *Journal of the American Society for Mass Spectrometry* **13**, pp. 300-307 (2002).
 29. A. B. Kanu and H. H. Hill, Jr. Drift Gas Selectivity with Thermal Desorption Ion Mobility Spectrometry. Gordon Research Conference. 2005.
 30. S. Sielemann, J. I. Baumbach, P. Pilzecker and G. Walendzik, Detection of trans-1,2-dichloroethene, trichloroethene and tetrachloroethene using Multi-Capillary Columns Coupled to Ion Mobility Spectrometers with UV-Ionization Sources, *International Journal for Ion Mobility Spectrometry* **2**, pp. 15-21 (1999).
 31. A. B. Kanu, C. Wu, and H. H. Hill, Jr. Rapid Pre-Separation for Eliminating False Positive Interferences from Drugs, Explosives and Chemical Warfare Agents in Ion Mobility Spectrometry. Gordon Research Conference. 2005.
 32. A. P. Snyder, C. S. Harden, A. H. Brittain, M. G. Kim, N. S. Arnold and H. L. C. Meuzelaar, Portable Hand-Held Gas-Chromatography Ion Mobility Spectrometry Device, *Analytical Chemistry* **65**, pp. 299-306 (1993).
 33. C. Bialobrzewski, *Le Radium* **8**, p. 1 (1911).
 34. G. Jaffé, Über die Ionisation flüssiger Dielektrika durch Radiumstrahlen, *Annalen der Physik* **330**, pp. 257-284 (1908).
 35. I. Adamczewski, Mobilités des Ions dans la Série des carbures d'Hydrogène Liquides et Leur Rapport avec le Coefficient de Viscosité, *Annls de Physique* **8**, pp. 309-359 (1937).

36. R. L. Williams, Ionic Mobilities in Argon and Helium Liquids, *Canadian Journal of Physics* **35**, p. 134 (1957).
37. L. Meyer and F. Reif, Mobilities of He Ions in Liquid Helium, *Physical Review* **110**, pp. 279-280 (1958).
38. G. Careri, F. Scaramuzzi and J. O. Thomson, Heat Flush and Mobility of Electric Charges in Liquid Helium I. - Non Turbulent Flow, *Nuovo Cimento* **13**, pp. 186-196 (1959).
39. K. R. Atkins, Ions in Liquid Helium, *Physical Review* **116**, pp. 1339-1343 (1959).
40. O. Gzowski, Mobility of Ions in Liquid Dielectrics, *Nature* **194**, p. 173 (1962).
41. J. A. Kok, *Electrical Breakdown of Insulating Liquids*. Interscience Publishers, New York (1961).
42. M. J. Morant, Photo-Injection of Charge into Dielectric Liquids, *Nature (London)* **187**, pp. 48-49 (1960).
43. A. M. Sletten, Electric Strength and High-Field Conduction Current in n-Hexane, *Nature (London)* **183**, pp. 311-312 (1959).
44. G. Jaffé, Zur Theorie der Ionisation in Kolonnen, *Annalen der Physik* **347**, pp. 303-344 (1913).
45. J. F. Fowler and F. T. Farmer, Conductivity Induced in Unplasticized 'Perspex' by X-rays, *Nature (London)* **175**, pp. 516-517 (1955).
46. H. J. Plumley, Conduction of Electricity by Dielectric Liquids at High Field Strengths, *Physical Review* **59**, pp. 200-207 (1941).
47. I. Adamczewski, Liquid-filled Ionization Chambers as Dosimeters, *Colloques Internationaux du Centre National de la Recherche Scientifique* **179**, pp. 21-44 (1970).
48. A. O. Allen, M. P. Haas and A. Hummel, Measurement of Ionic Mobilities in Dielectric Liquids by Means of Concentric Cylindrical Electrodes, *Journal of Chemical Physics* **64**, pp. 2587-2592 (1976).
49. N. Houser and R. C. Jarnagin, Electron Ejection from Triplet State in Fluid Solutions, *Journal of Chemical Physics* **52**, pp. 1069-1078 (1970).
50. S. K. Lim, M. E. Burba and A. C. Albrecht, Mobilities of Radical Cations and Anions, Dimer Radical Anions, and Relative Electron Affinities by Times of Flight in n-hexane, *Journal of Physical Chemistry* **98**, pp. 9665-9675 (1994).
51. K. S. Haber and A. C. Albrecht, Time-of-Flight Technique for Mobility Measurements in the Condensed Phase, *Journal of Physical Chemistry* **88**, pp.

6025-6030 (1984).

52. M. E. Burba, S. K. Lim and A. C. Albrecht, Relative Electron Affinity of C₆₀ and C₇₀ and the Stokes' Law Radius of the C₇₀ Radical Anion in n-Hexane by Time-of-Flight Mobility Measurements, *Journal of Physical Chemistry* **99**, pp. 11839-11843 (1995).
53. A. M. Tyndall, *The Mobility of Positive Ions in Gases*. Cambridge University Press, Cambridge, U.K. (1938).
54. M. Tam and H. H. Hill, Jr. Electrodispersion Ionization in Liquids, **Submitted** (2006).
55. A. P. Snyder, C. S. Harden, A. H. Brittain, M-G Kim, N. S. Arnold and H. L. C. Meuzelaar, Portable Hand-Held Gas Chromatography/Ion Mobility Spectrometry Device, *Analytical Chemistry* **65**, pp. 299-306 (1993).
56. A. B. Kanu, P. E. Haigh and Jr. H. H. Hill, Surface Detection of Chemical Warfare Agent Simulants and Degradation Products, *Analytica Chimica Acta* **553**, pp. 148-159 (2005).
57. J. I. Baumbach, S. Sielemann and P. Pilzecker, Coupling of Multi-Capillary Columns with two Different Types of Ion Mobility Spectrometer, *International Journal for Ion Mobility Spectrometry* **3**, pp. 28-37 (2000).
58. J. Xu, W. B. Whitten and J. M. Ramsey, Space Charge Effects on Resolution in a Miniature Ion Mobility Spectrometer, *Analytical Chemistry* **72**, pp. 5787-5791 (2000).

Figure Captions

Figure 1: Schematic of the liquid phase resistive glass ion mobility tube. The aqueous sample was ionized by the electrodispersion ionization source (A) into the liquid medium, contained inside a Pyrex dish (B), and transported through the resistive glass tube (C) by an electric field. The current was measured by the Faraday plate (D).

Figure 2: Schematic of the enclosed stacked-ring liquid phase ion mobility spectrometer. The units comprising the spectrometer were: (A) Teflon blocks, (B) stainless steel electrodes, (C) Faraday plate, (D) liquid medium entry, (E) liquid medium exit, and (F) sample inlet.

Figure 3: This plot showed the effect of the electric field of the ion mobility spectrometer on (a) the total ion current and (b) the ionization and ion transport efficiency of ESI in air and EDI in hexane. The background current levels in air and hexane were shown for comparison in (a).

Figure 4: The effectiveness of (a) Bradbury-Nielsen shutter and (b) Tyndall shutter in stopping ion current in liquid phase ion mobility spectrometry.

Figure 5: Ion current of solvent blank, 10 μM basic fuchsin, and 1 μM tetraethylammonium bromide. The Tyndall shutter was closed from 0 s – 10 s and opened from 10 s – 20 s.

Figure 6: LPIMS spectra in mineral oil. The blue trace represented the background spectrum in the absence of sample. The black trace represented the spectrum when 50 ppm NH_4NO_3 was introduced.

Figure 7: LPIMS spectra in mineral oil. The blue trace represented the background spectrum in the absence of sample. The black trace represented the spectrum when 50 ppm NaCl was introduced.

Figure 8: Pulsed electrodispersion ionization-liquid mobility spectrum of 10 μM basic fuchsin, dissolved in methanol-water (90:10, v/v), drifting in hexane. The mobility tube was 5-mm long and the ionization pulse was 0.5 s. The insert displayed the spectrum in full scale.

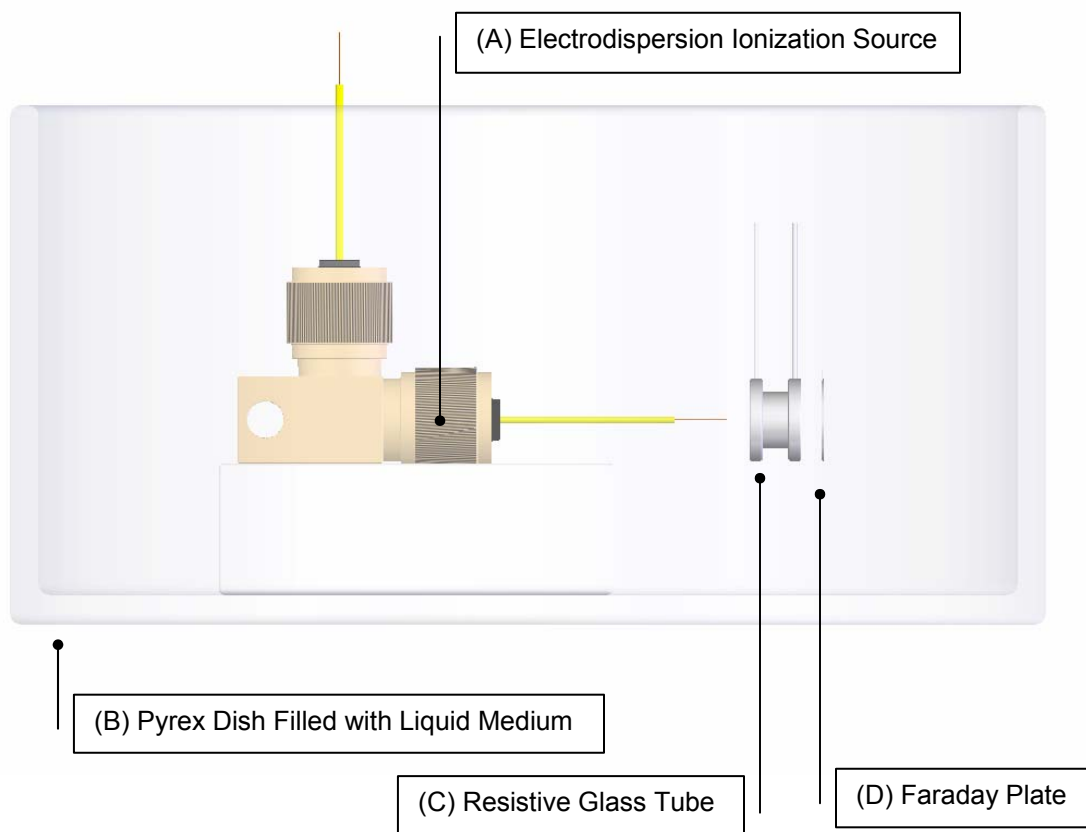


Figure 1: Schematic of the liquid phase resistive glass ion mobility tube. The aqueous sample was ionized by the electrodispersion ionization source (A) into the liquid medium, contained inside a Pyrex dish (B), and transported through the resistive glass tube (C) by an electric field. The current was measured by the Faraday plate (D).

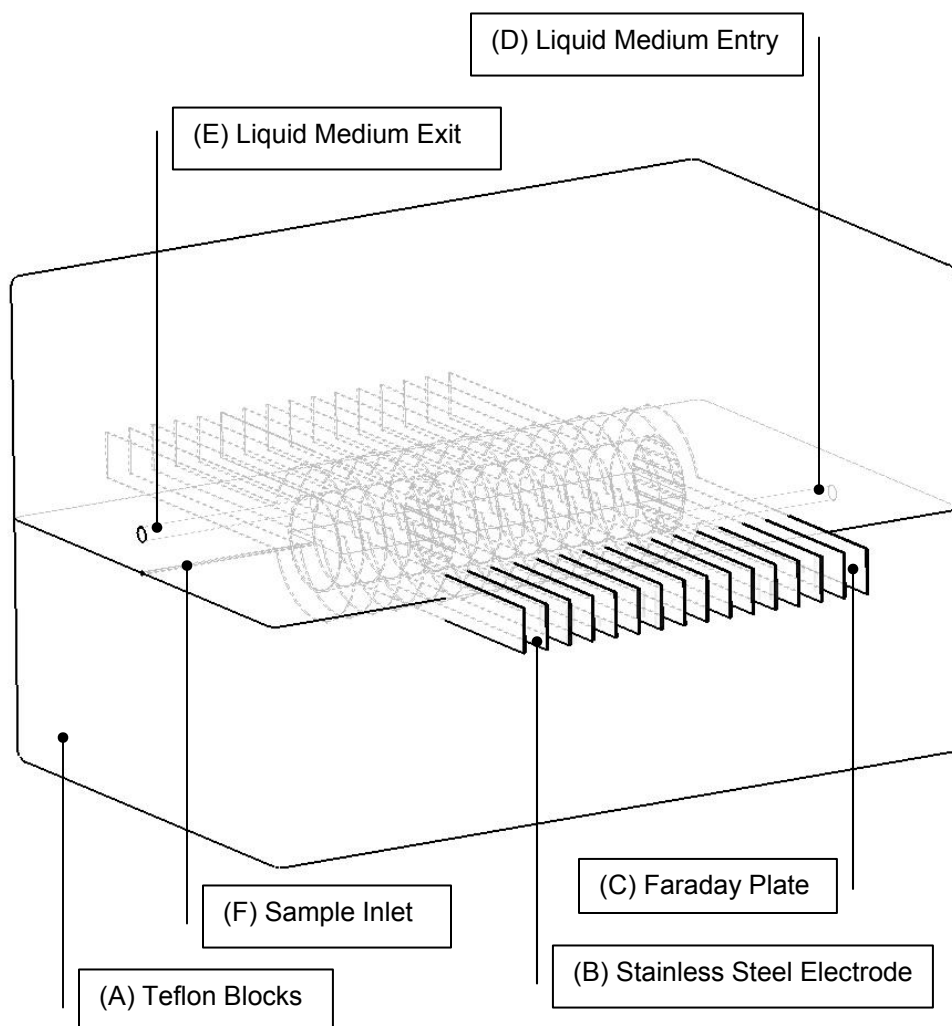


Figure 2: Schematic of the enclosed stacked-ring liquid phase ion mobility spectrometer. The units comprising the spectrometer were: (A) Teflon blocks, (B) stainless steel electrodes, (C) Faraday plate, (D) liquid medium entry, (E) liquid medium exit, and (F) sample inlet.

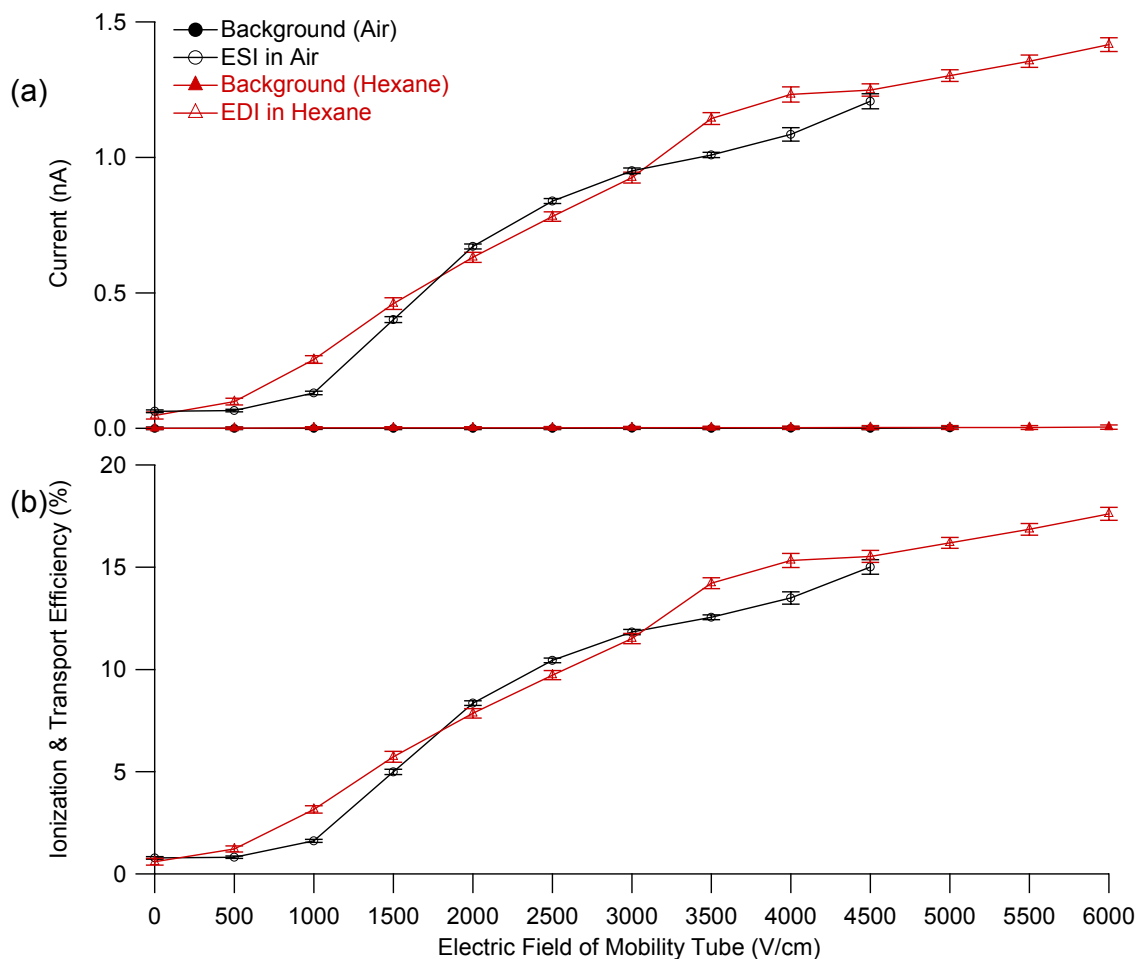


Figure 3: This plot showed the effect of the electric field of the ion mobility spectrometer on (a) the total ion current and (b) the ionization and ion transport efficiency of ESI in air and EDI in hexane. The background current levels in air and hexane were shown for comparison in (a).

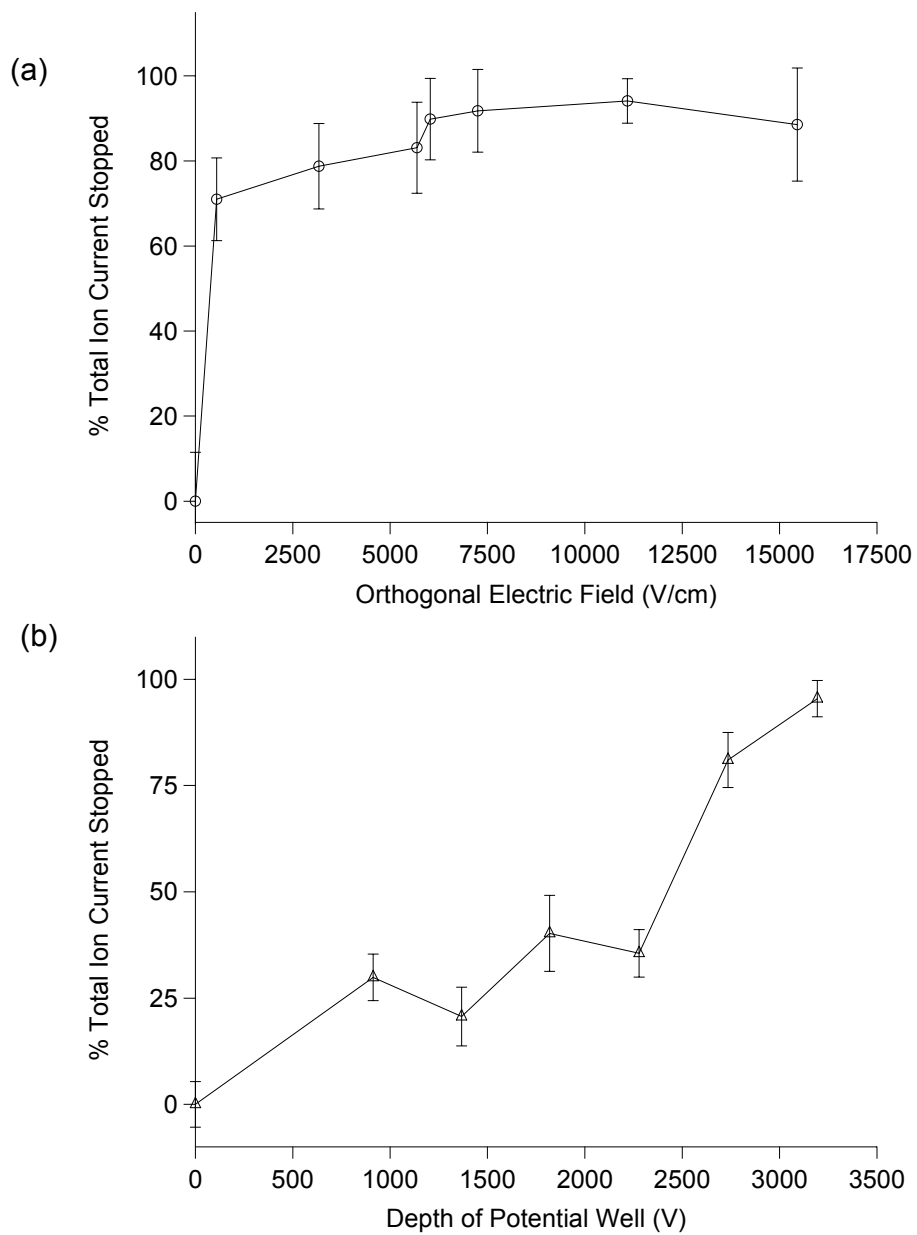


Figure 4: The effectiveness of (a) Bradbury-Nielsen shutter and (b) Tyndall shutter in stopping ion current in liquid phase ion mobility spectrometry.

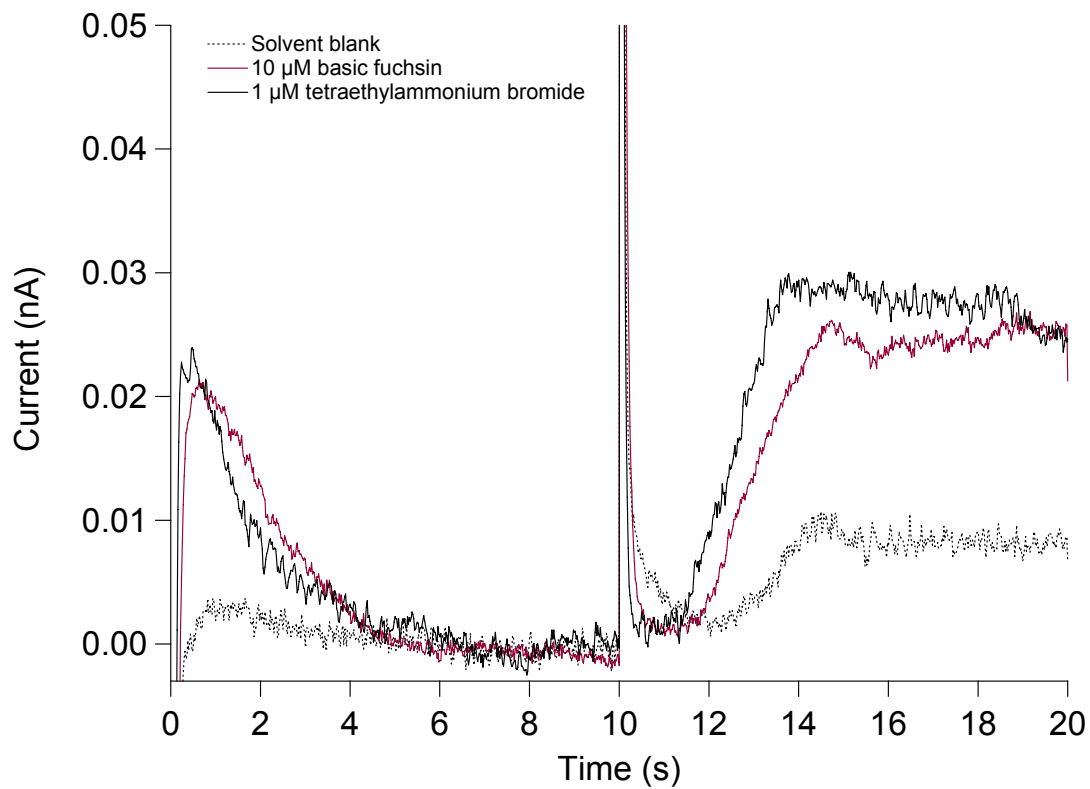


Figure 5: Ion current of solvent blank, 10 μM basic fuchsin, and 1 μM tetraethylammonium bromide. The Tyndall shutter was closed from 0 s – 10 s and opened from 10 s – 20 s.

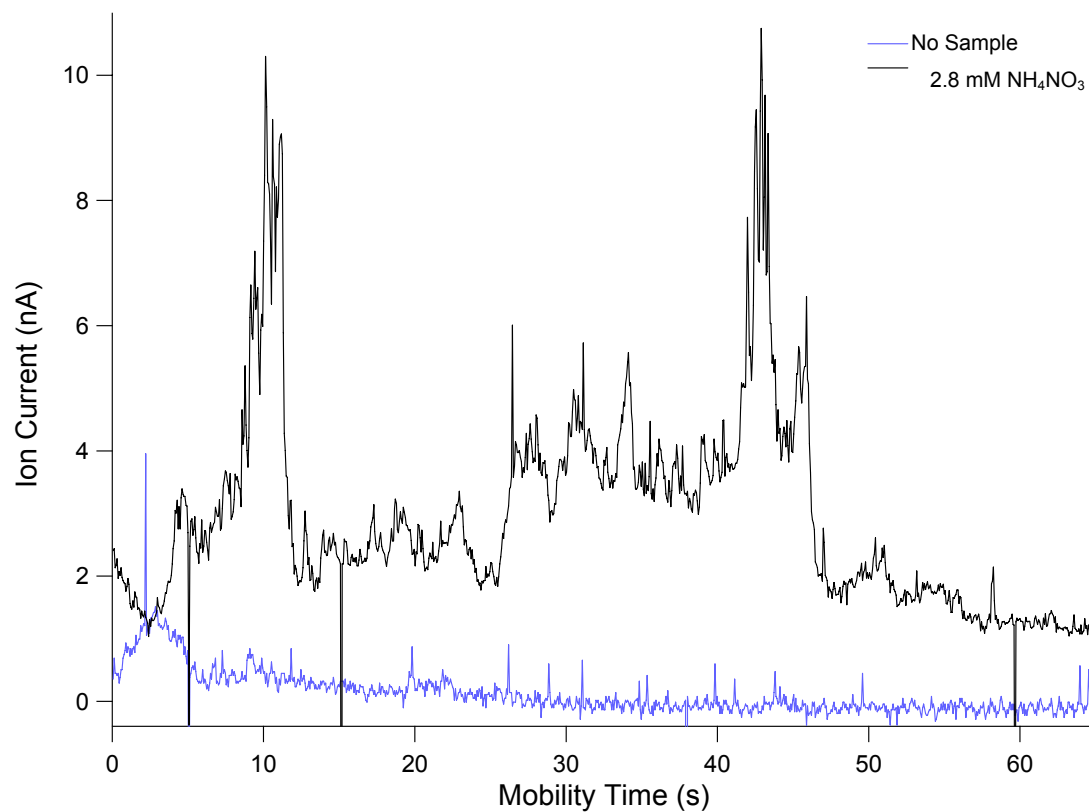


Figure 6: LPIMS spectra in mineral oil. The blue trace represented the background spectrum in the absence of sample. The black trace represented the spectrum when 2.8 mM ammonium nitrate was introduced.

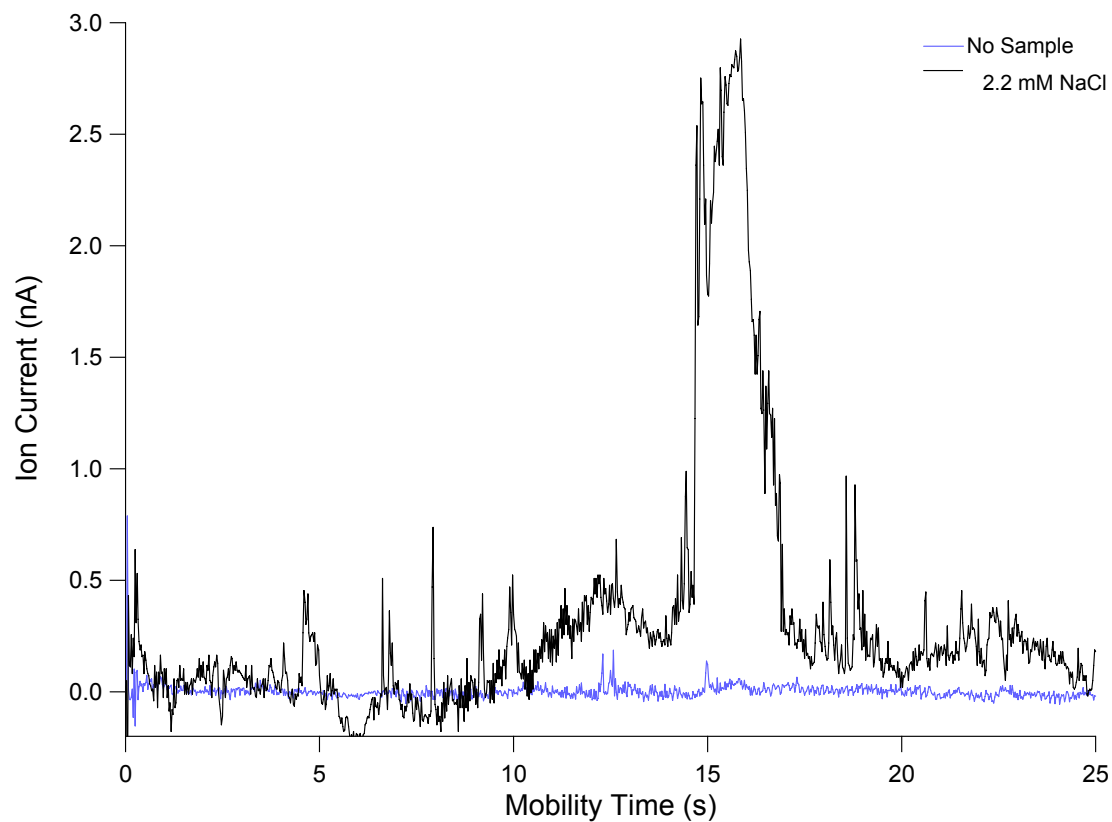


Figure 7: LPIMS spectra in mineral oil. The blue trace represented the background spectrum in the absence of sample. The black trace represented the spectrum when 2.2 mM sodium chloride was introduced.

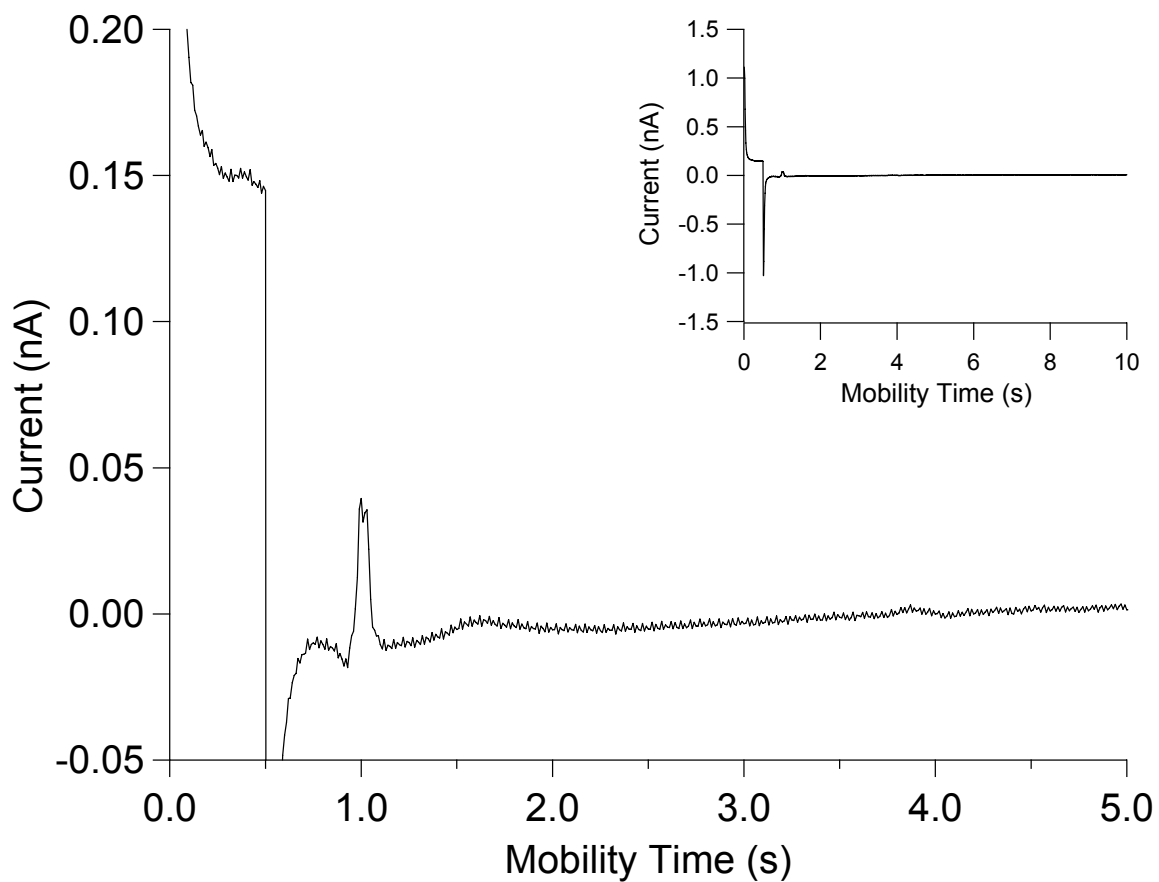


Figure 8: Pulsed electrodispersion ionization-liquid mobility spectrum of 10 μM basic fuchsin, dissolved in methanol-water (90:10, v/v), drifting in hexane. The mobility tube was 5-mm long and the ionization pulse was 0.5 s. The insert displayed the spectrum in full scale. The spectrum was averaged 50 times.

Chapter Four

Design, Construction, and Evaluation of an Integrated Liquid Phase Ion Mobility Spectrometer

Abstract

This paper presents two integrated miniaturized liquid phase ion mobility spectrometry devices. Counterflow of liquid medium was necessary to remove uncharged analyte in liquid phase ion mobility spectrometer. While this could not be achieved in existing instruments, new designs were explored to address this particular issue. In addition, alternative fabrication processes were considered in terms of cost-effective mass production. Low temperature co-fired ceramics and poly(dimethylsiloxane) are widely used in production of miniaturized and microfluidic instruments. Liquid phase ion mobility spectrometers fabricated from these two materials were evaluated based on the ability of liquid containment, electrical integrity, and ion transport efficiency.

Introduction

Liquid phase ion mobility spectrometry (LPIMS) has recently been developed as a novel analytical separation technique in the non-electrolyte containing liquids [1-3]. Liquid phase ions, produced from electrodispersion ionization (EDI) [4], are moved along the spectrometer by an electric field. The electric field is established, not by electrolytes in the liquid medium, but by multiple guard rings stationed along the spectrometers.

The two existing designs for miniaturized LPIMS instrument. The first prototype was an arrangement of guard rings sealed inside two pieces of Teflon block. It was a 1:10 model of the unidirectional stacked-ring gas phase ion mobility spectrometers (IMS) in our laboratory. Half cylinders of 5-mm i.d. were hollowed out from two Teflon blocks. The guard rings, inserted into slits of the Teflon blocks, were connected in series by resistors and electrically insulated from one another. The two Teflon blocks were sealed to form a liquid phase ion mobility spectrometer with an i.d. of 5 mm and a length of 20 mm. An electric field was established by applying a voltage to the first guard ring, and grounding the last guard ring through a resistor. Ion signal were collected as a discharge current on a Faraday plate.

The second prototype utilized resistive glass tubes (Burle Technologies Inc., Lancaster, PA). Resistive glass tubes had been used in gas phase ion mobility spectrometry in 1980s by Spangler [5;6]. Results obtained from the resistive coated mobility tube were compared to those obtained from a conventional stacked-ring

mobility tube. It was found that while the resolving power was similar between the two systems, the resistive coated mobility tube offered better sensitivity, possibly due to the more uniform electric field in the resistive coated mobility tube [5]. The resistive glass tubes (Burle) were fabricated from proprietary lead silicate glass, which surface was converted to semi-conductor by reducing in hydrogen. The great reduction in parts and assembly requirements were suitable for constructing miniaturized LPIMS instrument. Individual guard rings, resistors, and their connections, were replaced by a single piece of resistive glass tube. The resistive glass LPIMS prototype had 4.1 mm i.d., 5.4 mm o.d., 5 mm length, and total resistance of 8 M Ω to 10 M Ω . Electrodes were attached to either ends of the resistive glass tube to provide electrical contact. The front electrode was used for applying voltage to the spectrometer, while the end electrode was grounded via a resistor.

Although the two existing prototypes demonstrated the feasibility of LPIMS, the inherent design problems need to be addressed. The first prototype encountered leakage problem. Subsequent LPIMS experiments were conducted by removing the top Teflon block and immersing the prototype in a container of liquid medium. Without proper containment, the second resistive glass LPIMS prototype were also immersed in a container of liquid medium. Previous LPIMS results suggested the need for a counterflow of liquid medium to remove uncharged analyte molecules from the spectrometer (Chapter 5).

Low-temperature co-fired ceramic (LTCC), a type of ceramic sheet that was frequently used in integrated microelectronic packaging, ceramic printed wiring boards, and radiofrequency modules. LTCC comprises of alumina particles, lead oxide and silicon dioxide glass particles, and proprietary organic binding compounds. Before subjecting to high heat in a furnace, or the firing process, the LTCC sheet is flexible and machineable. Electronic circuits can be printed onto the ceramic sheet by applying conductive and resistive pastes. During the firing process, the organic binder is burnt off, and glass and alumina fuse into a monolithic structure. This process benefits miniaturization of ion mobility instruments because the electronic circuits are printed embedded within the mobility tube, and eliminates the need for external resistors. LTCC, with its breakdown voltage of 40 kV mm^{-1} and chemical inertness, is suitable for the application of LPIMS. Much of the LTCC fabrication process can be performed automatically by machines. Given the low cost of the LTCC sheets, this would be a cost-effective way of mass-producing LPIMS devices. Pfeifer et al explored LTCC as a potential solution for mass-producing miniaturized gas phase IMS [7]. Their rolled design eliminated many parts by machine-printing electrodes and resistors onto an unfired sheet of pliable low temperature co-fire ceramic. The printed low temperature co-fire ceramic was rolled into the required size. After subjected to high heat treatment, the rolled tube with the printed electrodes and resistors fused with the ceramic into one piece. Only minimal manual connections were required for this fabrication process.

Poly(dimethylsiloxane) (PDMS), also known as dimethicone, which had previously been used to produce chip-based microfluidic systems for electrophoresis, DNA sequencing, polymerase chain reaction, and immunoassays [8;9].The first capillary

zone electrophoresis on a PDMS chip was reported in 1997 by Effenhauser [10]. PDMS is a polymeric structure with repeating $[\text{SiO}(\text{CH}_3)_2]$ monomeric units. Polycarbonate and polymethylmethacrylate (PMMA) are two other polymeric substrates that have been used for microfluidic systems. The unique properties of PDMS make it suitable for preparing microfluidic devices. It is optically transparent (down to 240 nm), gas permeable, water impermeable, flexible, and inexpensive. It has low chemical reactivity, high dielectric strength (20 kV/mm), and a high operating temperature range (-50 to 200°C). The viscoelasticity property of PDMS lends itself to be useful as adhesives, lubricants, damping fluids, and heat transfer fluids. The non-toxic, non-flammable, and biocompatible nature of PDMS have allowed its use in other applications, including being used as an anti-caking agent by the food industry, as an anti-foaming agent by the pharmaceutical industry, as knuckle replacement implants and breast implants by the medical device industry. PDMS is also suitable for constructing the ionization source. An electrospray ionization source fabricated by PDMS was recently reported [11], where the hydrophobicity of PDMS was stated to improve electrospray ionization by forming smaller Taylor cone from. This suggested that integrating electrodispersion ionization source with LPIMS in a single device would be viable.

The design objectives for an integrated LPIMS device should include all the requisite components (an inlet for the electrodispersion ionization source, a liquid medium inlet and outlet, insulated and contained housing, embedded electrodes and resistors), with undemanding fabrication process, and have the capacity for mass production and further miniaturization. This study presents the design and fabrication

of integrated miniaturized devices of LPIMS with LTCC and PDMS materials. The devices were evaluated on basis of liquid containment, electrical integrity, and ion transport efficiency.

Design and Fabrication of Integrated Liquid Phase Ion Mobility Spectrometer

Design of Low Temperature Co-fired Ceramics LPIMS

The LPIMS ceramic device composed of the desolvation region, the ion shutter region, the drift region, the aperture grid/Faraday plate region, and an insulating base region. The mobility tube had a 3.8 mm i.d.. The LPIMS included 28 layers of LTCC in the desolvation region, 5 layers in the gate region, 42 layers in the drift region, 10 layers in the aperture grid/Faraday plate region, and 5 layers in the insulating end region. This amounted to a total length of 18.1 mm, a drift length of 10.4 mm, and a total resistance of 5.8 M Ω . The design should provide a very homogeneous electric field, having 50 electrodes per cm of drift length.

The obvious advantage of a LTCC device was the great reduction in electrical connections. The electrodes and resistors were connected by vias and embedded within the LTCC structure. The LTCC device had only five external connections for grounding, sensing ion shutter reference voltage, delivering ion shutter voltage and

drift tube voltage, and outputting ion signal. These five connections were located on the underside of the LTCC mobility tube.

The LTCC mobility tube was enclosed by three pieces of Teflon end caps. The first and second pieces of Teflon end caps sandwiched a septum membrane that fitted into the counter bore of the end cap. The fused silica capillary from EDI source was introduced through this septum. The second and the third pieces of Teflon end caps, located at either ends of the LTCC mobility tube, were sealed with two pieces o-rings. The three pieces of Teflon end caps were tightened physically with three screws. The third Teflon end cap supported five pogo pins, which pushed into the five external electrical connectors on the underside of the mobility tube. The pogo pins were connected to external electrical wire for inputting voltages, grounding, and outputting signal. The schematic of the complete LTCC-LPIMS device was illustrated in Figure 1, showing the position of the o-rings and septum within the device.

The LTCC (Green Tape 951, DuPont Microcircuit Materials, Research Triangle Park NC) was intended for layering up to 30 sheets. Since a LPIMS would require 90 sheets of LTCC, LPIMS was constructed in multiple segments that were bonded with pressure-sensitive adhesive to form the final mobility tube. In addition, the use of multiple segments allowed for integration of external electrodes, such as ion shutter and target screen, and for easy compilation of different mobility regions – the desolvation, the Tyndall gate, the drift tube, and the aperture grid/faraday regions.

Fabrication of Low Temperature Co-fired Ceramics LPIMS

The LTCC fabrication [12] began with transferring the design pattern, from a three-dimensional computer-aided design software (SolidWorks, Concord MA), onto a sheet of unfired LTCC by a CNC milling machine. A vacuum suction held down the unfired LTCC, while a 60,000 RPM mill bit drilled the pattern. Six segment patterns were arranged on each 4' x 4' LTCC sheet. The vias were filled with a silver paste, and the conductors and resistors were screen-printed. Five to six sheets of unfired LTCC were laminated together at 70°C for 10 minutes, and then at a pressure of 3000 psi for another 10 minutes. The perimeter of the six segments, each with five to six layers, were cut with milling tool. Multiple segments were aligned, bonded together with poly-2-ethyl-2-oxazoline (PEOX), a water-soluble adhesive, which burned off during the firing process segments, and subjected to a constrained lamination between 1000 and 1500 psi. The external conducting connections were soldered on the underside of the mobility tube. The mobility tube was fired in a furnace with a specific temperature profile at 350°C for six hours, 850°C for 10 to 15 minutes, and followed by a gradual decline to room temperature.

Design of Poly(dimethylsiloxane) LPIMS

The PDMS-LPIMS device was an enclosed system with two bonded layers of PDMS, which formed a microchannel 1000 μm wide, 400 μm deep, and 10 mm in length (Figure 2a). The bottom PDMS layer was bonded to a glass microscope slide for additional support. The microchannel had entries for liquid sample and liquid

medium at the front and end of the microchannel, respectively. A sample nozzle was designed to incorporate the EDI source onto the microchannel. The outside width of the nozzle was 20 μm , the inner width was 10 μm , and the depth was 10 μm .

Electrodispersion ionization took place in the Y-shaped region with two liquid exits. A close-up three-dimensional view and a top-view of the sample nozzle were illustrated in Figure 2b and 2c, respectively. Seven electrodes, with thickness of 0.35 μm , were deposited around the inside surfaces of the microchannel, such that the electrodes would be essentially rectangular. The EDI voltage was applied to the first electrode. The LPIMS voltage was applied to the second electrode. The second through sixth electrodes were externally connected in series with resistors. The sixth electrode was grounded through another resistor. The seventh electrode was used as a Faraday plate for measuring ion current.

Fabrication of Poly(dimethylsiloxane) LPIMS

PDMS channels are fabricated by soft lithography, a relatively new technique introduced by Whitesides [13;14]. Prior to the availability of soft lithography using polymeric substances, microchannels were fabricated by the conventional process of photolithography and microfabrication on glass and silicon substrates. Soft lithography prepares the microstructures using elastomeric stamp or mold on a soft substrate, such as PDMS and PMMA. Comparing to photolithography, soft lithography is more advantageous because it has simpler preparation, less time-consuming, lower cost, and better resolution. While photolithography can prepare

features down to 100 nm, soft lithography can reduce the size to 10 nm [13;15]. The fabrication of PDMS-LPIMS devices involved two phases of soft lithography [16;17]. The first phase of soft lithography involved patterning, which transferred the channel design onto a glass or silicon substrate, termed the master. The channel design was printed onto a high-resolution transparency to be used as a photomask. By exposing the system to light, the pattern from the photomask was transferred onto the master, which contained a layer of photoresist material. The depth of the PDMS channel was determined by the nature and thickness of the photoresist material. The master, which carried a positive relief of the photoresist, was used to produce replicates of PDMS channels. The second step of soft lithography was replica molding. Liquid PDMS prepolymer base (Sylgard 184, Dow Corning Inc., Midland, MI), mixed with its curing agent, was poured onto the master and cured for six hours at 80°C. The prepolymer base contains vinyl groups which react with the silicon hydride groups in the curing agent, to form a cross-linked solid polymer. This step yielded a PDMS layer with an open channel. After the titanium/platinum electrodes were deposited, the channel was sealed by bonding with a second layer of PDMS by oxygen plasma bonding. By exposing the surfaces of the two PDMS layers to an oxygen plasma discharge, the two layers were bonded irreversibly.

Results and Discussion

The properties of these two integrated designs of LPIMS were listed in Table 1. The properties of the previously reported LPIMS instruments were included for comparison.

A. Liquid Containment

i) Low Temperature Co-fired Ceramics LPIMS

The containment of the liquid medium within the LPIMS was achieved for both LTCC-LPIMS and PDMS-LPIMS devices. There were several noteworthy operational details. The end surfaces of the LTCC-LPIMS mobility tube was ground smooth to ensure a tight seal between the Teflon end caps and the mobility tube. The distance between the second and the third Teflon end caps was equal at all points around the circumference of the mobility tube for proper alignment between the external electrical connectors on the underside of the mobility tube and the pogo pins in the third end cap. This alignment was also necessary for sealing the mobility tube between the two end caps. The firing process had caused internal cracks, from the center channel to an alignment pinhole, within one structure, which caused liquid medium from the center channel to leak through the alignment pinhole. This was resolved by sealing the alignment pins inside their pinholes with epoxy.

ii) Poly(dimethylsiloxane) LPIMS

The infusion of non-polar organic solvent into the PDMS microchannel with was impeded by the nature of the PDMS surface. The surface of PDMS is hydrophobic due to the methyl groups. During the oxygen plasma process, which was used to bond two layers of PDMS, the methyl group on the PDMS surface is oxidized to silanol groups [9] (Figure 3)[18]. The PDMS surface remained hydrophilic if it were in contact with water, which was used to clean the microchannels following the fabrication process. However, the oxidation of surface methyl groups is reversible in

air within 30 minutes [9], and the infusion difficulty was overcome by injecting air through the microchannel for 30 minutes, prior to introduction of liquid medium. The typical resistivity values between pairs of adjacent electrodes of an empty PDMS microchannel were listed in Table 2. The resistance between adjacent pair of electrodes was usually in the 10^{11} Ω range for a freshly prepared microchannel. After rinsing the channel with air for 30 minutes, the surface of the microchannel returned to being hydrophobic and the resistance between adjacent pair of electrodes was normally in the 10^{12} Ω range.

B. Electrical Integrity

i) Low Temperature Co-fired Ceramics LPIMS

The LTCC mobility tube was made by stacking multiple layers of LTCC sheets with printed conducting electrodes and resistance materials. Electrical integrity was achieved by preventing misalignment. Two alignment holes were drilled at the same position for each layer. Alignment pins were used to arrange the multiple layers in a stacking position. The most significant disadvantage of the LTCC-LPIMS device was the 20% variation in resistivity of the resistance material. This problem could be solved by trimming the resistance material with laser after the firing process [7]. However, the laser trimming was not feasible for this LTCC device because the resistance materials were embedded. The large variance in resistivity would severely affect the homogeneity of the applied electric field, and thus lowering the resolving of the instrument. Improvement in layer-to-layer resistivity reproducibility would be

required to reach the full potential of an ultimate homogeneous field with 50 electrodes per cm of drift length that the LTCC-LPIMS could provide.

ii) Poly(dimethylsiloxane) LPIMS

Integrity of the deposited titanium/platinum electrodes was a major concern for PDMS-LPIMS. Cracks developed on deposited metal layer, due to the vast difference in Young modulus values between PDMS and metal, could disrupt the electrical connection [19]. This was prevented in our PDMS-LPIMS by providing a solid glass support for the PDMS microchannel. However, the deposited electrodes inside the microchannel appeared visibly less dense with use. Some electrodes were completely washed away after continual use. The density of the electrode surface decreased after 30 minutes of liquid flow in the absence of applied voltage. As a result, the electrodes were discontinued across the width of the microchannel and voltages were not delivered to the microchannel. This was caused by disrupted metal adhesion to the PDMS surface, where unreacted PDMS prepolymer on the polymer surface prevented the adhesion of metal [19]. Metal adhesion to PDMS could be improved by bombarding the PDMS surface with argon ions, followed by a hexane wash, as suggested by Bertrand et al [19].

C. Ion Transport Efficiency

i) Low Temperature Co-fired Ceramics LPIMS

Experiments had shown that the electrical circuit for the LTCC-LPIMS instrument to be working. Previous LPIMS experiments demonstrated that the total ion current

between 1 and 2 nA was obtained from ionizing an aqueous sample at 0.5 $\mu\text{L}/\text{min}$ with an EDI voltage of 1000 V above the target screen, for a drift distance of 2 mm. The LTCC-LPIMS had a drift length of 18.9 mm. The applied electric field of the drift region was 586 V/cm. The sample was an aqueous solution of 10 μM basic fuchsin, dissolved in methanol-water (90:10, vol/vol). The sample flow rate was 0.5 $\mu\text{L}/\text{min}$. The drift liquid, benzene, had a flow rate of 100 $\mu\text{L}/\text{min}$, or a linear velocity of 0.015 cm/s. The linear velocity of basic fuchsin in benzene at 586V/cm was anticipated to be 1 cm/s. Therefore, the counterflow of benzene should impede the migration of basic fuchsin ions by only 1.5% and would not hamper ion detection.

The EDI current data was tabulated in Table 3. When the EDI voltage and the LPIMS tube voltage were both zero, there was no current registered. When 2000V was applied to the mobility tube, 0.127 nA was measured. This current originated from the benzene background. When 2000V was applied to the EDI source, no ionization should occur because the EDI voltage equaled that of the target screen. There was no electric field between the EDI source and the LPIMS tube to induce ionization. However, a higher current of 0.137 nA was measured. As the EDI voltage increased, while maintaining the LPIMS voltage at 2000V, the total ion current also increased. When the EDI voltage was 1000V above that of the target screen, 0.145 nA was measured, which was 0.018 nA above the background current of 0.127 nA.

A control test was run at the end of the experiment set, the target screen was maintained at 2000V, but there was no applied EDI voltage. The current measured for the control test was 0.158 nA, which was the highest current level detected for

the experiment set. This indicated that the background current level rose with experimental time. The current was possibly arisen from water droplets contamination and not originating from EDI. The results for ion transport efficiency were inconclusive. Further testing will be necessary.

ii) Poly(dimethylsiloxane) LPIMS

To evaluate ion transport in PDMS-LPIMS microchannel, total ion current was measured with successive electrodes being used as the Faraday plate. The liquid medium, benzene, was flowing at a rate of 5 $\mu\text{L}/\text{min}$. The EDI voltage was applied to electrode 1 and was set at 1500V above that of the electrode 2. The electric field of the channel was set at +800V per electrode, except when the electrode 2 was used as the Faraday plate. For example, when the total ion current was being measured at the electrode 3, +800V was applied to the electrode 2; and when the total ion current was being measured at the electrode 7, +4000V, +3200V, +2400V, +1600V, and +800V were applied to the electrode 2, 3, 4, 5, and 6, respectively. Using electrode 2 as the Faraday plate was equivalent to measuring ion detection right after ionization. Measuring current at electrode 3 and beyond was equivalent to allowing the electrodispersed ion to travel along a length of ion mobility tube prior to ion detection. Therefore, effectiveness of ion transport can be determined by expressing the ion current detected as a fraction of the total electrodispersed current detected at the electrode 2.

The first set of experiments used benzene as the sample, and methanol-water (90:10, vol/vol) was used in the second set of experiments. The sample flow rate was 0.5 $\mu\text{L}/\text{min}$. Figure 4 showed the total ion current measured at successive electrodes along the PDMS channel in benzene with the two samples. The data showed that EDI signal of methanol-water was substantially greater than that of benzene. The EDI signal of methanol-water decreased with the increasing distance traveled. The ion transport efficiency declined to 32% of total electrodispersed ion current at electrode 3 and 0.45% at electrode 4. The results showed that the EDI signal could not be detected beyond the electrode 4, or a distance of 4 mm. The rapid reduction in ion transport efficiency with increasing migration distance could be hindered by the electrode design. The current electrodes were 1 mm wide and the electrodes spacing was also 1 mm. For the length of 10 mm from electrode 2 to electrode 7, there were 5 mm of zero-field region where the main ion movement was by diffusion. Future designs of PDMS-LPIMS should utilize narrower electrode widths.

Acknowledgements

This work was supported by the National Institutes of Biomedical Imaging and Bioengineering, National Institutes of Health (Grant R21EB001950).

References

1. M. Tam and H. H. Hill, Jr. Analytical Detection by Liquid Phase Ion Mobility Spectrometry. 54th American Society for Mass Spectrometry Conference on Mass Spectrometry. Seattle, WA. 2006.
2. H. H. Hill, Jr. and M. Tam. Ion Mobility Spectrometry Method and Apparatus. US Patent 7,071,465. 2006.
3. M. Tam and H. H. Hill, Jr. Liquid Phase Ion Mobility Spectrometry. 14th International Symposium on Ion Mobility Spectrometry. Paris, France. 2005.
4. M. Tam and Jr. H. H. Hill, Electrodispersion Ionization in Liquids, **Submitted** (2006).
5. J. P. Carrico, D. W. Sickenberger, G. E. Spangler and K. N. Vora, Simple Electrode Design for Ion Mobility Spectrometer, *J. Phys. E: Sci. Instrum.* **16**, pp. 1058-1062 (1983).
6. G. E. Spangler, K. N. Vora and J. P. Carrico, Miniature Ion Mobility Spectrometer Cell, *J. Phys. E: Sci. Instrum.* **19**, pp. 191-198 (1986).
7. K. B. Pfeifer and A. N. Rumpf, Measurement of Ion Swarm Distribution Functions in Miniature Low-Temperature Co-Fired Ceramic Ion Mobility Spectrometer Drift Tubes, *Analytical Chemistry* **77**, pp. 5215-5220 (2005).
8. P. A. Auroux, D. Iossifidis, D. R. Reyes and A. Manz, Micro Total Analysis Systems. 2. Analytical Standard Operations and Applications, *Analytical Chemistry* **74**, pp. 2637-2652 (2002).
9. S. K. Sia and G. M. Whitesides, Microfluidic Devices Fabricated in Poly(dimethylsiloxane) for Biological Studies, *Electrophoresis* **24**, pp. 3563-3576 (2003).
10. C. S. Effenhauser, G. J. M. Bruin, A. Paulus and M. Ehrat, Integrated Capillary Electrophoresis on Flexible Silicone Microdevices: Analysis of DNA Restriction Fragments and Detection of Single DNA Molecules on Microchips, *Analytical Chemistry* **69**, pp. 3451-3457 (1997).
11. K. Huikko, P. Östman, K. Grigoras, S. Tuomikoski, V. -M. Tianen, A. Soininen, K. Puolanne, A. Manz, S. Franssila, R. Kostainen and T. Kotiaho, Poly(dimethylsiloxane) Electro spray Devices Fabricated with Diamond-like Carbon-Poly(dimethylsiloxane) Coated SU-8 Masters, *Lab Chip* **3**, pp. 67-72 (2003).
12. Donald Gene Plumlee, Fabrication of a Miniature Ion Mobility Spectrometry in

Low Temperature Co-fired Ceramics, Boise State University, Boise, Idaho (2003).

13. Y. Xia and G. M. Whitesides, Soft Lithography, *Angewandte Chemie International Edition* **37**, pp. 550-575 (1998).
14. J. C. McDonald and G. M. Whitesides, Poly(dimethylsiloxane) as a Material for Fabricating Microfluidic Devices, *Accounts of Chemical Research* **35**, pp. 491-499 (2002).
15. W. W. Y. Chow, K. F. Lei, G. Shi, W. J. Li and Q. Huang, Microfluidic Channel Fabrication by PDMS-Interface Bonding, *Smart Materials and Structures* **15**, p. S112-S116 (2006).
16. H. Cui, K. Horiuchi, P. Dutta and C. F. Ivory, Isoelectric Focusing in a Poly(dimethylsiloxane) Microfluidic Chip, *Analytical Chemistry* **77**, pp. 1303-1309 (2005).
17. N. H. Al Mamum, Fabrication of a Microchip Device for Liquid Phase Ion Mobility Spectrometry, Washington State University, Pullman, WA (2006).
18. D. C. Duffy, J. C. McDonald, O. J. A. Schueller and G. M. Whitesides, Rapid Prototyping of Microfluidic Systems in Poly(dimethylsiloxane), *Analytical Chemistry* **70**, pp. 4974-4984 (1998).
19. A. Delcorte, S. Befany, C. Poleunis, M. Troosters and P. Bertrand, Improvement of Metal Adhesion to Silicone Films: a TOF-SIMS Study. In *Adhesion Aspects of Thin Films* (Edited by K. L. Mittal), VSP, The Netherlands (2005).

Table 1: Properties and dimensions of the previously reported and integrated LPIMS devices.

	Previously Reported Devices		Integrated Devices	
	Teflon	Resistive Glass	LTCC	PDMS
Housing Material:	Teflon	Pyrex	LTCC	PDMS
Channel Properties:				
<i>Shape Cross Section</i>	Cylindrical 4.76 mm i.d.	Cylindrical 4.1 mm i.d.	Cylindrical 3.8 mm i.d.	Rectangular 1.0 mm (w) 0.4 mm (h)
<i>Total Length (mm)</i>	20.0	14.5	18.1	10.0
<i>Drift Length (mm)</i>	13.3	5.0	10.4	10.0
Resistors:	External	Surface	Embedded	External
Number of electrodes:	16	Continuous	65	6
Insulator:				
<i>Material</i>	Teflon	n/a	LTCC	PDMS
<i>Resistivity (ohm-cm)</i>	10^{18}	n/a	10^{14}	10^{13}
<i>Dielectric Strength (kV/mm)</i>	60	n/a	20	21
Sample Introduction:	Fused silica capillary	Fused silica capillary	Fused silica capillary	Sample nozzle incorporated into main channel

Table 2: Typical Resistivity Values between a Pair of Adjacent Electrodes in an empty PDMS-LPIMS

Electrodes Pair	Resistivity Between Electrodes ($\Omega \cdot \text{mm}$)	
	10 hours after plasma bonding	After injecting air for 30 minutes
#2 and #3	1.0×10^{11}	1.2×10^{12}
#3 and #4	2.0×10^{10}	2.0×10^{12}
#4 and #5	2.0×10^{10}	2.5×10^{12}
#5 and #6	1.0×10^{12}	3.1×10^{12}
#6 and #7	8.0×10^{11}	3.8×10^{12}

Table 3: Total ion current obtained from LTCC-LPIMS.

EDI Voltage (V)	Target Screen (V)	EDI Voltage above Target Screen (V)	Total Ion Current (nA)
0	0	0	0.000 ± 0.003
0	2000	-2000	0.127 ± 0.006
2000	2000	0	0.137 ± 0.006
2500	2000	500	0.140 ± 0.006
3000	2000	1000	0.145 ± 0.007
3500	2000	1500	0.148 ± 0.007
4000	2000	2000	0.150 ± 0.007
0	2000	-2000	0.158 ± 0.006

Figure Captions

Figure 1: Schematic of the LTCC-LPIMS (A) with its sealing Teflon end caps (B), external electrical connections (C), liquid medium entry (D) and exit (E). The three pieces of Teflon end caps were tightened with three screws (F), and sealed with two pieces of o-rings (G) and a membrane (H) that fitted into the counter bore of the end caps.

Figure 2: (a) Top-view schematic of the third generation of PDMS-LPIMS prototype. The PDMS channel was 1000 μm wide, 400 μm deep and 1 cm long. (b) Close-up three-dimensional view and (c) top-view of the sample nozzle. The outside width of the nozzle was 50 μm , the inner width was 10 μm , and the depth was 10 μm .

Figure 3: The surface methyl groups of poly(dimethylsiloxane) are oxidized to hydroxyl group by oxygen plasma. The oxidation reaction is reversible in air within 30 minutes.

Figure 4: Plot of total ion current being measured at successive electrodes along the PDMS channel in benzene. The sample used were benzene (●) and methanol-water (90:10, vol/vol) (⊖).

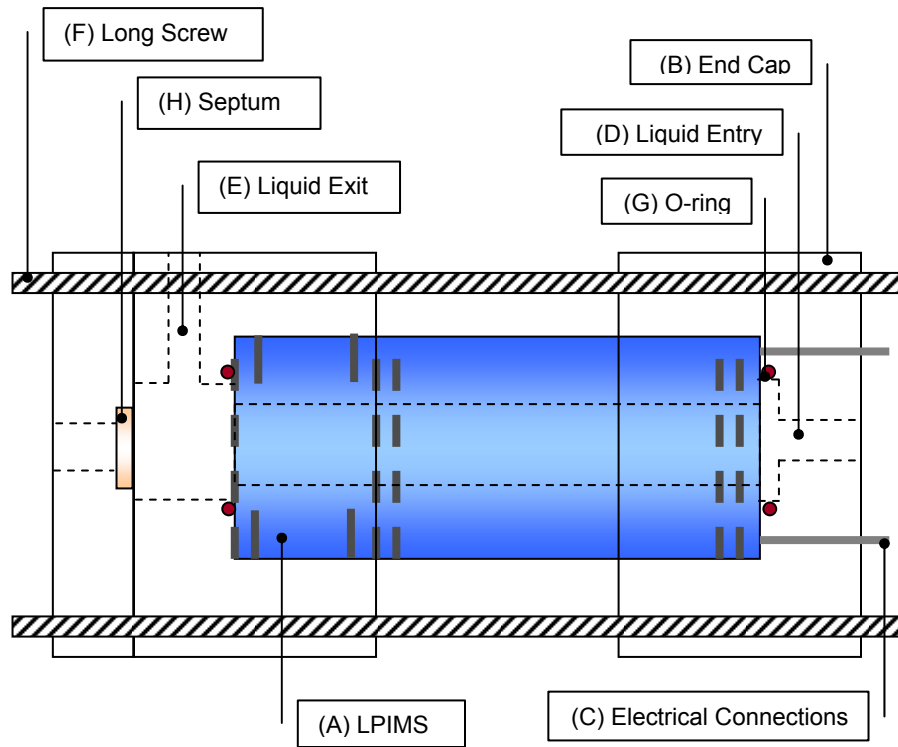


Figure 1: Schematic of the LTCC-LPIMS (A) with its sealing Teflon end caps (B), external electrical connections (C), liquid medium entry (D) and exit (E). The three pieces of Teflon end caps were tightened with three screws (F), and sealed with two pieces of o-rings (G) and a membrane (H) that fitted into the counter bore of the end caps.

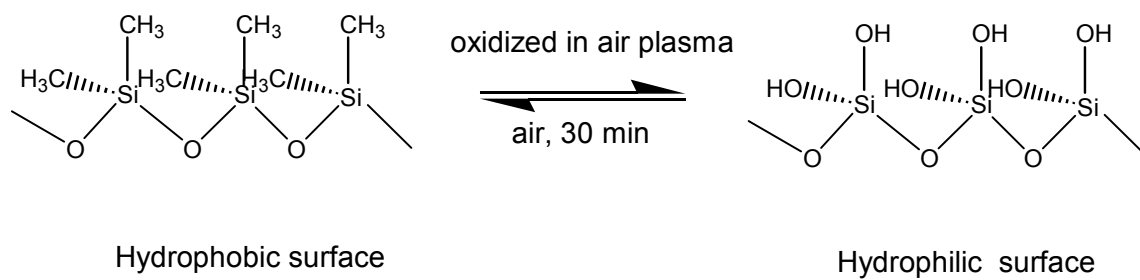


Figure 3: The surface methyl groups of poly(dimethylsiloxane) are oxidized to hydroxyl group by oxygen plasma. The oxidation reaction is reversible in air within 30 minutes.

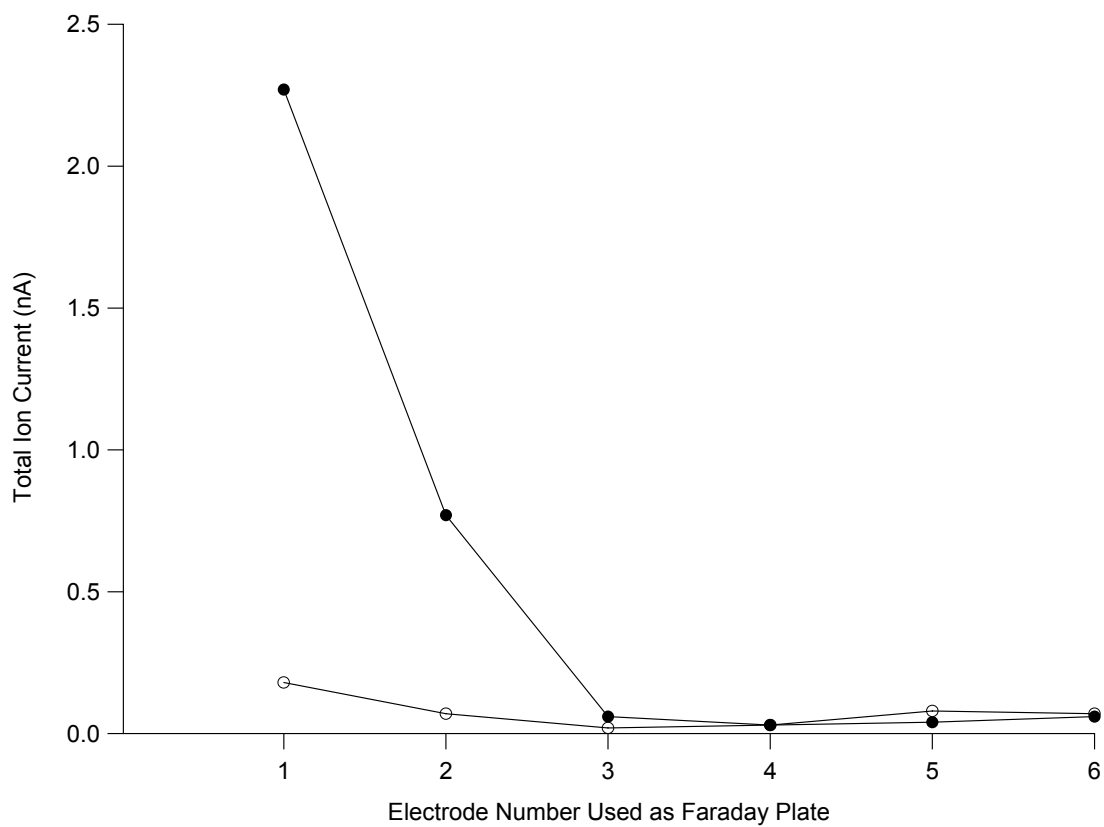


Figure 4: Plot of total ion current being measured at successive electrodes along the PDMS channel in benzene. The sample used were benzene (●) and methanol-water (90:10, vol/vol) (○).

Chapter Five

Evaluation of Pulsed Electrodispersion Ionization

Source for Liquid Phase Ion Mobility

Spectrometry

Abstract

Pulsed electrodispersion ionization source was developed and evaluated for liquid phase ion mobility spectrometry in liquid hexane. The pulsed electrodispersion was achieved by alternating the voltage applied to the ionization source, between a voltage sufficient to induce electrodispersion and a lower voltage. A miniaturized resistive glass liquid phase mobility spectrometer of 5 mm length was used. The use of a pulsed ionization eliminated the need for an ion shutter. Liquid phase ion mobility spectra of methanol-water solvent, tetramethylammonium, tetrabutylammonium, and bradykinin demonstrated the capability of pulsed electrodispersion ionization as a multipurpose ionization source for liquid phase ion mobility spectrometry. This study presented pulsed electrodispersion ionization as a multipurpose ionization source for generating liquid phase ions. Three important instrumental processes were merged into a single source: sample introduction, sample ionization, and pulsed ion injection.

Introduction

Liquid phase ion mobility spectrometry (LPIMS) is a newly developed analytical separation technique [1-3]. The separation is based upon the difference in mobilities of ions traveling through a non-electrolytic liquid medium under the influence of an externally established electric field. Ionization in LPIMS was achieved by electrodispersion ionization (EDI) [4], which was designed to deliver aqueous ions into non-aqueous liquid medium. LPIMS is a time-of-flight analyzer that detects ion signal as a function of the analyte arrival time. Because EDI is a continuous ionization source, an ion shutter was used to introduce short pulses of ions into LPIMS [5]. It is anticipated that a pulsed ionization source would be appropriate for LPIMS.

Other time-of-flight analyzer, time-of-flight mass spectrometer (TOF-MS) and gas-phase ion mobility spectrometer (IMS), interface well with pulsed ionization sources. Pulsed glow discharge-TOF-MS is used to provide rapid elemental and molecular analyses through its sequential “hard” and “soft” ionization processes [6-11]. Matrix-assisted laser desorption ionization is a widely used ionization source for TOF-MS, performing routine mass measurements of peptides and proteins [12-14] and enabling analysis of biomolecules and synthetic polymers up to 350 kDa with sub picomole sensitivities [15-17].

Early works of gas-phase IMS were conducted with pulsed ionization sources, such as electron-impact [18-23], Townsend discharge [24-26], thermionic emitter [19;27],

and spark discharge sources [28]. These ion mobility spectrometers contained no physical ion shutters because the ionization pulses were short, in comparison to the drift times. The pulsing of the ionization source doubled as the gating mechanism. Bradbury-Nielsen shutter [29] and Tyndall shutter [30] were implemented into ion mobility spectrometers to provide more precise timing of ions [31-35]. With the introduction of ion shutters, continuous ionization sources, such as radioactive ionization and electrospray ionization, are made compatible with IMS. Radioactive ionization sources (^{63}Ni , ^{241}Am , and Tritium) are frequently employed in portable and handheld IMS instruments because they require neither power supply nor maintenance. Radioactive ionization-IMS has been used for detecting a diversity of compounds, from atmospheric [36;37] and environmental [38-42] pollutants, explosives [43-45], drugs [46-49], chemical warfare agent simulants [50;51], to derivatized whole cell bacteria [52]. Electrospray ionization-IMS was introduced in the late 1980s [53] that had become invaluable in the research of proteomics [54-60], glycomics [61-63], and metabolomics [64]. In addition to these popular continuous ionization sources, there are current reports in exploring pulsed ionization sources for IMS. Pulsed corona discharge ionization and distributed plasma ionization were developed as alternative non-radioactive ionization sources [65-70]. MALDI was used as a interchangeable replacement of EDI to make use of its capability to form primarily singly charged ions and its ability to ionize bio- and synthetic polymers [71-76].

EDI is the liquid phase analogue of electrospray ionization (ESI). Like ESI, which was recently developed in pulsation mode with mass spectrometry [77-80], EDI can operate in continuous and pulsing modes. The pulsing of EDI is controlled by

adjusting the applied EDI voltage relative to the sample flow rate [4]. The goal of this study was to demonstrate the merge of three important instrumental processes: sample introduction, sample ionization, and ion gating, in pulsed EDI for miniaturized liquid phase ion mobility spectrometry.

Experimental Section

Instrumentation

The pulsed EDI-LPIMS system consisted of a pulsed electrodispersion ionization source and a liquid phase ion mobility spectrometer (Figure 1). The pulsed EDI source comprised of a standard electrodispersion ionization source [4] and a pulsed voltage circuit. Aqueous sample was introduced by a syringe that was connected through a grounded metal union to a fused silica capillary. EDI voltage was applied to a second metal union. A micro-elbow junction allowed for a 90° bend of the fused silica capillary. The pulsed voltage circuit contained four 2.5 M Ω resistors in series and was controlled by a Double Pole Single Throw (DPST) two-way switch, constructed by Technical Services of Washington State University. The EDI voltage was alternated between an upper voltage and a lower voltage. The upper voltage was sufficient to induce electrodispersion ionization, which was 2200V above the voltage of the spectrometer. There was no ionization at the lower voltage, which was half the value of the upper voltage. The pulsed voltage circuit was capable of switching a maximum voltage of 10 kV. The pulse width and frequency was synchronized with a LabView (National Instruments, Austin, TX)-based data

acquisition program [81]. At the beginning of each mobility experiment, a 5-V signal was sent by the data acquisition program to the two-way switch, opening the first two-way switch and closing the second two-way switch for the duration of the pulse width, 0.05 s, at a frequency of 0.1 Hz. At the end of the 0.05 s pulse, the first two-way switch closed and the second two-way switch opened.

The liquid phase ion mobility spectrometer consisted of a resistive glass tube (Burle Electro-Optics Inc., Sturbridge MA) and a Faraday plate (Figure 1). The resistive glass tube had a 4.1-mm i.d., 5-mm length, and a total inner surface resistance of 10 M Ω . There were electrodes attached to either ends of the spectrometer. +500 V was applied to the front electrode of the spectrometer. The spectrometer was grounded through a 430 k Ω resistor at the end electrode. The Faraday plate was located 2 mm behind the spectrometer. The current signal was amplified at 10⁹ volts/ampere by a Keithley 427 model (Keithley Instruments, Cleveland, OH) and acquired by the data acquisition program.

Materials and Reagents

The liquid medium, through which ions drifted, was hexane (J. T. Baker, Phillipsburg, NJ). Tetraalkylammonium salts and bradykinin (Sigma-Aldrich, St. Louis, MO) in micro-molar concentrations were used as the sample analytes. The samples were prepared in methanol-water (90:10, vol/vol) with HPLC grade methanol (J. T. Baker, Phillipsburg, NJ) and 18.1 M Ω water. Tetramethylammonium bromide and tetrabutylammonium bromide were individually dissolved as 10 mM solutions and

further diluted to 10 μM and 100 μM . Bradykinin was prepared from bradykinin acetate as 10 mM solutions and diluted to 100 μM . The solvent blank was methanol-water (90:10, vol/vol).

Calculations

Liquid phase ion mobility (μ) was calculated as the ratio of ion velocity (v) to the applied electric field (E). In terms of the spectrometer length (L) and the mobility time (t), the liquid phase ion mobility was expressed as:

$$\mu = \frac{L}{E \cdot t} \quad (1)$$

Because the liquid phase ion mobility spectrometry was miniaturized, with a length of 5 mm (L_1), the distance between the end of the resistive glass mobility spectrometer and the Faraday plate (L_2) became significant. It would be necessary to take into consideration the electric field between the end of the spectrometer and the Faraday plate for the mobility calculation. The distance of L_2 was 2 mm. When a voltage of +507 V was applied to the front electrode of the spectrometer, the end electrode had a voltage of +18 V. Therefore, the electric field across L_1 was +978 V/cm (E_1) and the electric field across L_2 was +90V/cm (E_2). Therefore, the mobility value was more accurately represented as:

$$\mu = \left(\frac{L_1}{E_1} + \frac{L_2}{E_2} \right) \cdot \frac{1}{t} \quad (2)$$

The expected mobility values of ions in hexane ($\mu_{\text{in hexane}}$) were estimated by adjusting the literature mobility values of ions in water ($\mu_{\text{in water}}$) for the viscosity difference between the two liquid medium.

$$\mu_{\text{in hexane}} = \mu_{\text{in water}} \times \frac{\eta_{\text{water}}}{\eta_{\text{hexane}}} \quad (3)$$

Water has a viscosity of 0.89 cP, while the less viscous hexane has a viscosity of 0.326 cP [82]. Consequently, analytes are expected to have 2.7 times faster mobilities in hexane than in water, as the mobility of ions is inversely proportional to the viscosity of the liquid medium [83].

Results and Discussion

LPIMS Spectra of Solvent Blank

Liquid phase ion mobility spectra of the methanol-water solvent blank were obtained using pulsed electrodispersion ionization for sample introduction, sample ionization, and ion gating. 179 spectra were collected consecutively over 30 minutes at 10-s intervals. An EDI voltage of +2700 V was applied for a pulse width of 0.05 s.

The solvent peaks shifted to longer mobility time over the course of the experiment. The first 8.5 minutes of the data (51 averages), the last 2.5 minutes of data (15 averages), and the entire 30 minutes of data (179 averages) were compared (Figure

2). There were two solvent peaks, at 0.49 s and 0.54 s, observed in the averaged spectrum for the first 8.5 minutes of the experiment (Figure 2a). The solvent peaks had shifted to 0.62 s, 0.67 s, 0.73 s, and 0.80 s in the averaged spectrum in the last 2.5 minutes of the experiment (Figure 2b). The solvent peaks were assumed to be solvated proton ions. The fact that the mobility time of the solvent peaks increased with experimental duration suggested that the solvent ions were surrounded by an increasing amount of solvation molecules. Conventional gas phase ion mobility spectrometry has a unidirectional counter flow of drift gas that keep the drift region clean by continuously sweeping out neutral molecules [84]. Because the liquid hexane medium was stationary in this study, any uncharged solvent molecules would remain inside the spectrometer. Subsequent ion-molecule reactions, between ionized and uncharged solvent molecules, produced ions of increasing sizes and longer drift times.

The three-dimensional plot of current intensity, mobility time, and consecutive spectrum number (Figure 3) revealed that two populations of ions were present: a major group of ions with a drift time of 0.51 s (A in Figure 3) and a minor group of ions with drift times between 1 s and 2 s (B in Figure 3). The minor group of ions, also observed in Figure 2c as a broad peak, was presumably larger cluster ions of the solvent.

Figure 3 showed that the solvent peaks shifted progressively from 0.51 ± 0.05 s at the start of the experiment, to 0.71 ± 0.06 s towards the end of the experiment. The mobility value of the solvent ions, calculated with equation 2, had decreased from

$(5.4 \pm 0.5) \times 10^{-3} \text{ cm}^2/\text{V}\cdot\text{s}$ to $(3.8 \pm 0.3) \times 10^{-3} \text{ cm}^2/\text{V}\cdot\text{s}$. The estimated mobility value of proton in hexane, was calculated by adjusting the literature mobility value of proton in water, $(3.623 \times 10^{-3} \text{ cm}^2/\text{V}\cdot\text{s})$ [85], for the viscosity difference (equation 3). The estimated mobility value of proton in hexane was $9.9 \times 10^{-3} \text{ cm}^2/\text{V}\cdot\text{s}$. However, migration of proton in water involves a transfer process of proton among water molecules through forming and disrupting hydrogen bonds. This mechanism of proton migration, first proposed by Grotthuss [86] in 1806, is continually being studied and modeled [87-89]. The Grotthuss mechanism was assumed to have negligible effect in the liquid medium used in this experiment, as there are no hydrogen bonds formed between the protons and the non-polar hexane. Therefore, the migration of proton in hexane involves the actual movement of proton molecules through hexane. The mobilities of solvated proton ions in hexane are therefore expected to be slower than the estimated mobility of $9.9 \times 10^{-3} \text{ cm}^2/\text{V}\cdot\text{s}$ in the absence of proton migration by Grotthuss mechanism. The experimental mobility value of $5.4 \times 10^{-3} \text{ cm}^2/\text{V}\cdot\text{s}$ for the solvent ions in hexane was indeed slower than the estimated mobility of proton in hexane by 1.8 times.

LPIMS Spectra of Analytes

Pulsed EDI-LPIMS of tetramethylammonium bromide, tetrabutylammonium bromide, and bradykinin were conducted in hexane in the positive mode. The samples were dissolved in the solvent blank of methanol-water (90:10, vol/vol) at a concentration of $100 \mu\text{M}$. The sample flow rates were $0.1 \mu\text{L}/\text{min}$. An EDI voltage of $+2650 \text{ V}$ was applied for a pulse width of 0.05 s .

The EDI-LPIMS spectra of tetramethylammonium, tetrabutylammonium ions, and bradykinin were shown in Figure 4a – 4c. All the analyte spectra showed a sharp and intense peak. Both tetraalkylammonium spectra featured a 0.28 s peak and the bradykinin spectrum had a 0.19 s peak. It was assumed that the 0.19 s and the 0.28 s peaks were not an analyte peak since it had a faster mobility time than the solvent ions. Tetramethylammonium spectrum had a unique peak at 0.76 s, with a corresponding mobility value of $3.6 \times 10^{-3} \text{ cm}^2/\text{V}\cdot\text{s}$; while tetrabutylammonium spectrum had a characteristic peak at a slower mobility time of 0.89 s, with a mobility value of $3.1 \times 10^{-3} \text{ cm}^2/\text{V}\cdot\text{s}$. The bradykinin spectrum had overlapping peaks between 0.6 s and 1.7 s, with the two most intense peaks at 0.67 s and 1.18 s. The 0.67 s peak in the bradykinin spectrum was most likely solvent ions, because its mobility value of $4.1 \times 10^{-3} \text{ cm}^2/\text{V}\cdot\text{s}$ was in close proximity to that of the solvent ions.

The experimental mobility values of tetramethylammonium, tetrabutylammonium, and bradykinin were compared with the literature mobility values in water and the estimated mobility values in hexane (Table 1). The mobility value of bradykinin in water was not available in literature and thus, the mobility value for a fluorescein isothiocyanate (FITC)-labeled bradykinin was provided instead. The FITC label increased the mass of bradykinin from 1060 Da to 1436 Da [90]. While the mobility value of the solvent ions were slower than that expected in hexane, due to the absence of Grotthus mechanism in non-polar hexane, the three analytes all had faster mobilities than anticipated. Tetramethylammonium, with its mobility value of $3.6 \times 10^{-3} \text{ cm}^2/\text{V}\cdot\text{s}$, was 2.8 times faster than its estimated mobility value in hexane; tetrabutylammonium, with its mobility value of $3.6 \times 10^{-3} \text{ cm}^2/\text{V}\cdot\text{s}$, was 5.6 times

faster; and bradykinin, with its mobility value of $2.3 \times 10^{-3} \text{ cm}^2/\text{V}\cdot\text{s}$, was 6 times faster. Ions in water are surrounded by a shell of solvation sphere due to the ion-dipole interaction with water molecules [85]. Singh et al previously reported that, in aqueous solutions of acetonitrile, the solvation sphere surrounding copper ions consisted of acetonitrile molecules [91]. The replacement of solvation molecules, from water to acetonitrile molecules, increased the hydrodynamic radius of the copper ions. The mobility of copper ions was, therefore, slower in the aqueous acetonitrile solution, compared with its mobility in water. Based on the same line of reasoning, ions in hexane would not have a shell of solvation sphere due to the lack of ion-dipole interaction between the ions and the non-polar hexane. As a result, mobility of ions in hexane was faster than predicted.

Conclusions

Electrodispersion ionization is a liquid phase ionization source capable of generating ions in short pulses. Pulsed electrodispersion ionization source is useful for pulsed injection of aqueous ions in liquid phases. This is useful for liquid phase ion mobility spectrometry, especially in a miniaturized instrument. A pulsed ionization source eliminates the need for a physical ion shutter, thus simplifying the manufacturing process. A pulsed ionization source also reduces sample consumption. The results suggest that a counterflow of liquid medium will be useful in removing uncharged molecule in the liquid phase ion mobility spectrometer.

Acknowledgements

This work was supported by the National Institutes of Biomedical Imaging and Bioengineering, National Institutes of Health (Grant R21EB001950).

References

1. H. H. Hill, Jr. and M. Tam. Ion Mobility Spectrometry Method and Apparatus. US Patent 7,071,465. July 4, 2006.
2. M. Tam and H. H. Hill, Jr. Liquid Phase Ion Mobility Spectrometry. 14th International Symposium on Ion Mobility Spectrometry. Paris, France. 2005.
3. M. Tam and H. H. Hill, Jr. Analytical Detection by Liquid Phase Ion Mobility Spectrometry. 54th American Society for Mass Spectrometry Conference on Mass Spectrometry. Seattle, WA. 2006.
4. M. Tam and H. H. Hill, Jr. Electrodispersion Ionization in Liquids, **Submitted** (2006).
5. M. Tam and H. H. Hill, Jr. Liquid Phase Ion Mobility Spectrometry, *Manuscript in Preparation* (2006).
6. W. Hang, W. O. Walden and W. W. Harrison, Microsecond Pulsed Glow Discharge as an Analytical Spectroscopic Source, *Analytical Chemistry* **68**, pp. 1148-1152 (1996).
7. R. E. Steiner, C. L. Lewis and V. Majidi, Consideration of a Millisecond Pulsed Glow Discharge Time-of-Flight Mass Spectrometer for Concurrent Elemental and Molecular Analysis, *Journal of Analytical Atomic Spectrometry* **14**, pp. 1537-1541 (1999).
8. D. Fliefel, K. Fuhrer, M. Gonin and D. Gunther, Evaluation of a Pulsed Glow Discharge Time-of-Flight Mass Spectrometer as a Detector for Gas Chromatography and the Influence of the Glow Discharge Source Parameters on the Information Volume in Chemical Speciation Analysis, *Analytical and Bioanalytical Chemistry* **386**, pp. 169-179 (2006).
9. R. E. Steiner, C. L. Lewis and F. L. King, Time-of-Flight Mass Spectrometry with a Pulsed Glow Discharge Ionization Source, *Analytical Chemistry* **69**, pp. 1715-1721 (1997).
10. L. Li, C. M. Barshick, J. T. Millay, A. V. Welty and F. L. King, Determination of Bromine in Flame-Retardant Plastics Using Pulsed Glow Discharge Mass Spectrometry, *Analytical Chemistry* **75**, pp. 3953-3961 (2003).
11. L. Li, J. T. Millay, J. P. Turner and F. L. King, Millisecond Pulsed Radio Frequency Glow Discharge Time of Flight Mass Spectrometry: Temporal and Spatial Variations in Molecular Energetics, *Journal of the American Society for Mass Spectrometry* **15**, pp. 87-102 (2004).

12. M. Mann, R. C. Hendrickson and A. Pandey, Analysis of Proteins and Proteomes by Mass Spectrometry, *Annual Review of Biochemistry* **70**, pp. 437-473 (2001).
13. W. Pusch and M. Kostrzewa, Application of MALDI-TOF Mass Spectrometry in Screening and Diagnostic Research, *Current Pharmaceutical Design* **11**, pp. 2577-2591 (2005).
14. B. Spengler and R. J. Cotter, Ultraviolet-Laser Desorption Ionization Mass-Spectrometry of Proteins above 100000 Daltons by Pulsed Ion Extraction Time-of-Flight Analysis, *Analytical Chemistry* **62**, pp. 793-796 (1990).
15. R. Kaufmann, Matrix-Assisted Laser Desorption Ionization (MALDI) Mass Spectrometry: a Novel Analytical Tool in Molecular Biology and Biotechnology, *Journal of Biotechnology* **41**, pp. 155-175 (1995).
16. H. J. Rader and W. Schrepp, MALDI-TOF Mass Spectrometry in the Analysis of Synthetic Polymers, *Acta Polymerica* **49**, pp. 272-293 (1998).
17. S. E. M. Moore, A. R. Hemsley, A. N. French, E. Dudley and R. P. Newton, New Insights from MALDI-TOF MS, NMR, and GC-MS: Mass Spectrometry Techniques Applied to Palynology, *Protoplasma* **228**, pp. 151-157 (2006).
18. D. L. Albritton, T. M. Miller, D. W. Martin and E. W. McDaniel, Mobilities of Mass-Identified H_3^+ and H^+ Ions in Hydrogen, *Physical Review* **171**, pp. 94-102 (1968).
19. T. M. Miller, J. T. Moseley, D. W. Martin and E. W. McDaniel, Reactions of H^+ in H_2 and D^+ in D_2 ; Mobilities of Hydrogen and Alkali Ions in H_2 and D_2 Gases, *Physical Review* **173**, pp. 115-123 (1968).
20. J. T. Moseley, R. M. Snuggs, D. W. Martin and E. W. McDaniel, Mobilities, Diffusion Coefficients, and Reaction Rates of Mass-Identified Nitrogen Ions in Nitrogen, *Physical Review* **178**, pp. 240-248 (1969).
21. J. Heimerl, R. Johnsen and M. A. Biondi, Ion-Molecule Reactions, $He^+ + O_2$ and $He^+ + N_2$, at Thermal Energies and Above, *Journal of Chemical Physics* **51**, pp. 5041-5048 (1969).
22. H. L. B. a. M. A. B. R. Johnsen, Ion-Molecule Reactions Involving N_2^+ , N^+ , O_2^+ , and O^+ Ions from 300K to ~ 1 eV, *Journal of Chemical Physics* **52**, pp. 5080-5084 (1970).
23. R. M. S. D. W. M. a. E. W. M. J. T. Moseley, Longitudinal and Transverse Diffusion Coefficients of Mass-Identified N^+ and N_2^+ Ions in Nitrogen, *Physical Review Letters* **21**, pp. 873-875 (1968).
24. J. A. Hornbeck, Microsecond Transient Currents in the Pulsed Townsend Discharge, *Physical Review* **58**, pp. 374-379 (1951).

25. J. A. Hornbeck, The Drift Velocities of Molecular and Atomic Ions in Helium, Neon, and Argon, *Physical Review* **84**, pp. 615-620 (1951).
26. R. N. Varney, Drift Velocities of Ions in Krypton and Xenon, *Physical Review* **88**, pp. 362-364 (1952).
27. J. T. Moseley, I. R. Gatland, D. W. Martin and E. W. McDaniel, Measurement of Transport Properties of Ions in Gases; Results for K^+ Ions in N_2 , *Physical Review* **178**, pp. 234-239 (1969).
28. E. W. McDaniel, D. W. Martin and W. S. Barnes, Drift Tube-Mass Spectrometer for Studies of Low-Energy Ion-Molecule Reactions, *Review of Scientific Instruments* **33**, pp. 2-7 (1962).
29. N. E. Bradbury and R. A. Nielsen, Absolute Values of the Electron Mobility in Hydrogen, *Physical Review* **49**, pp. 388-393 (1936).
30. A. M. Tyndall, *The Mobility of Positive Ions in Gases*. Cambridge University Press, Cambridge, U.K. (1938).
31. K. B. McAfee, D. Sipler and D. Edelson, Mobilities and Reactions of Ions in Argon, *Physical Review* **160**, pp. 130-135 (1967).
32. L. G. McKnight, Drift Velocities and Interactions of Negative Ions in Oxygen, *Physical Review A* **2**, pp. 762-770 (1970).
33. L. G. McKnight and J. M. Sawina, Drift Velocities and Interactions of Negative Ions in Oxygen. II O_4^- , *Physical Review A* **4**, pp. 1043-1046 (1971).
34. R. P. Creaser, Measured Mobility and Derived Interaction Potentials for K^+ Ions in Rare Gases, *Journal of Physics B: Atomic and Molecular Physics* **7**, pp. 529-540 (1974).
35. P. L. Patterson, Mobilities of Negative Ions in SF_6 , *Journal of Chemical Physics* **53**, pp. 696-704 (1970).
36. J. H. Cross, T. F. Limero, J. L. Lane and F. S. Wang, Determination of Ammonia in Ethylene Using Ion Mobility Spectrometry, *Talanta* **45**, pp. 19-23 (1997).
37. L. Myles, T. P. Meyers and L. Robinson, Atmospheric Ammonia Measurement with an Ion Mobility Spectrometer, *Atmospheric Environment* **40**, pp. 5745-5752 (2006).
38. J. W. Leonhardt, A New ppb-Gas Analyzer by Means of GC-Ion Mobility Spectrometry (GC-IMS), *Journal of Radioanalytical and Nuclear Chemistry* **257**, pp. 133-139 (2003).
39. K. Tuovinen, H. Paakkanen and A. Hanninen, Detection of Pesticides from Liquid Matrices by Ion Mobility Spectrometry, *Analytica Chimica Acta* **404**, pp.

7-17 (2000).

40. M. T. Jafari and M. Azimi, Analysis of Sevin, Amitraz, and Metalaxyl Pesticides Using Ion Mobility Spectrometry, *Analytical Letters* **39**, pp. 2061-2071 (2006).
41. O. Raatikainen, V. Reinikainen, P. Minkkinen, T. Ritvanen, P. Muje, J. Pursianinen, T. Hiltunen, P. Hyvonen, A. von Wright and S. P. Reinikainen, Multivariate Modelling of Fish Freshness Index Based on Ion Mobility Spectrometry Measurements, *Analytica Chimica Acta* **544**, pp. 128-134 (2005).
42. F. W. Karasek and O. S. Tatone, Plasma Chromatography of the Mono-Halogenated Benzenes, *Analytical Chemistry* **44**, pp. 1758-1763 (1972).
43. A. H. Lawrence and P. Neudorfl, Detection of Ethylene Glycol Dinitrate Vapors by Ion Mobility Spectrometry Using Chloride Reagent Ions, *Analytical Chemistry* **60**, pp. 104-109 (1988).
44. G. E. Spangler, J. P. Carrico and D. N. Campbell, Recent Advances in Ion Mobility Spectrometry for Explosives Vapor Detection, *J. Test. Eval.* **13**, pp. 234-240 (1985).
45. F. W. Karasek and D. W. Denney, Detection of 2,4,6-trinitrotoluene Vapors in Air by Plasma Chromatography, *Journal of Chromatography A* **93**, pp. 141-147 (1974).
46. F. W. Karasek, D. E. Karasek and S. H. Kim, Detection of Lysergic Acid Diethylamide, Δ^9 -Tetrahydrocannabinol and Related Compounds by Plasma Chromatography, *Journal of Chromatography A* **105**, pp. 345-352 (1975).
47. F. W. Karasek, Jr. H. H. Hill and S. H. Kim, Plasma Chromatography of Heroin and Cocaine with Mass-Identified Mobility Spectra, *Journal of Chromatography A* **117**, pp. 327-336 (1976).
48. A. Miki, Th. Keller, P. Regenscheit, R. Dirnhofer, M. Tatsuno, M. Katagi, M. Nishikawa and H. Tsuchihashi, Application of Ion Mobility Spectrometry to the Rapid Screening of Methamphetamine Incorporated in Hair, *Journal of Chromatography B* **692**, pp. 319-328 (1997).
49. A. H. Lawrence, Ion Mobility Spectrometry/Mass Spectrometry of Some Prescription and Illicit Drugs, *Analytical Chemistry* **58**, pp. 1269-1272 (1986).
50. W. E. Steiner, B. H. Clowers, P. E. Haigh and Jr. H. H. Hill, Secondary Ionization of Chemical Warfare Agent Simulants: Atmospheric Pressure Ion Mobility Time-of-Flight Mass Spectrometry, *Analytical Chemistry* **75**, pp. 6068-6076 (2003).
51. A. B. Kanu, P. E. Haigh and Jr. H. H. Hill, Surface Detection of Chemical Warfare Agent Simulants and Degradation Products, *Analytica Chimica Acta* **553**, pp. 148-159 (2005).

52. M. L. Ochoa and P. B. Harrington, Chemometric Studies for the Characterization and Differentiation of Microorganisms Using in situ Derivatization and Thermal Desorption Ion Mobility Spectrometry, *Analytical Chemistry* **77**, pp. 854-863 (2005).
53. C. B. Shumate and Jr. H. H. Hill, Coronaspray Nebulization and Ionization of Liquid Samples for Ion Mobility Spectrometry, *Analytical Chemistry* **61**, pp. 601-606 (1989).
54. D. Wittmer, B. K. Luckenbill, H. H. Hill and Y. H. Chen, Electrospray-Ionization Ion Mobility Spectrometry, *Analytical Chemistry* **66**, pp. 2348-2355 (1994).
55. R. R. Hudgins, J. Woenckhaus and M. F. Jarrold, High Resolution Ion Mobility Measurements for Gas Phase Proteins: Correlation between Solution Phase and Gas Phase Conformations, *International Journal of Mass Spectrometry* **165**, pp. 497-507 (1997).
56. S. C. Henderson, S. J. Valentine, A. E. Counterman and D. E. Clemmer, ESI/Ion Trap/Ion Mobility/Time-of-Flight Mass Spectrometry for Rapid and Sensitive Analysis of Biomolecular Mixtures, *Analytical Chemistry* **71**, pp. 291-301 (1999).
57. T. Wyttenbach, P. R. Kemper and M. T. Bowers, Design of a New Electrospray Ion Mobility Mass Spectrometer, *International Journal of Mass Spectrometry* **212**, pp. 13-23 (2001).
58. A. A. Shvartsburg, F. M. Li, K. Q. Tang and R. D. Smith, Characterizing the Structures and Folding of Free Proteins Using 2-D Gas-Phase Separations: Observation of Multiple Unfolded Conformers, *Analytical Chemistry* **78**, pp. 3304-3315 (2006).
59. J. A. Taraszka, R. Kurulugama, R. A. Sowell, S. J. Valentine, S. L. Koenigler, R. J. Arnold, D. F. Miller, T. C. Kaufman and D. E. Clemmer, Mapping the Proteome of Drosophila Melanogaster: Analysis of Embryos and Adult Heads by LC-IMS-MS Methods , *Journal of Proteome Research* **4**, pp. 1223-1237 (2005).
60. B. T. Ruotolo and D. H. Russell, Gas-Phase Conformations of Proteolytically Derived Protein Fragments: Influence of Solvent on Peptide Conformation, *Journal of Physical Chemistry B* **108**, pp. 15321-15331 (2004).
61. D. S. Lee, C. Wu and H. H. Hill, Detection of Carbohydrates by Electrospray Ionization Ion Mobility Spectrometry following Microbore High-Performance Liquid Chromatography, *Journal of Chromatography A* **822**, pp. 1-9 (1998).
62. B. H. Clowers, B. Bendiak, P. Dwivedi, W. E. Steiner and Jr. H. H. Hill, Separation of Sodiated Isobaric Disaccharides Using Electrospray Ionization-Atmospheric Pressure Ion Mobility-Time of Flight Mass Spectrometry, *Journal of the American Society for Mass Spectrometry* **16** , pp. 660-669 (2005).

63. B. H. Clowers and H. H. Hill, Mass analysis of Mobility-Selected Ion Populations using Dual Gate, Ion Mobility, Quadrupole Ion Trap Mass Spectrometry, *Analytical Chemistry* **77**, pp. 5877-5885 (2005).
64. P. Wu, P. Dwivedi, S. J. Klopsch, G. J. Puzon, L. Xun and Jr. H. H. Hill, Metabolic Profiling by Ion Mobility Mass Spectrometry (IMMS), **Manuscript in Preparation**, (2006).
65. M. Tabrizchi, T. Khayamian and N. Taj, Design and Optimization of a Corona Discharge Ionization Source for Ion Mobility Spectrometry, *Review of Scientific Instruments* **71**, pp. 2321-2328 (2000).
66. A. J. Marr, S. N. Cairns, D. M. Groves and M. L. Lanford, Development and Preliminary Evaluation of a Radio-Frequency Discharge Ionization Source for Use in Ion Mobility Spectrometry, *International Journal for Ion Mobility Spectrometry* **4**, pp. 126-128 (2001).
67. C. A. Hill and C. L. P. Thomas, A Pulsed Corona Discharge Switchable High Resolution Ion Mobility Spectrometer-Mass Spectrometer, *Analyst* **128**, pp. 55-60 (2003).
68. P. Dwivedi, W. C. Blanchard and Jr. H. H. Hill, Evaluation of Novel Distributed Plasma Ionization Source (DPIS) for Detection of Drugs and Environmental Pollutants Using Ion Mobility-Quadrupole Mass Spectrometry, *Manuscript in Preparation* (2006).
69. R. G. Ewing, M. Waltman, K. Cotter, R. Lee, and W. C. Blanchard. A Comparison of the Negative Ion Molecule Reactions Occurring in Air for Both Corona Discharge and Ni-63 Ionization Sources with Relevance to Explosives Detection. 14th International Symposium on Ion Mobility Spectrometry. 2005.
70. W. C. Blanchard , M. J. Crawford, and R. G. Ewing. A New Distributed Plasma Ion Source. Pittsburg Conference. 2005.
71. W. E. Steiner, B. H. Clowers, W. A. English and Jr. H. H. Hill, Atmospheric Pressure Matrix-Assisted Laser Desorption/Ionization with Analysis by Ion Mobility Time-of-Flight Mass Spectrometry, *Rapid Communications in Mass Spectrometry* **18**, (2004).
72. A. S. Woods, J. M. Koomen, B. T. Ruotolo, K. J. Gillig, D. H. Russell, K. Fuhrer, M. Gonin, T. F. Egan and J. A. Schultz, A Study of Peptide-Peptide Using MALDI-Ion Mobility o-TOF and ESI Mass-Spectrometry, *Journal of the American Society for Mass Spectrometry* **13**, pp. 166-169 (2002).
73. J. M. Koomen, B. T. Ruotolo, K. J. Gillig, J. A. Mclean, D. H. Russell, M. J. Kang, K. R. Dunbar, K. Fuhrer, M. Gonin and J. A. Schultz, Oligonucleotide Analysis with MALDI-Ion Mobility-TOFMS, *Anal. Bioanal. Chem.* **373**, pp. 612-617 (2002).
74. K. J. Gillig, B. Ruotolo, E. G. Stone, D. H. Russell, K. Fuhrer, M. Gonin and A.

- J. Schultz, Coupling High-Pressure MALDI with Ion Mobility/Orthogonal Time-of-Flight Mass Spectrometry, *Analytical Chemistry* **72**, pp. 3965-3971 (2000).
75. J. Gidden, M. T. Bowers, A. T. Jackson and J. H. Scrivens, Gas-Phase Conformations of Cationized Poly(styrene) Oligomers, *Journal of the American Society for Mass Spectrometry* **13**, pp. 499-505 (2002).
 76. S. Lee, T. Wyttenbach and M. T. Bowers, Gas-Phase Structures of Sodiated Oligosaccharides by Ion Mobility Ion Chromatography Methods, *International Journal of Mass Spectrometry* **167**, pp. 605-614 (1997).
 77. Y. Lu, F. Zhou, W. Shui, L. Bian, Y. Guo and P. Yang, Pulsed Electrospray for Mass Spectrometry, *Analytical Chemistry* **73**, pp. 4748-4753 (2001).
 78. L. Y. Yeo, D. Lastochkin, S. C. Wang and H. C. Chang, A New AC Electrospray Mechanism by Maxwell-Wagner Polarization and Capillary Resonance, *Physical Review Letters* **92**, pp. 133902-1-133902-4 (2004).
 79. B. F. Chao, C. J. Chen, F. A. Li and G. R. Her, Sheathless Capillary Electrophoresis-Mass Spectrometry Using a Pulsed Electrospray Ionization Source, *Electrophoresis* **27**, pp. 2083-2090 (2006).
 80. J. Wei, W. Shui, F. Zhou, Y. Lu, K. Chen, G. Xu and P. Yang, Naturally and Externally Pulsed Electrospray, *Mass Spectrometry Reviews* **21**, pp. 148-162 (2002).
 81. B. H. Clowers, Separation of Gas Phase Isomers Using Ion Mobility and Mass Spectrometry, Washington State University, Pullman WA (2005).
 82. D. R. Lide, *CRC Handbook of Chemistry and Physics* (85th Edn). CRC Press, Boca Raton, FL (2004).
 83. D. R. Baker, *Capillary Electrophoresis*. John Wiley & Sons, Inc., New York, NY (1995).
 84. M. A. Baim and Jr. H. H. Hill, Tunable Selective Detection for Capillary Gas Chromatography by Ion Mobility Spectrometry, *Analytical Chemistry* **54**, pp. 38-43 (1982).
 85. P. W. Atkins, *Physical Chemistry* (5th Edn). W. H. Freeman and Company, USA (1994).
 86. C. J. T. von Grothuss, Sur la Décomposition de l'eau et des Corps qu'elle Tient en Dissolution à l'aide de L'électricité Galvanique, *Ann. Chim.* **LVIII**, pp. 54-74 (1806).
 87. M. Eigen and L. de Maeyer, Self-Dissociation and Protonic Charge Transport in Water and Ice, *Proceedings of the Royal Society of London. Series A* **247**, pp. 505-533 (1958).

88. Y. Wu and G. A. Voth, A Computer Simulation Study of the Hydrated Proton in a Synthetic Proton Channel, *Biophysical Journal* **85**, pp. 864-875 (2003).
89. U. W. Schmitt and G. A. Voth, The Computer Simulation of Proton Transfer in Water, *Journal of Chemical Physics* **111**, pp. 9361-9381 (1999).
90. D. E. Raymond, A. Manz and H. M. Widmer, Continuous Separation of High Molecular Weight Compounds Using a Microliter Volume Free-Flow Electrophoresis Microstructure, *Analytical Chemistry* **68**, pp. 2515-2522 (1996).
91. I. D. MacLeod, D. M. Muir, A. J. Parker and P. Singh, Solvation of Ions. Some Applications. II. Electrolysis of Copper (I) Sulphate in Water-Nitrile Mixtures, *Australian Journal of Chemistry* **30**, pp. 1423-1437 (1977).
92. R. A. Robinson and R. H. Stokes, *Electrolyte Solutions* (Second Edn). Butterworths Publications Limited, London, England (1965).

Table 1: Experimental, literature, and expected mobility values of the aqueous analytes

Aqueous Sample	Mobility Values (10^{-3} cm ² /V·s)		
	Experimental (in Hexane)	Literature (in Water)	Expected (in Hexane)
Solvent Blank (Methanol-water)	5.4	3.623 (H ⁺) [84]	9.9
	3.8		
Tetramethylammonium	3.6	0.466 [91]	1.27
Tetrabutylammonium	3.1	0.202 [91]	0.551
Bradykinin	2.3	0.139 (FITC-labeled) [89]	0.379

Figure Captions

Figure 1: Schematic of liquid phase ion mobility spectrometer (LPIMS) with pulsed electrodispersion ionization (EDI). The components included a pulsed electrodispersion ionization source, a resistive glass ion mobility spectrometer, and a Faraday plate, all of which were rested inside a Pyrex dish filled with the liquid medium.

Figure 2: Pulsed electrodispersion ionization – liquid phase ion mobility spectra of the solvent blank (methanol-water, 90:10 vol/vol) for (a) the first 8.5 minutes (51 averages), (b) the final 2.5 minutes (15 averages), and (c) the entire 30 minutes (179 averages).

Figure 3: Pulsed electrodispersion ionization – liquid phase ion mobility spectra of the solvent blank (methanol-water, 90:10 vol/vol) was obtained over 30 minutes (179 spectra) in the positive mode. The 3D plot showed that there were two populations of ions, the first group of ions with higher current intensity (A) and the second group of ions with lower current intensity (B).

Figure 4a: Pulsed electrodispersion ionization – liquid phase ion mobility spectrum of 100 μM tetramethylammonium bromide in the positive mode.

Figure 4b: Pulsed electrodispersion ionization – liquid phase ion mobility spectrum of 100 μM tetrabutylammonium bromide.

Figure 4c: Pulsed electrodispersion ionization – liquid phase ion mobility spectrum of 100 μ M bradykinin in the positive mode.

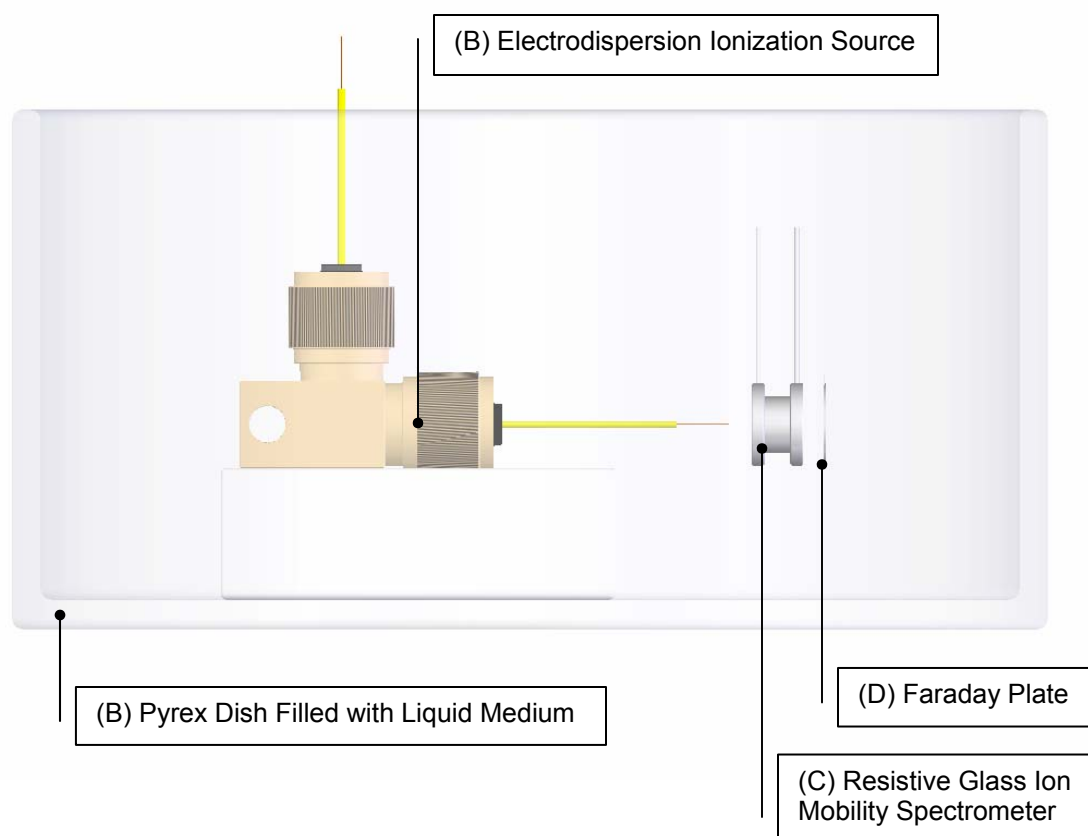


Figure 1: Schematic of liquid phase ion mobility spectrometer (LPIMS) with pulsed electrodispersion ionization (EDI). The components included a pulsed electrodispersion ionization source, a resistive glass ion mobility spectrometer, and a Faraday plate, all of which were rested inside a Pyrex dish filled with the liquid medium.

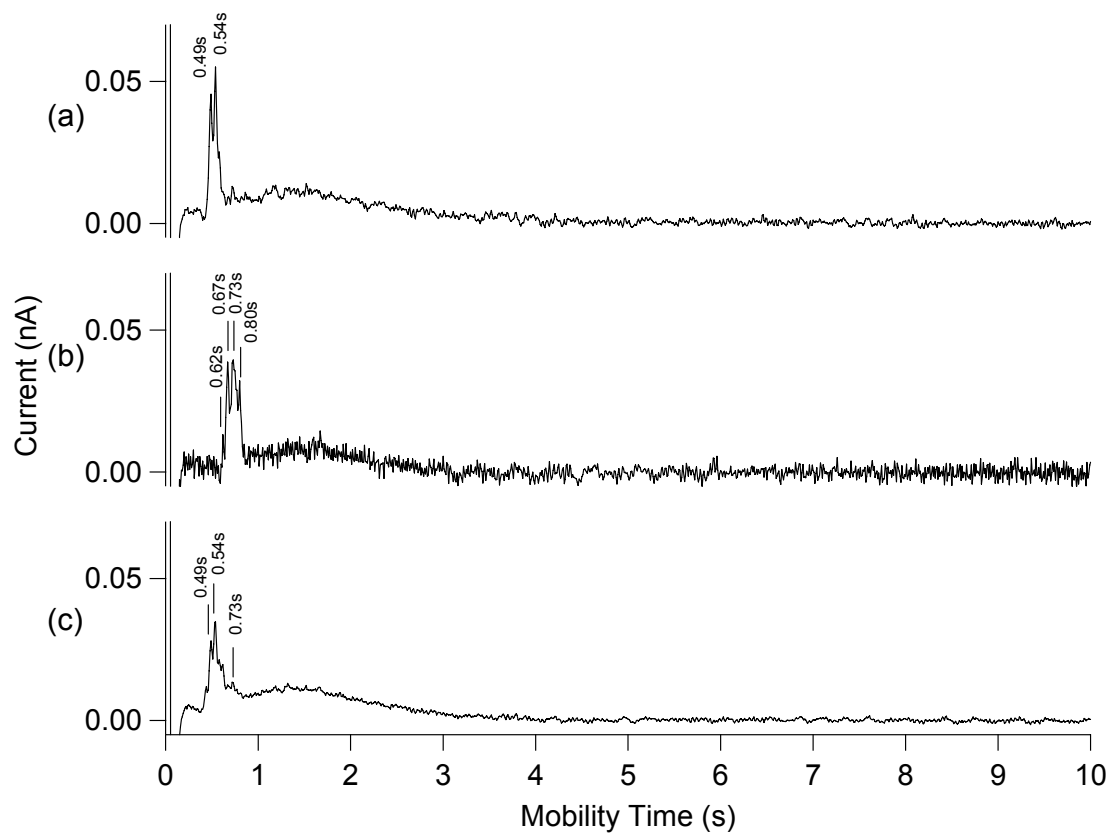


Figure 2: Pulsed electrodispersion ionization – liquid phase ion mobility spectra of the solvent blank (methanol-water, 90:10 vol/vol) for (a) the first 8.5 minutes (51 averages), (b) the final 2.5 minutes (15 averages), and (c) the entire 30 minutes (179 averages).

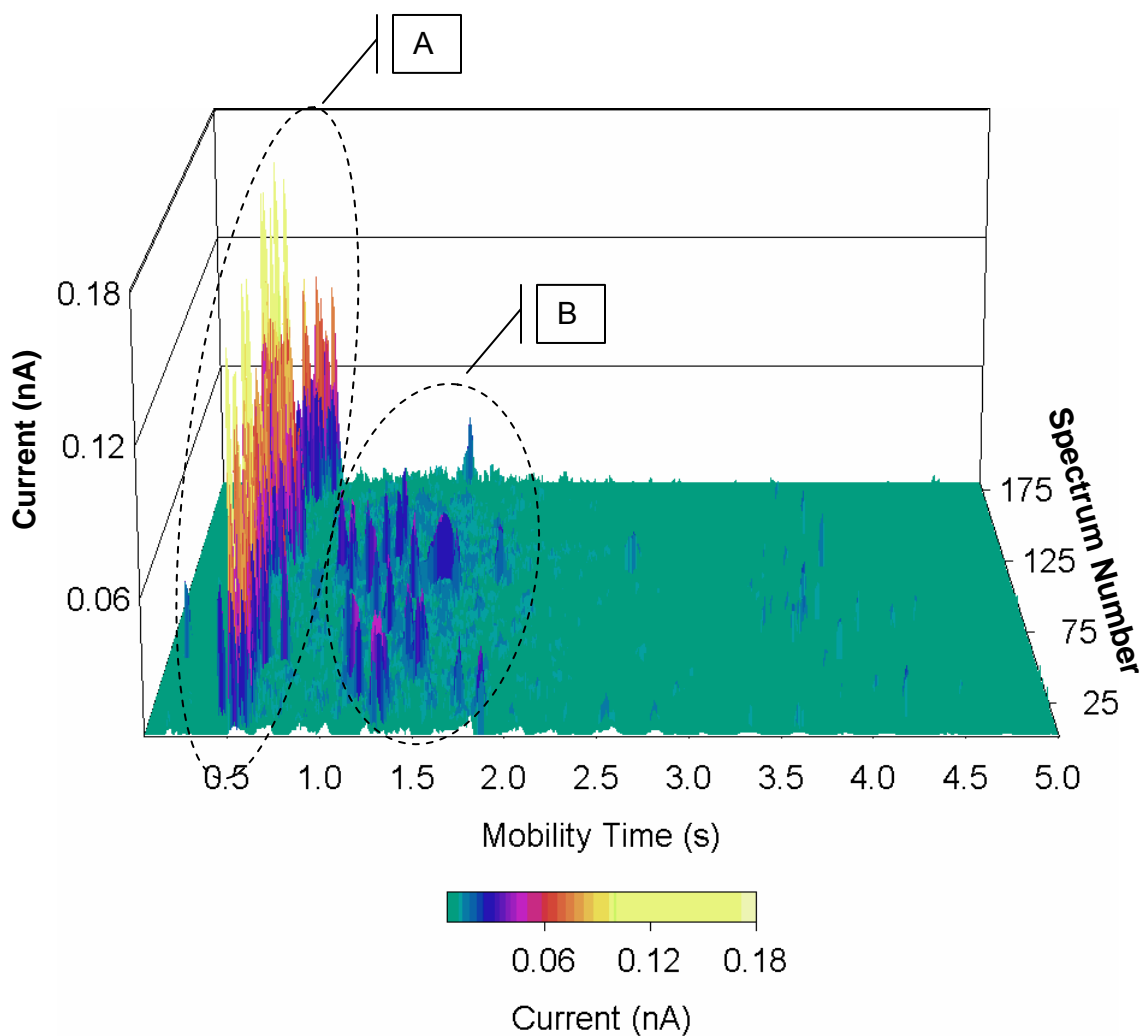


Figure 3: Pulsed electrodispersion ionization – liquid phase ion mobility spectra of the solvent blank (methanol-water, 90:10 vol/vol) was obtained over 30 minutes (179 spectra) in the positive mode. The 3D plot showed that there were two populations of ions, the first group of ions with higher current intensity (A) and the second group of ions with lower current intensity (B).

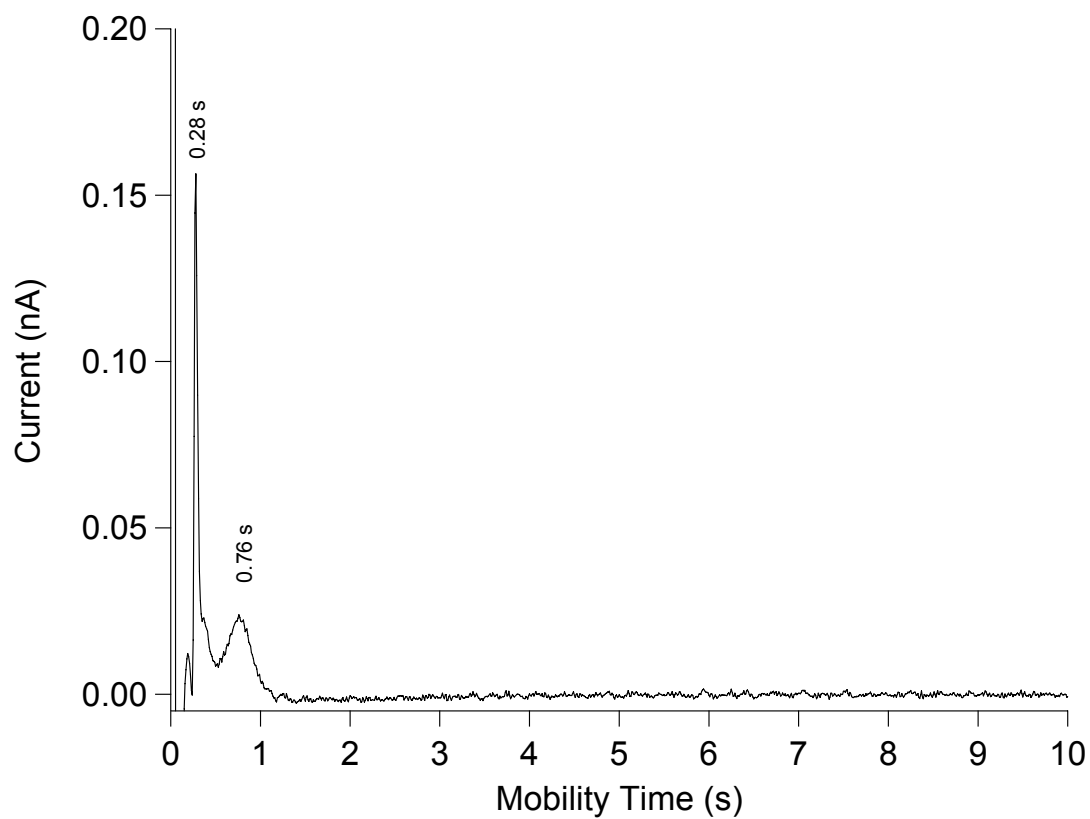


Figure 4a: Pulsed electrodispersion ionization – liquid phase ion mobility spectrum of 100 μM tetramethylammonium bromide in the positive mode.

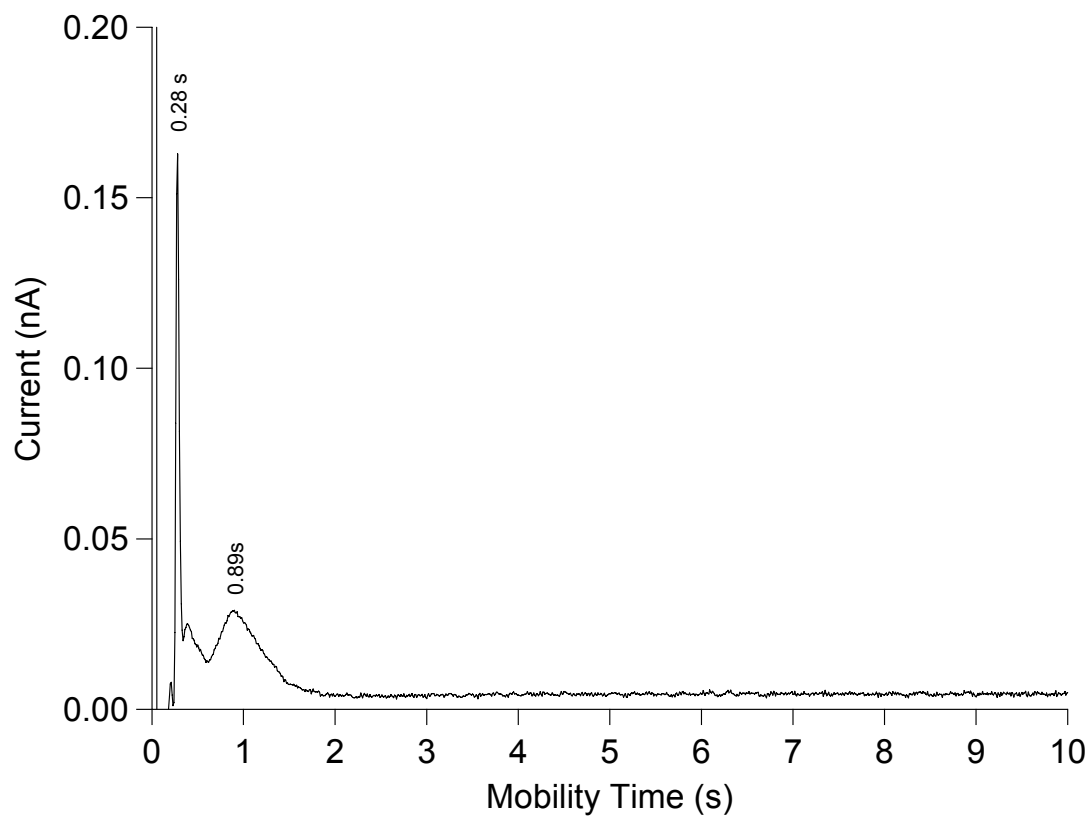


Figure 4b: Pulsed electrodispersion ionization – liquid phase ion mobility spectrum of 100 μM tetrabutylammonium bromide.

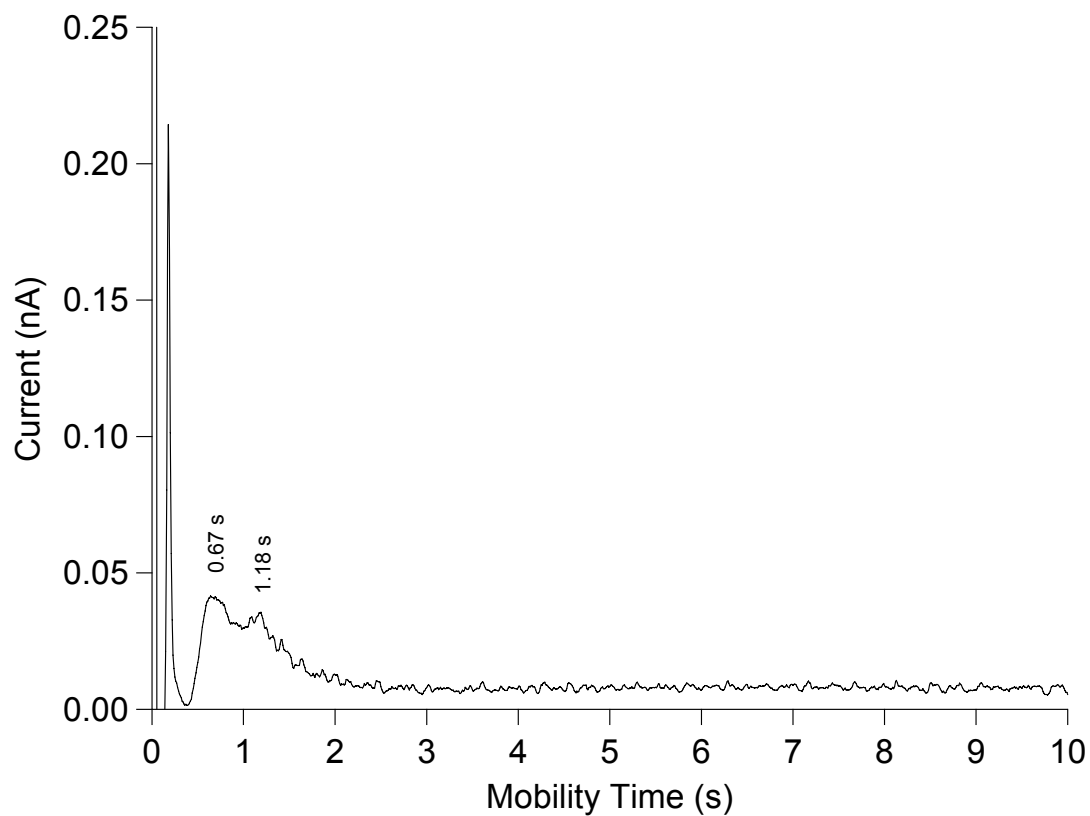


Figure 4c: Pulsed electrodispersion ionization – liquid phase ion mobility spectrum of 100 μ M bradykinin in the positive mode.

Chapter Six

Conclusions

Portable devices based on gas phase ion mobility spectrometry are widely employed by first responders for the rapid detection of explosives and warfare agents because of its simple instrumentation, low maintenance, and milliseconds-fast analysis time. However, improving separation efficiency has been especially challenging in miniaturized IMS. The maximum attainable resolving power is proportional to the square root of the IMS drift length. Therefore, separation power of IMS suffers at the expense of miniaturization. With the concept of the maximum resolving power also being proportional to the square root of the operational pressure, this project introduced a novel analytical method, called liquid phase ion mobility spectrometry.

i) Electrodispersion ionization was developed as a suitable ionization source for liquid phase ion mobility spectrometry.

Prior to the development of liquid phase ion mobility spectrometry (LPIMS), it was critical to identify a suitable ionization source. Without an appropriate ion source, LPIMS, whose separation and detection required the conversion of the analytes into charged particles, could not be demonstrated. The potential ionization source should have the capability to ionize aqueous solution of analytes in a non-electrolyte containing liquid medium. Since the measurement of discharge current by Faraday plate was the intended detection method, the ionization source should selectively ionize the aqueous analyte, and not the liquid medium. Additionally, it would be ideal for the ionization source to be non-radioactive. The inclusion of radioactive material and generation of radioactive waste would hinder the implementation of LPIMS as a portable and rapid personal diagnostic tool.

A new ionization source, called electrodispersion ionization, was developed to address these criteria. EDI produced ions from aqueous phase analytes in non-electrolyte containing liquids. EDI was effective in delivering pre-existent positive and negative ions from aqueous sample solution and dispersing them into the organic liquid medium. Its ionization efficiency was dependent upon the sample flow rate. Visualization of the electrodispersed droplets was demonstrated with aqueous solutions of two dyes, basic fuchsin and bromothymol blue. Continuous and stable current from EDI was measured for inorganic and organic ions by Faraday plate. Quantitative ionization of the method was investigated for several amino acids with detection limits measured in the low ppm range.

Under certain operation conditions, combinations of applied voltage and sample flow rate can lead to pulsing of the ion current for the EDI source. Control of this pulsing phenomenon may lead to the elimination of the need for an ion gate in such applications as liquid phase ion mobility spectrometry. EDI may be especially useful in combination with liquid phase ion mobility spectrometry and other liquid phase separation methods for ions. In addition, EDI may be useful for the creation of ions or the dispersion of reactants into non-aqueous phases for chemical syntheses.

ii) Ion transport in liquid phase ion mobility spectrometry was demonstrated.

Efficiency of Bradbury-Nielsen shutter and Tyndall shutter were investigated in the liquid phase.

Ions produced from EDI were moved along by an electric field along the LPIMS in a liquid medium. Liquid phase ion mobility spectrometry with electrodispersion ionization was demonstrated for the first time. The LPIMS spectra of ammonium nitrate and sodium chloride were inadequately resolved possibly due to the extension of analyte solvation and the inefficiency of the ion shutters.

The efficiency of two types of ion shutters, Tyndall and Bradbury-Nielsen shutters, for LPIMS was investigated. The total ion current leaking pass the ion shutters decreased with increasing orthogonal field of Bradbury-Nielsen shutter and with increasing reverse field of Tyndall gate. 95% of the total ion could be stopped with an orthogonal field 32 times greater and a reverse field 8.5 times greater than the electric field of the LPIMS for the Bradbury-Nielsen shutter and Tyndall shutter, respectively.

iii) Integrated system of liquid phase ion mobility spectrometry were designed, constructed, and evaluated.

Directing the research towards the ultimate goal of using LPIMS as a personal diagnostic tool, attempts were made to integrate the components of LPIMS into an inexpensive and disposable composite device which could be mass produced cost effectively. New instrument designs and alternative fabrication processes were explored: low temperature co-fired ceramics (LTCC) and poly(dimethylsiloxane) (PDMS) fabricated with Micro-Electro-Mechanical Systems technology. 90 sheets of LTCC sheet, with embedded conducting electrodes and resistors, were fused into a single LTCC-LPIMS device. The electrical connections for LTCC-LPIMS were limited to only five inputs and outputs. The instrumental parts and fabrication process time of LPIMS were further reduced with the incorporation of the EDI source into the PDMS-LPIMS. Identical PDMS-LPIMS microchannels could be replicated with ease after a master, which carried a positive relief of the LPIMS microchannel pattern, was patterned. Ion transport efficiency was a major issue for both LTCC-LPIMS and PDMS-LPIMS that needed to be solve.

iv) Liquid phase ion mobility spectrometry with pulsed electrodispersion ionization was demonstrated.

As with other time-of-flight analyzer, it was anticipated that LPIMS would interface well with a pulsed ionization source. The use of a pulsed ionization eliminated the need for an ion shutter in LPIMS and thus simplifying the fabrication process. A pulsed ionization source also required smaller sample volumes.

Previous experiments showed that pulsing of the ion current for the EDI source was controlled by combinations of applied voltage and sample flow rate. Pulsed EDI was achieved by alternating the voltage applied to the ionization source, between a voltage sufficient to induce electrodispersion and a lower voltage. Pulsed EDI-LPIMS of methanol-water solvent blank in hexane showed that the amount of solvation for the solvent ions increased with experimental duration. This suggested the necessity of a counter flowing liquid medium for the removal of uncharged molecule in the LPIMS. Mobility values of tetramethylammonium, tetrabutylammonium, and bradykinin, obtained from pulsed EDI-LPIMS spectra, were three to five times faster than those predicted for singly charged analyte in hexane. It was speculated that the absence of ion-dipole interaction between the ions and the non-polar hexane displaced the solvation sphere that would otherwise exist in aqueous solution.

APPENDIX

Appendix I

Additional Data from Parametric Studies of Electrodispersion Ionization

Figure Captions

Figure 1: Schematic of the electrodispersion ionization apparatus.

Figure 2: Plot of total ion current versus electrodispersion ionization voltage for sample of methanol-water and 100 μM ammonium chloride at a flow rate of 0.1 $\mu\text{L}/\text{min}$ in benzene and decane, in the positive mode. The total ion current increased with EDI voltage. The onset voltage of EDI was 300V, 250V, 400V, and 450V, for methanol-water in benzene, ammonium chloride in benzene, methanol-water in decane, and ammonium chloride in decane, respectively.

Figure 3: Effect of sample flow rate on electrodispersion ionization efficiency for a sample of methanol-water (90:10) in benzene. The sample flow rate studied were 0.05 $\mu\text{L}/\text{min}$ (\square), 0.1 $\mu\text{L}/\text{min}$ (\times), 0.2 $\mu\text{L}/\text{min}$ (\triangle), and 0.5 $\mu\text{L}/\text{min}$ (\circ).

Figure 4: Effect of sample flow rate on electrodispersion ionization efficiency for a sample of methanol-water (90:10) and 100 μM ammonium chloride, in benzene and decane. The range of sample flow rates was from 0.02 $\mu\text{L}/\text{min}$ to 2.0 $\mu\text{L}/\text{min}$. The EDI voltage was +750V.

Figure 5: Effect of sample flow rate on electrodispersion ionization efficiency for a sample of methanol-water (90:10) and 100 μM ammonium chloride, in benzene and decane. The sample flow rate studied were from 0.02 $\mu\text{L}/\text{min}$ to 2.0 $\mu\text{L}/\text{min}$. The EDI voltage was -750V.

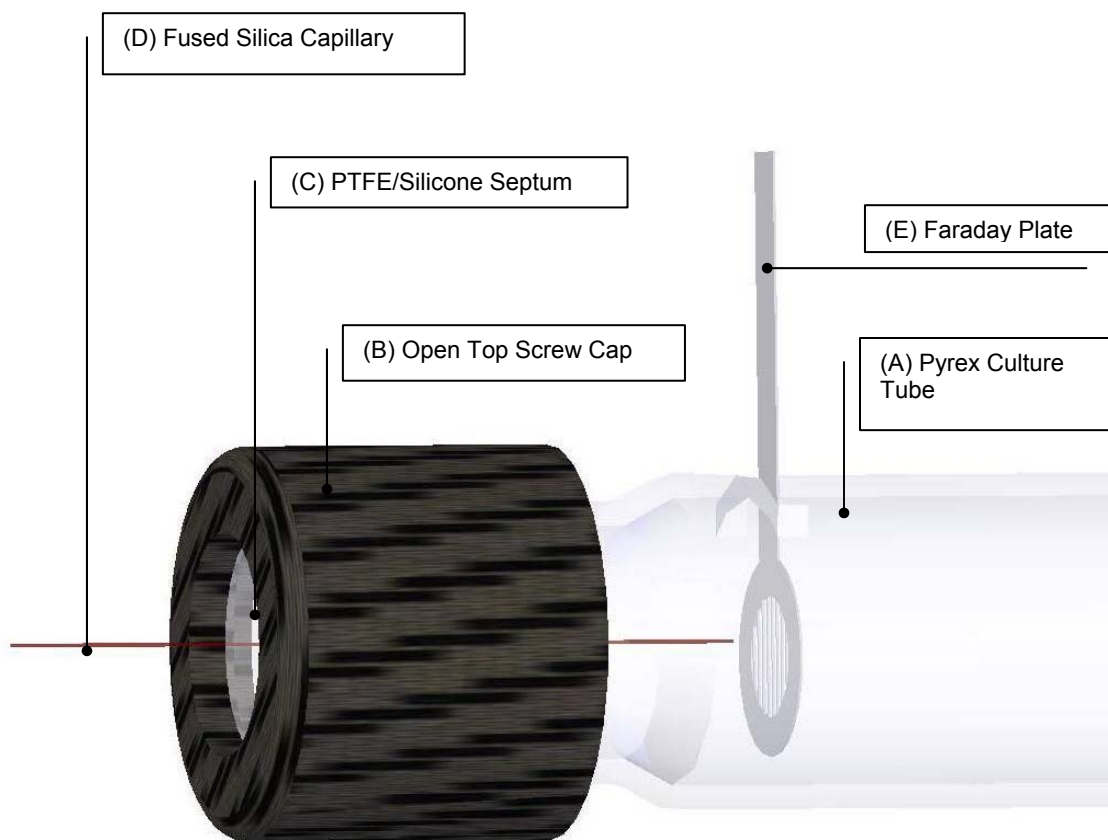


Figure 1: Schematic of the electrodispersion ionization apparatus.

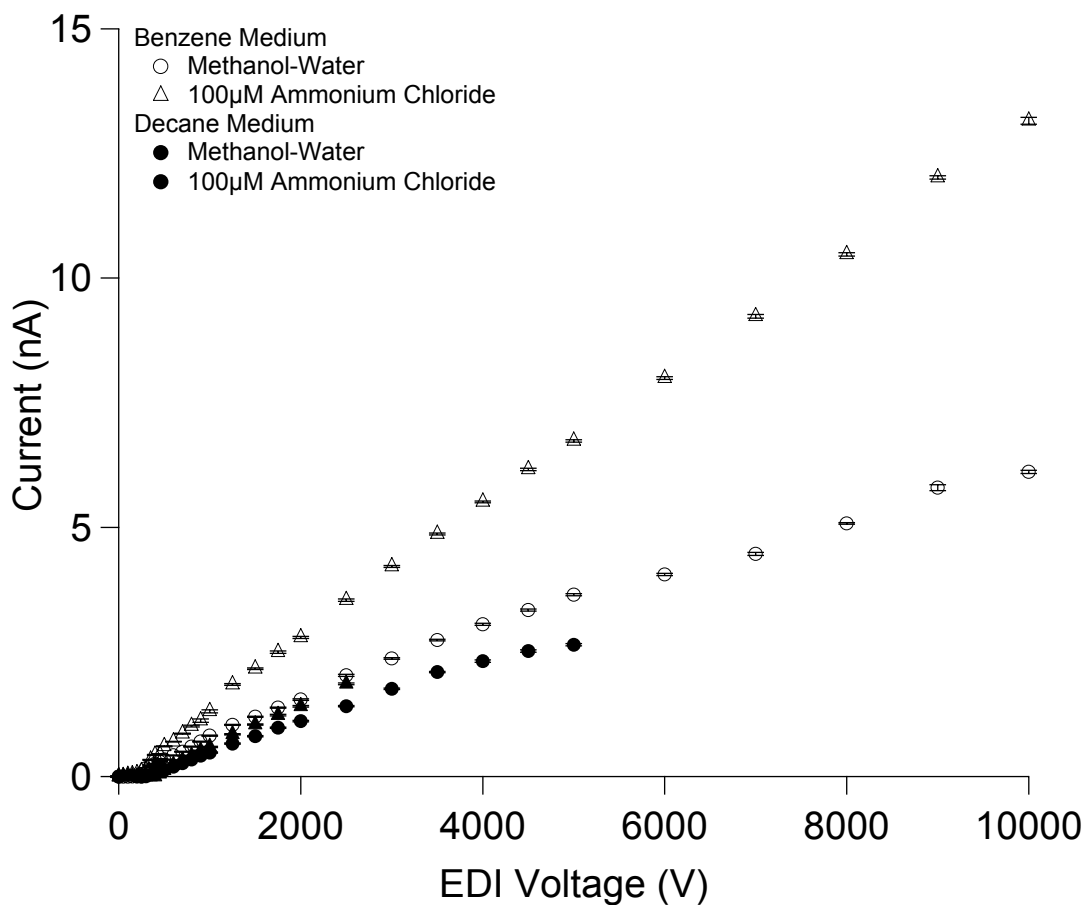


Figure 2: Plot of total ion current versus electrodispersion ionization voltage for sample of methanol-water and 100 μM ammonium chloride at a flow rate of 0.1 $\mu\text{L}/\text{min}$ in benzene and decane, in the positive mode. The total ion current increased with EDI voltage. The onset voltage of EDI was 300V, 250V, 400V, and 450V, for methanol-water in benzene, ammonium chloride in benzene, methanol-water in decane, and ammonium chloride in decane, respectively.

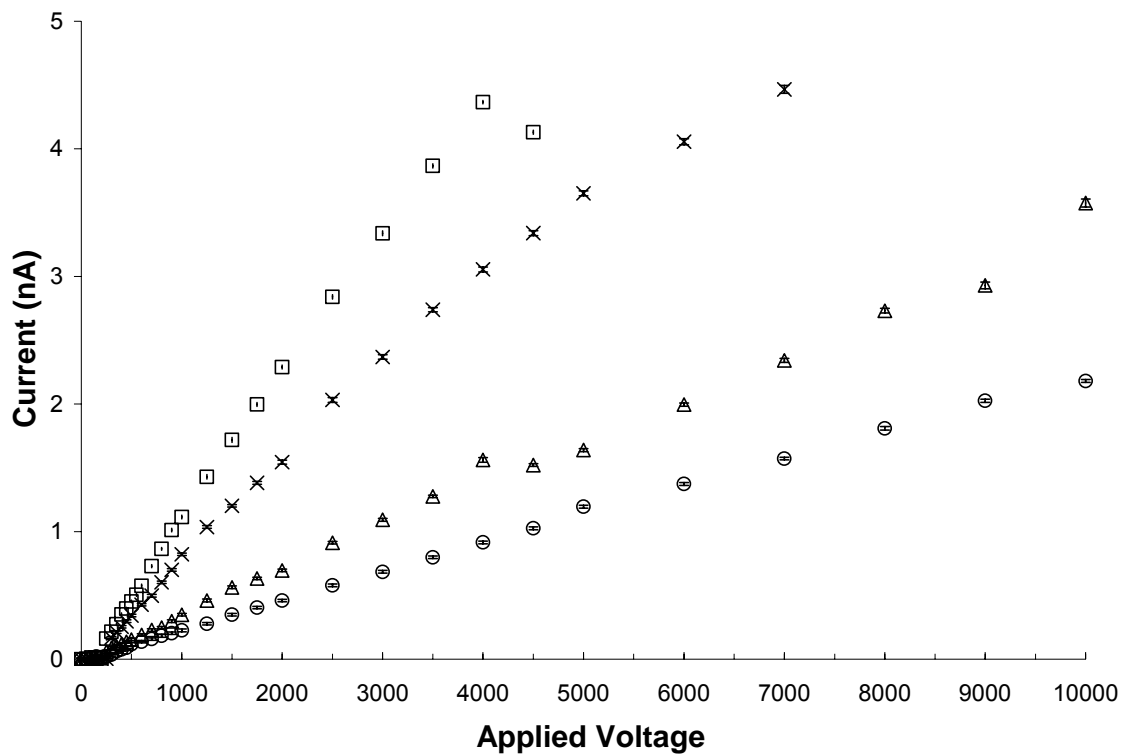


Figure 3: Effect of sample flow rate on electrodispersion ionization efficiency for a sample of methanol-water (90:10) in benzene. The sample flow rate studied were 0.05 $\mu\text{L}/\text{min}$ (\square), 0.1 $\mu\text{L}/\text{min}$ (\times), 0.2 $\mu\text{L}/\text{min}$ (\triangle), and 0.5 $\mu\text{L}/\text{min}$ (\circ).

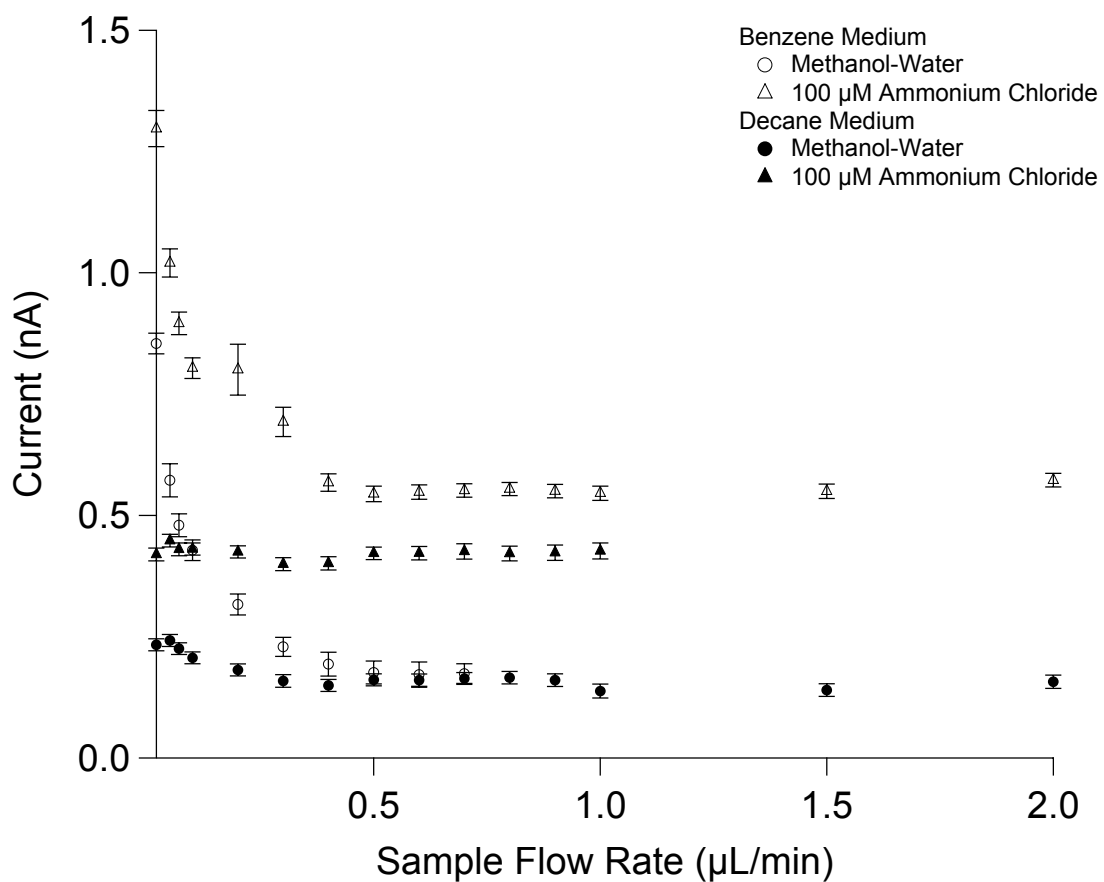


Figure 4: Effect of sample flow rate on electrodispersion ionization efficiency for a sample of methanol-water (90:10) and 100 µM ammonium chloride, in benzene and decane. The range of sample flow rates was from 0.02 µL/min to 2.0 µL/min. The EDI voltage was +750V.

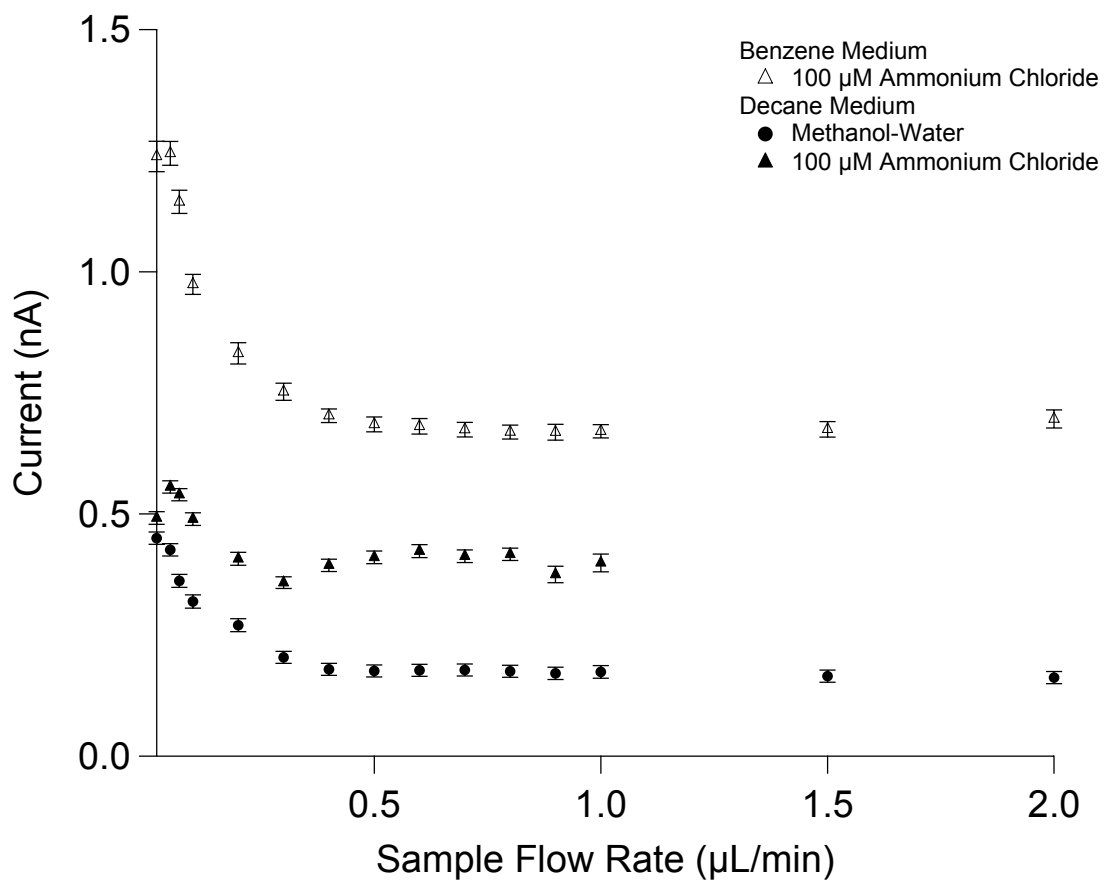


Figure 5: Effect of sample flow rate on electrodispersion ionization efficiency for a sample of methanol-water (90:10) and 100 µM ammonium chloride, in benzene and decane. The sample flow rate studied were from 0.02 µL/min to 2.0 µL/min. The EDI voltage was -750V.

Appendix II

Additional Graphic Representations of Liquid

Phase Ion Mobility Spectrometers

Figure Captions

Figure 1: Liquid phase ion mobility spectrometer (LPIMS), constructed from a Pyrex culture tube. The electric field was established by multiple stainless steel electrodes connected in series with resistors. The photograph also showed the sample inlet, liquid medium inlet and outlet, and the electrical connections.

Figure 2: Mobility tube of LPIMS, fabricated from low temperature co-fired ceramic (LTCC). The photograph showed that the diameter of the device was smaller than that of a quarter.

Figure 3: The complete prototype of low temperature co-fired ceramic-liquid phase ion mobility spectrometer (LTCC-LPIMS): photograph displaying the LPIMS mobility tube (A), the sealing Teflon end caps (B – D), the external electrical connections (E), the liquid medium entry (F), and the liquid medium exit (G). The three pieces of Teflon end caps were physically tightened with three screws and sealed with two pieces of o-rings and a membrane that fitted into the counter bore of the end caps.

Figure 4: Schematic of the LTCC-LPIMS prototype, showing (A) the internal electrical connections, and (B) the alignment holes and the external electrical connections: (1) aperture grid, where the spectrometer voltage was grounded via an external resistor, (2) ion shutter sense line, (3) ion shutter voltage input, (4) spectrometer voltage input, and (5) Faraday plate.

Figure 5: Photograph of the first generation of poly(dimethylsiloxane)-liquid phase ion mobility spectrometer (PDMS-LPIMS). The PDMS-LPIMS microchannel was 1000 μm wide, 400 μm deep, and 5 cm long. There were 24 sputtered gold electrodes. The sample inlet was a fused silica capillary inserted at the front end of the LPIMS-PDMS.

Figure 6: Photograph of the second generation of poly(dimethylsiloxane)-liquid phase ion mobility spectrometer (PDMS-LPIMS). The PDMS channel was 1000 μm wide, 400 μm deep and 5 cm long. There were 26 machine-sputtered gold electrodes. The sample inlet and the drift liquid inlet were polyethylene tubing, located at the front and back end of the PDMS channel. Electrical wires were connected to each of the 26 gold electrodes with conducting silver paste.

Figure 7: Three-dimensional schematic of the third generation of PDMS-LPIMS. The PDMS channel was 1000 μm wide, 400 μm deep and 1 cm long. The sample inlet was incorporated into the PDMS design.

Figure 8: Top-view schematic of the third generation of PDMS-LPIMS. The microchannel was 1000 μm wide, 400 μm deep and 1 cm long. There were 6 sputtered platinum electrodes. EDI voltage was applied at electrode 0. The sample nozzle was incorporated into the PDMS design near electrode 1. Electrode 6 was used as the Faraday plate.

Figure 9: Photograph of the fourth generation of PDMS-LPIMS prototype, showing the polyethylene capillaries, which carried in the liquid medium and sample, and the electrical connections. The bottom PDMS layer was bonded to a glass microscope slide for additional support.

Figure 10: Photograph of a resistive glass-LPIMS. A miniature Bradbury-Nielsen gate was inserted between two resistive glass tubes, one being used as the desolvation region and another for the drift region. The sample was introduced via a fused silica capillary and ionized by electrodispersion ionization. The instrument was held steady by a poly(dimethylsiloxane) cover, and immersed into a Pyrex beaker filled with the liquid medium.

Figure 11: Photograph of the miniaturized Bradbury-Nielsen gate, with a 4.56 mm i.d., 9.30 mm o.d., and a wire spacing of 0.64 mm.

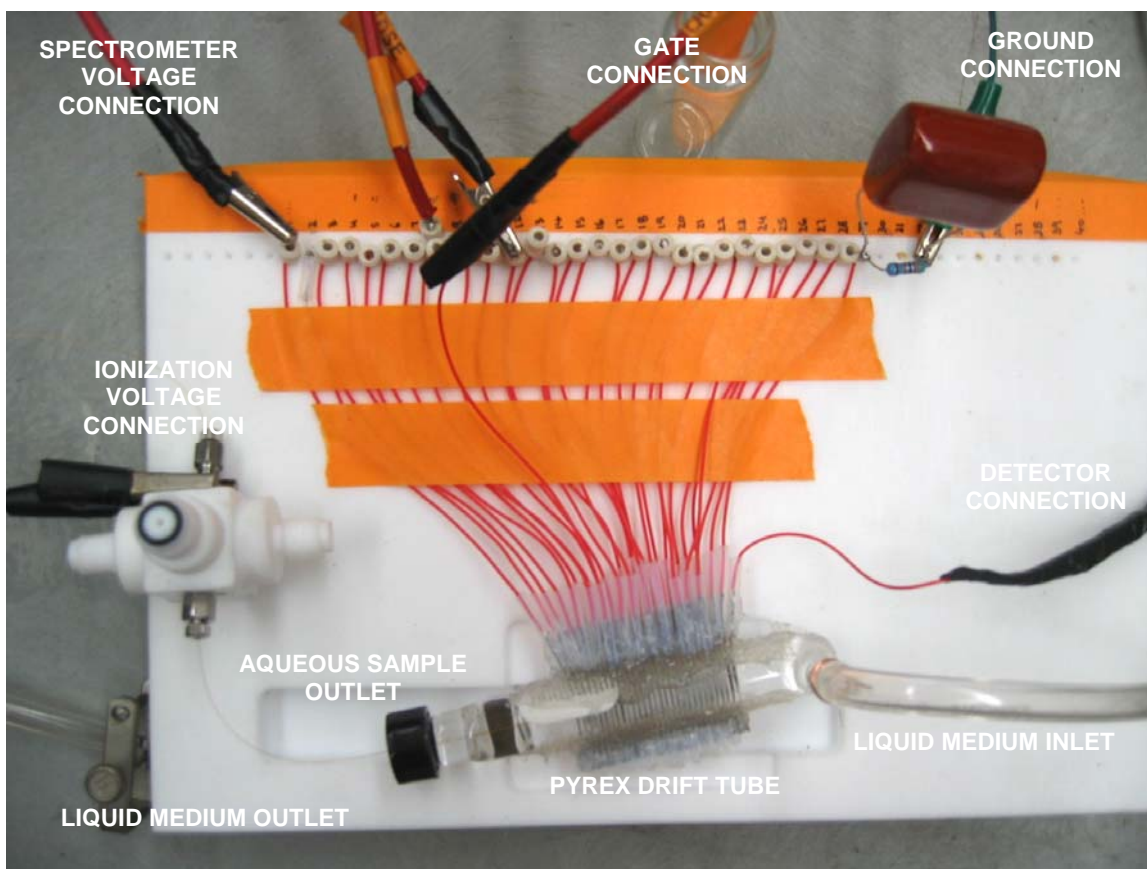


Figure 1: Liquid phase ion mobility spectrometer (LPIMS), constructed from a Pyrex culture tube. The electric field was established by multiple stainless steel electrodes connected in series with resistors. The photograph also showed the sample inlet, liquid medium inlet and outlet, and the electrical connections.



Figure 2: Mobility tube of LPIMS, fabricated from low temperature co-fired ceramic (LTCC). The photograph showed that the diameter of the device was smaller than that of a quarter.

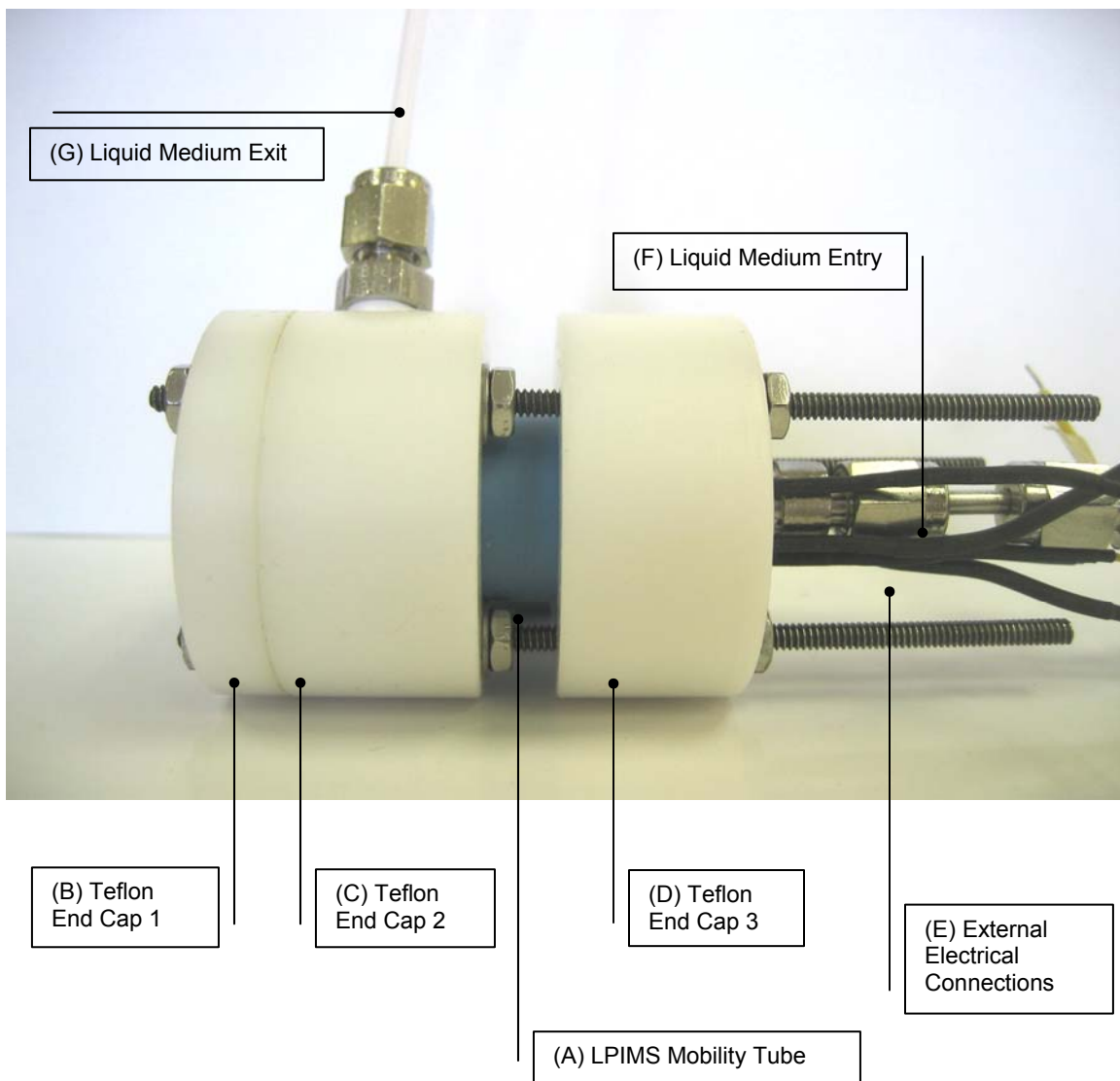


Figure 3: The complete prototype of low temperature co-fired ceramic-liquid phase ion mobility spectrometer (LTCC-LPIMS): photograph displaying the LPIMS mobility tube (A), the sealing Teflon end caps (B – D), the external electrical connections (E), the liquid medium entry (F), and the liquid medium exit (G). The three pieces of Teflon end caps were physically tightened with three screws and sealed with two pieces of o-rings and a membrane that fitted into the counter bore of the end caps.

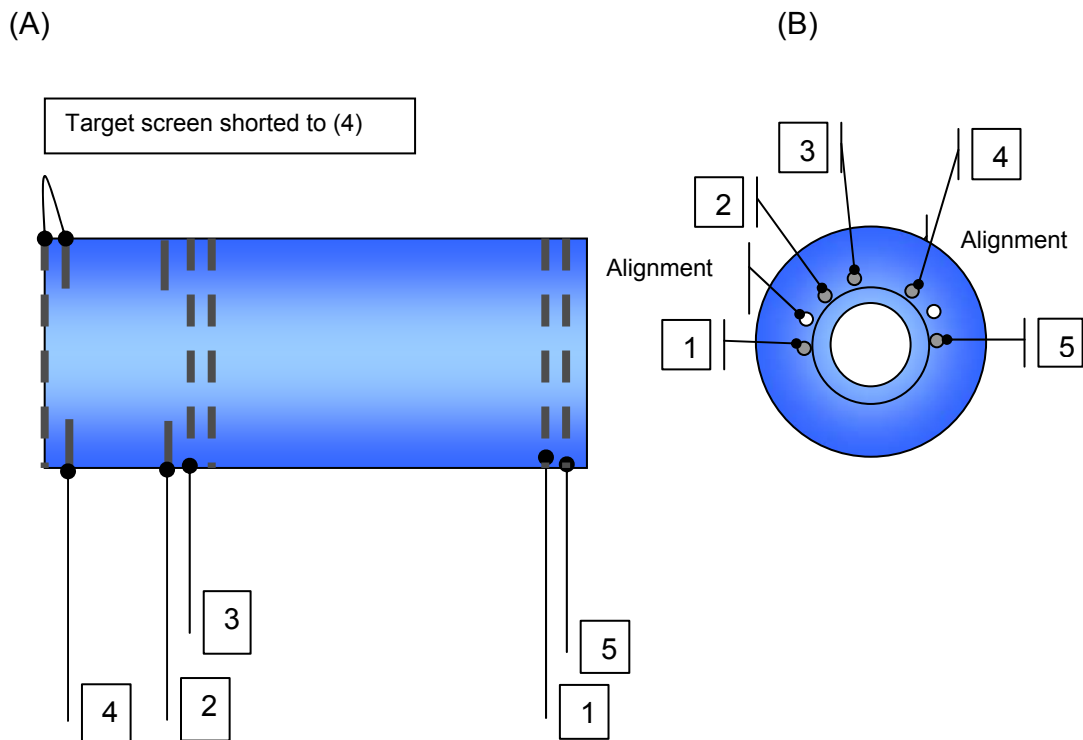


Figure 4: Schematic of the LTCC-LPIMS prototype, showing (A) the internal electrical connections, and (B) the alignment holes and the external electrical connections: (1) aperture grid, where the spectrometer voltage was grounded via an external resistor, (2) ion shutter sense line, (3) ion shutter voltage input, (4) spectrometer voltage input, and (5) Faraday plate.

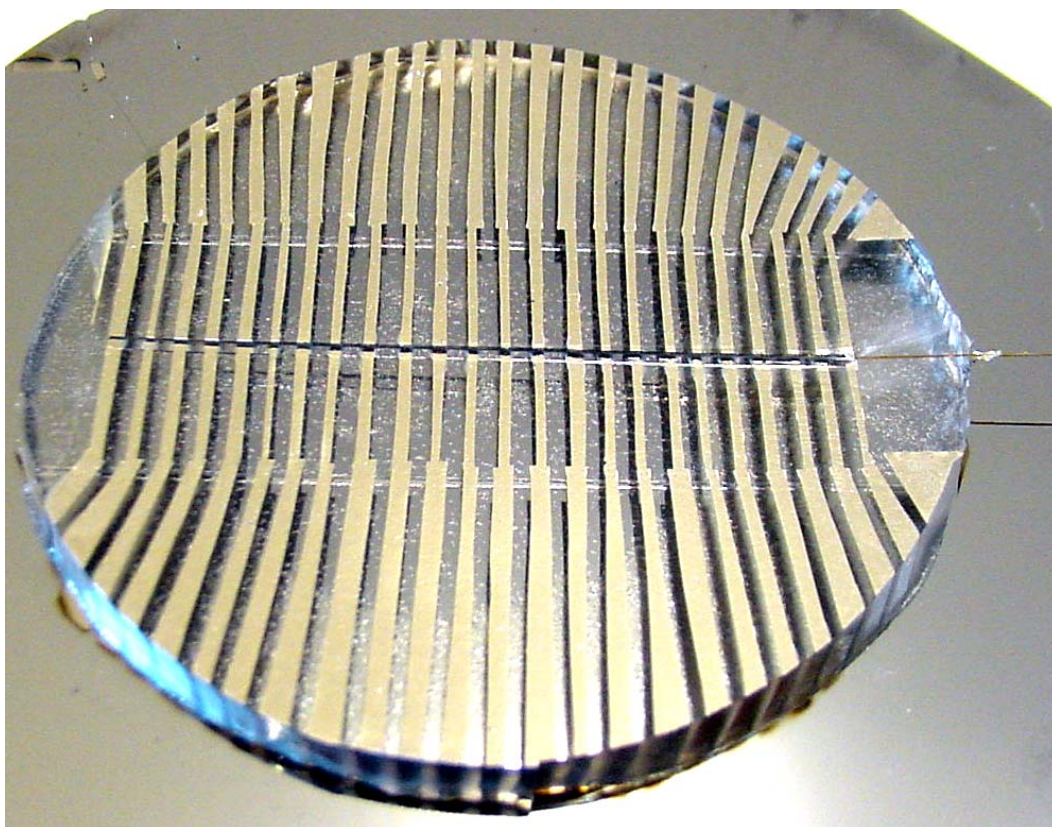


Figure 5: Photograph of the first generation of poly(dimethylsiloxane)-liquid phase ion mobility spectrometer (PDMS-LPIMS). The PDMS-LPIMS microchannel was 1000 μm wide, 400 μm deep, and 5 cm long. There were 24 sputtered gold electrodes. The sample inlet was a fused silica capillary inserted at the front end of the LPIMS-PDMS.

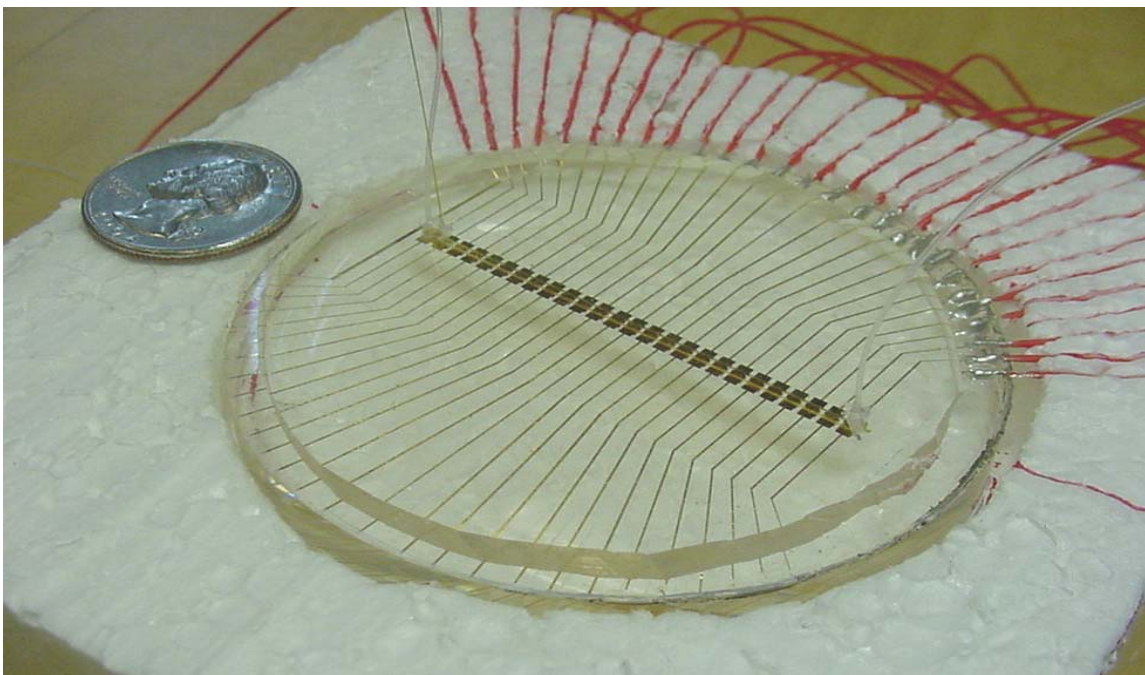


Figure 6: Photograph of the second generation of poly(dimethylsiloxane)-liquid phase ion mobility spectrometer (PDMS-LPIMS). The PDMS channel was 1000 μm wide, 400 μm deep and 5 cm long. There were 26 machine-sputtered gold electrodes. The sample inlet and the drift liquid inlet were polyethylene tubing, located at the front and back end of the PDMS channel. Electrical wires were connected to each of the 26 gold electrodes with conducting silver paste.

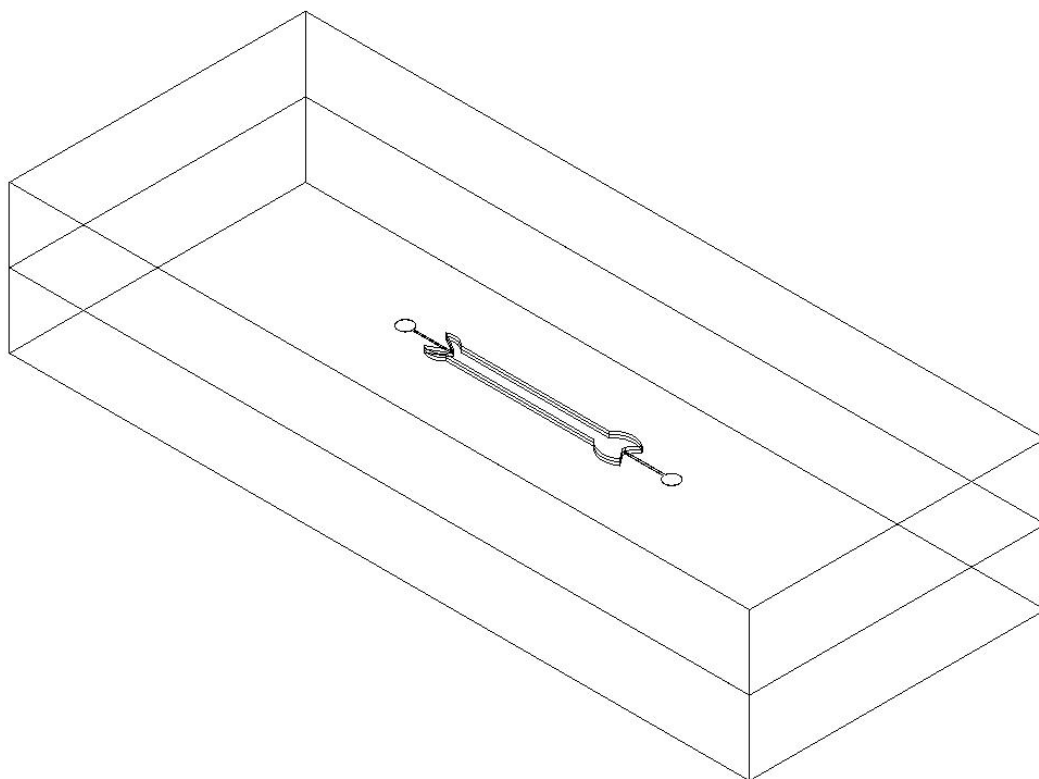


Figure 7: Three-dimensional schematic of the third generation of PDMS-LPIMS. The PDMS channel was 1000 μm wide, 400 μm deep and 1 cm long. The sample inlet was incorporated into the PDMS design.

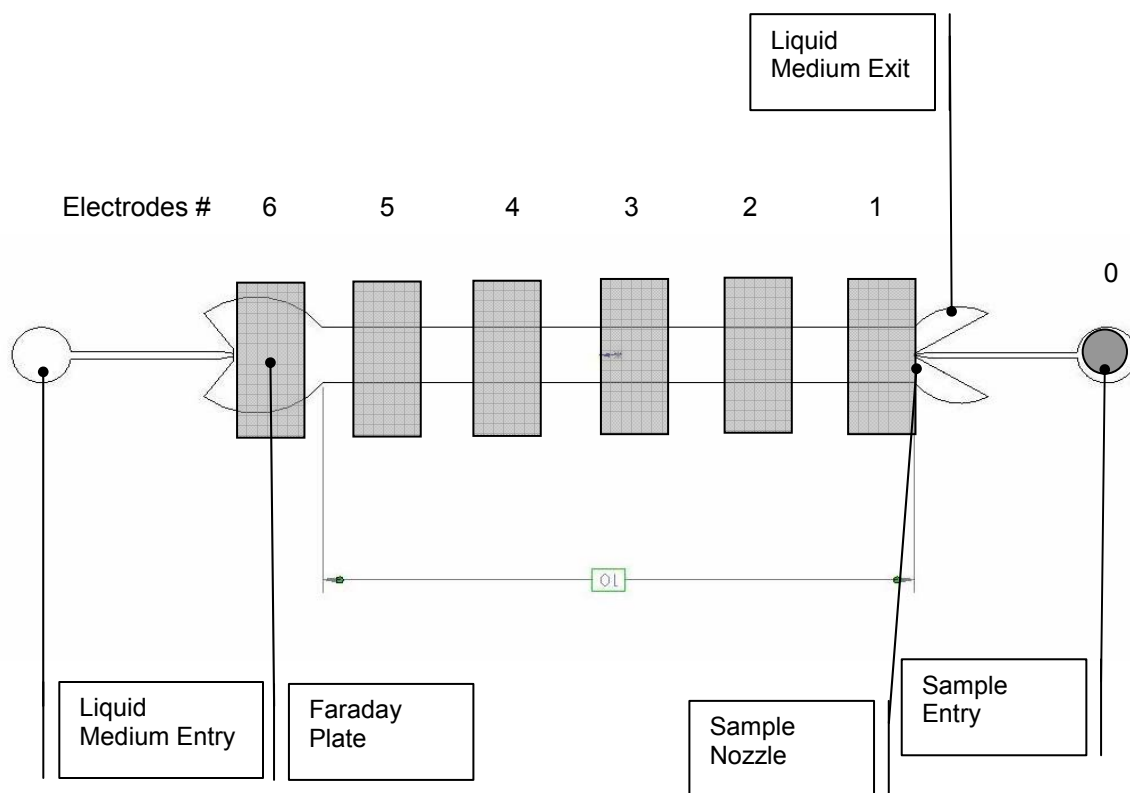


Figure 8: Top-view schematic of the third generation of PDMS-LPIMS. The microchannel was 1000 μm wide, 400 μm deep and 1 cm long. There were 6 sputtered platinum electrodes. EDI voltage was applied at electrode 0. The sample nozzle was incorporated into the PDMS design near electrode 1. Electrode 6 was used as the Faraday plate.

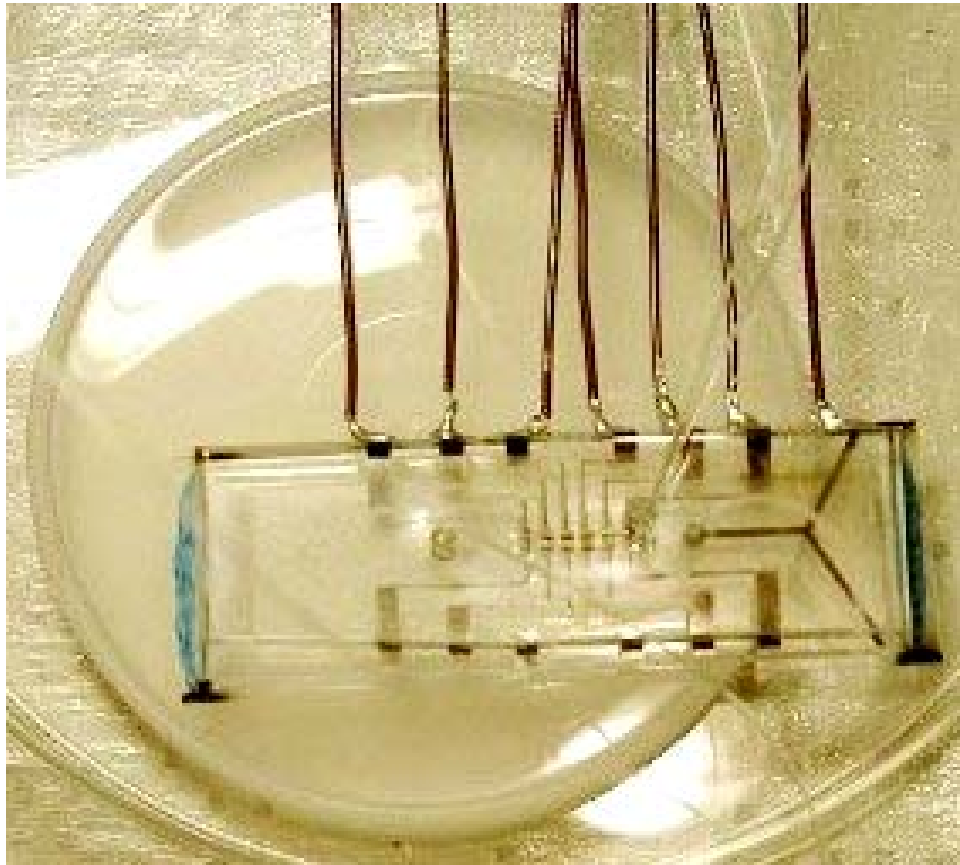


Figure 9: Photograph of the fourth generation of PDMS-LPIMS prototype, showing the polyethylene capillaries, which carried in the liquid medium and sample, and the electrical connections. The bottom PDMS layer was bonded to a glass microscope slide for additional support.

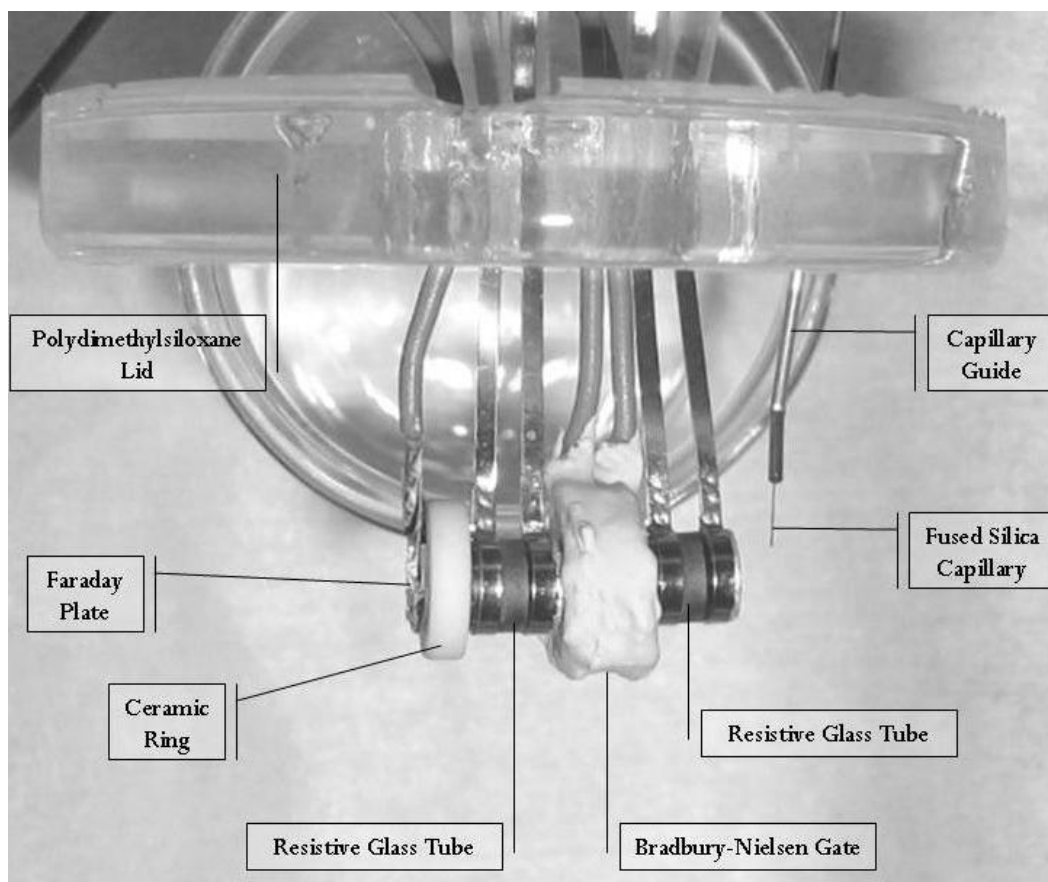


Figure 10: Photograph of a resistive glass-LPIMS. A miniature Bradbury-Nielsen gate was inserted between two resistive glass tubes, one being used as the desolvation region and another for the drift region. The sample was introduced via a fused silica capillary and ionized by electrodispersion ionization. The instrument was held steady by a poly(dimethylsiloxane) cover, and immersed into a Pyrex beaker filled with the liquid medium.



Figure 11: Photograph of the miniaturized Bradbury-Nielsen gate, with a 4.56 mm i.d., 9.30 mm o.d., and a wire spacing of 0.64 mm.

Appendix III

Electric Circuit for Pulsed Electrodispersion

Ionization Source

The electrical connections for pulsed electrodispersion ionization was shown in Figure 1. Aqueous sample was introduced by a syringe pump. The syringe was connected to a fused silica capillary through a grounded metal union. EDI voltage was applied to the second metal union. A micro-elbow junction allowed a 90° bend of the capillary. The pulsing of the electrodispersion ionization source was controlled by a Double Pole Single Throw (DPST) two-way switch, designed and constructed by Technical Services at Washington State University. The two-way switch consisted of two reed switches (HSR-10K, Hermetic Switch Inc., Chickasha, OK), current coils, electronic circuits and supporting power supplies. The function of two-way switch was to alter the voltage applied to the electrodispersion ionization source between a voltage high enough to cause electrodispersion and a lower voltage. The two-way switch was also used for controlling the voltage applied to the ion shutter. The schematic of the two-way switch circuit and the electrical connections for pulsed electrodispersion ionization was shown in Figure 1.

The HSR-10K reed switch could toggle voltages up to a maximum of 10 kV. Each reed switch had two overlapping ferromagnetic reeds with tungsten contacts, hermetically sealed inside a glass capsule. A coil of wire wrapped around the glass capsule (187 turns). Contact between the two reeds was made by a magnetic field, generated by passing a current through the coil. The two reeds “bounced” when the contact was made and a steady state was reached within 100 μ s. The contact was broken with the removal of the magnetic field. The first reed switch operated as the normally close (NC) switch, with its two reeds closed at its unactuated position. The first reed switch was connected to a voltage insufficient for electrodispersion ionization. The second reed switch operated as the normally open (NO) switch, with its two reeds open at its unactuated position. The second reed switch was connected to a voltage sufficient for electrodispersion ionization.

At the beginning of each mobility run, a 5-V pulse was sent by the LabView data acquisition system to the two-way switch that opened the first reed switch (NC) and closed the second reed switch (NO). The duration of this 5-V pulse was dictated by the user at the LabView computer interface. The typical pulse was 50 ms. After the indicated pulse, the first switch (NC) would be closed and the second reed switch (NO) would be opened.

Figure Captions

Figure 1: Schematic of liquid phase ion mobility spectrometer (LPIMS) with pulsed electrodispersion ionization (EDI). The components included a pulsed electrodispersion ionization source, a resistive glass ion mobility spectrometer, and a Faraday plate, all of which were rested inside a Pyrex dish filled with the liquid medium. Aqueous sample was introduced by a syringe pump. The syringe was connected to a fused silica capillary through a grounded metal union. EDI voltage was applied to the second metal union. A micro-elbow junction allowed a 90° bend of the capillary. R_1 , R_2 , R_3 , and R_4 were 2.5 M Ω resistors. NC was the normally closed reed switch of the two-way switch for controlling the EDI pulse and NO was the normally open reed switch. LPIMS voltage (HV_1) was applied to the front electrode. The end electrode of LPIMS was grounded through a 430 k Ω resistor (R_5).

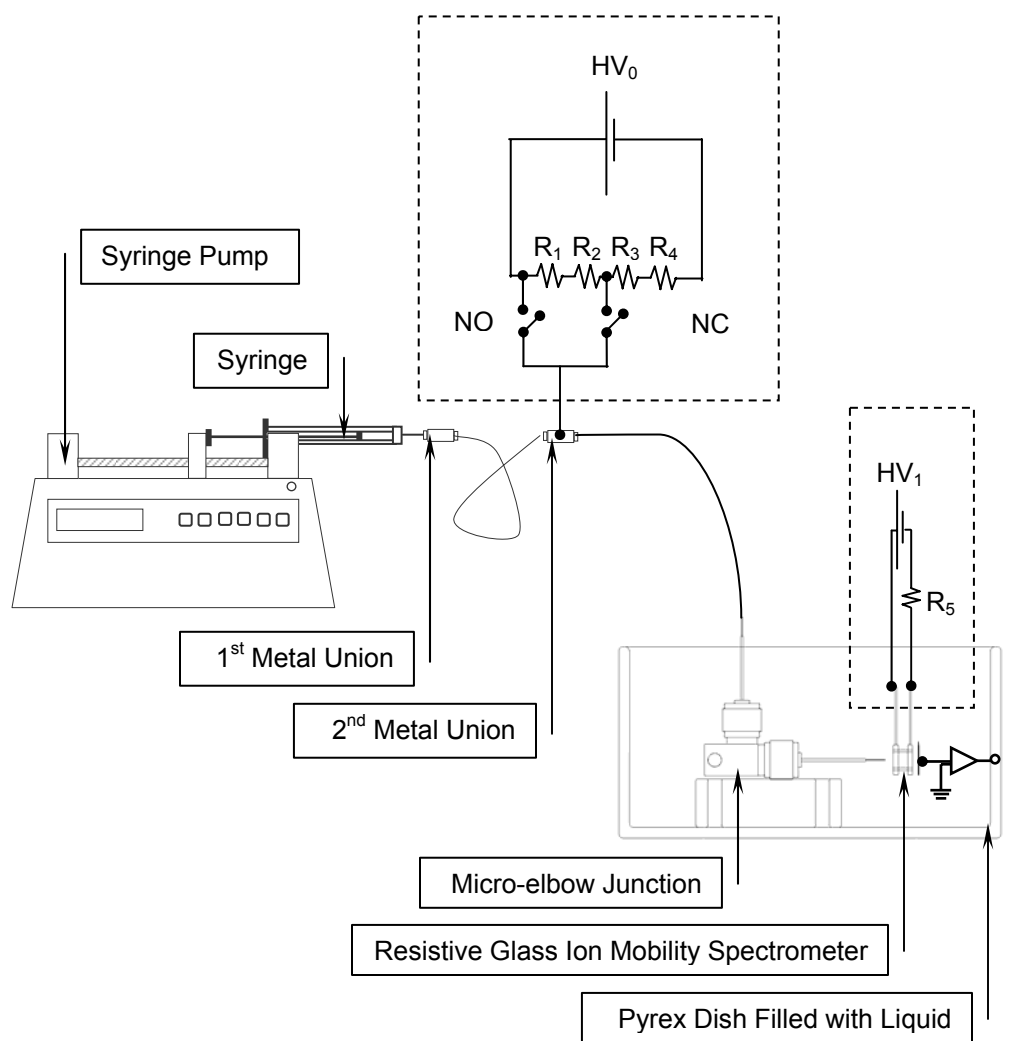


Figure 1: Schematic of liquid phase ion mobility spectrometer (LPIMS) with pulsed electrodispersion ionization (EDI). The components included a pulsed electrodispersion ionization source, a resistive glass ion mobility spectrometer, and a Faraday plate, all of which were rested inside a Pyrex dish filled with the liquid medium. Aqueous sample was introduced by a syringe pump. The syringe was connected to a fused silica capillary through a grounded metal union. EDI voltage was applied to the second metal union. A micro-elbow junction allowed a 90° bend of the capillary. R₁, R₂, R₃, and R₄ were 2.5 MΩ resistors. NC was the normally closed reed switch of the two-way switch for controlling the EDI pulse and NO was the normally open reed switch. LPIMS voltage (HV₁) was applied to the front electrode. The end electrode of LPIMS was grounded through a 430 kΩ resistor (R₅).

Appendix IV

Secondary Electrospray Ionization-Ion Mobility

Spectrometry for Explosive Vapor Detection

Abstract

The unique capability of secondary electrospray ionization (SESI) as a non-radioactive ionization source to detect analytes in both liquid and gaseous samples was evaluated using aqueous solutions of three common military explosives: cyclo-1,3,5-trimethylene-2,4,6-trinitramine (RDX), nitroglycerin (NG) and pentaerythritol tetranitrate (PETN). The adducts formed between the compounds and their respective dissociation product, $\text{RDX}\cdot\text{NO}_2^-$, $\text{NG}\cdot\text{NO}_3^-$ and $\text{PETN}\cdot\text{NO}_3^-$, gave the most intense signal for the individual compound but were more sensitive to temperature than other species. These auto-adducts were identified as $\text{RDX}\cdot\text{NO}_2^-$, $\text{NG}\cdot\text{NO}_3^-$ and $\text{PETN}\cdot\text{NO}_3^-$ and had maximum signal intensity at 137, 100, and 125°C, respectively. The reduced mobility values of the three compounds were constant over the temperature range from 75 °C to 225 °C. The signal-to-noise ratios for RDX, NG and PETN at 50 mg/L in methanol-water were 340, 270, and 170, respectively, with a nominal noise of 8 ± 2 pA. In addition to the investigation of auto-adduct formation,

the concept of doping the ionization source with non-volatile adduct-forming agents was investigated and described for the first time. The SESI-IMS detection limit for RDX was 116 $\mu\text{g/L}$ in the presence of a traditional volatile chloride dopant and 5.30 $\mu\text{g/L}$ in the presence of a non-volatile nitrate dopant. In addition to a lower detection limit, the nitrate dopant also produced a greater response sensitivity and a higher limit of linearity than did the traditional volatile chloride dopant.

Introduction

Ion mobility spectrometry (IMS) is the established method of choice for the detection of explosives,¹⁻⁷ in which radioactive ^{63}Ni ionization source is used to ionize explosive vapors thermally desorbed from solid particles. A volatile dopant is frequently employed in ^{63}Ni -IMS to provide a reactant ion.⁸ The most common dopant is methylene chloride.^{3;5;8-16} Other dopants have also been experimented, including o-dichlorobenzene,³ carbon tetrachloride,^{4;15} hexachloroethane,⁶ methyl chloride,¹⁵ trichloromethane,¹⁵ chlorobenzene,¹⁵ methylene bromide,^{9;11;16} methyl bromide,¹⁵ methyl iodide^{9;15} and nitrogen dioxide.¹⁰ The use of dopants is also common in explosives detection by liquid chromatography mass spectrometry (LC-MS) with electrospray ionization or atmospheric pressure chemical ionization. The dopant was either added to the LC mobile phase or added post-column. Salts of ammonium were often used including ammonium acetate¹⁷⁻¹⁹, ammonium formate^{20;21}, ammonium chloride,^{22;23} and ammonium nitrate²³.

The use of a radioactive ionization source such as the ^{63}Ni source in IMS explosive detection increases the bureaucracy associated with using these detectors in the field and limits the type of doping agents that can be employed to produce sensitive and selective reactant ions. Electrospray ionization²⁴ and corona discharge^{25;26} have been examined as an alternative non-radioactive ionization source. In this study a novel non-radioactive ionization source called secondary electrospray ionization (SESI)^{27;28} was investigated for the detection of explosives.

Secondary electrospray ionization was first introduced by Chen and Hill²⁷ in 1994 when they demonstrated that electrospray ionization (ESI) not only could ionize solvated analytes, but ESI could also be used to produce reactant ions, from electrospraying a solvent, to ionize neutral gaseous analytes. Later, Wu et al²⁸ evaluated the analytical figures of merit of SESI, in comparison with ESI, in the analysis of illicit drugs, and concluded that SESI was a more sensitive ionization technique than ESI.

The ionization mechanism for SESI is similar to that of atmospheric pressure chemical ionization, where gas phase reactant ions are produced in the ionization source and reacted with the sample analyte in the gas-phase forming a charged analyte, which can then be separated and detected by IMS. In SESI, reactant ions are produced from the electrospray process. Wu et al²⁸ reported that SESI had higher ionization efficiency than ESI in the IMS analysis of illicit drug samples.

The primary purposes of this study was to evaluate the unique capability of SESI to ionize both liquid and gaseous samples using three common military explosives and to demonstrate the use of non-volatile doping agents for the production of unique reactant ions. Additionally, this paper investigated the temperature effect on the stability of the response ions of these explosives, reporting the effect of temperature on both K_0 and sensitivity of the compounds studied.

Experimental Section

Instrumentation. The SESI-IMS system was constructed at Washington State University (Figure 1). The SESI-IMS system consisted of a water-cooled ESI source, a sample introduction unit and an ion mobility spectrometer.

The water-cooled ESI source used in this study has been described in detail by Clowers et al.²⁹ A voltage of -10 kV was applied to the electrospray needle. The electrospray solvent was delivered by a Micro-Tech Ultra Plus II MicroLC system (Micro-Tech Scientific, Vista, CA) at 10 μ L/min via a fused silica capillary. Nitrogen carrier gas flowed at 50 mL/min inside the cooling cavity of the ESI source. In these studies, the sample was not introduced into the IMS through the electrospray process as in normal electrospray IMS.

The sample introduction unit was an assembly of a stainless steel Tee tube fitting ($1/8$ "") and a perforated stainless steel sample inlet ring connected via a Teflon tubing. The sample, which was pumped at 10 μ L/min by a Harvard syringe pump "11" (Harvard Apparatus, Holliston, MA), entered the Tee tube fitting through a fused silica capillary (75 μ m I.D.) and was carried to the sample inlet ring by nitrogen gas flowing at 573 ml/min. The sample introduction unit was heated to approximately 210 °C with heating tape. The elevated temperature of the sample introduction unit ensured that the sample was completely volatilized before entering the ion mobility

tube. The sample inlet ring was located between the electrospray needle and the ion entrance gate. In the ESI-IMS experiments, the explosive compounds were introduced through the electrospray. In the SESI-IMS experiments, the explosive compounds were introduced through the sample introduction unit in Figure 1.

The ion mobility spectrometer was made of a stack of stainless steel guard rings (47 mm I.D.), which were connected in series by resistors and insulated from one another with alumina rings. The drift region was 14.1 cm in length, with a constant electric field of -379 V/cm, unless stated otherwise. A Bradbury-Nielsen type shutter gate was used.³⁰ A target screen and an aperture grid were located at the front and at the end of the ion mobility tube respectively. Nitrogen drift gas flowed at 800 mL/min countercurrent to the direction at which ions were traveling. The temperature of the IMS housing was varied between 75 and 225 °C. The TNT experiments were operated at approximately 235 °C.

Signal was detected by a faraday plate, collected and amplified (10^9 gain) by a Keithley 427 current amplifier (Keithley Instruments, Cleveland, OH), then processed by a LabView (National Instruments, Austin, TX) based data acquisition system written in-house. Spectra were collected at either 25 or 30 ms interval with a pulse width of 0.2 ms and were averaged 500 times.

The ITEMISER® (Ion Track Instruments, Wilmington, MA), a commercial ⁶³Ni-IMS instrument, was operated in the explosive mode with purified air as drift gas and methylene chloride as dopant. 10 μL of 10 mg/L sample solution was pipetted on a

pre-cleaned microscope slide (Becton Dickinson Labware, Franklin Lakes, NJ), which was then placed in the vapor desorption unit of the instrument after solvent had evaporated. This 10 ng sample was then introduced to the IMS by thermal desorption at 175 °C. The sampling time was 5 s. Spectra were collected at 15 ms interval and were averaged 70 times.

Chemicals and solvents. The explosives used in this study were trinitrotoluene (TNT), cyclo-1,3,5-trimethylene-2,4,6-trinitramine (RDX), nitroglycerin (NG) and pentaerythritol tetranitrate (PETN) (Radian International, Austin, TX). Test solutions ranged in concentrations from 0.1 mg/L to 50 mg/L were prepared by diluting a 1000 mg/L stock standard in acetonitrile with HPLC grade methanol-water (9:1, v/v) solution (J. T. Baker, Phillipsburg, NJ). Methylene chloride, sodium nitrite (Fisher Scientific, Fair Lawn, NJ), sodium chloride (J. T. Baker, Phillipsburg, NJ), and sodium nitrate (Sigma Chemical, St. Louis, MO) solutions were made by dissolving the respective compound in methanol-water (9:1, v/v) solution.

Calculations. Reduced mobilities were calculated from the following equation:

$$K_0 = \frac{L}{t_d \cdot E} \cdot \frac{P}{760} \cdot \frac{273}{T} \quad (1)$$

where L is the length of ion mobility drift region (cm); t_d is the drift time of the species in seconds; E is the electric field strength of ion mobility drift region (V/cm); P is the pressure (Torr) and T is the temperature of ion mobility tube (K).

Results and Discussion

Non-volatile dopants. The IMS spectra of TNT ionized by ESI (Figure 2a), SESI (Figure 2b) and ^{63}Ni in the presence of a methylene chloride dopant (Figure 2c) illustrated that TNT responded well in IMS with different ionization sources. All three spectra showed an intense TNT peak with a reduced mobility value, K_0 , of $1.54 \text{ cm}^2/\text{V}\cdot\text{s}$.

The ESI-IMS and SESI-IMS of TNT both operated with an electric field of -270 V/cm . The ESI-IMS spectrum was run at $233 \text{ }^\circ\text{C}$ and 705 Torr , while SESI-IMS at $236 \text{ }^\circ\text{C}$ and 702 Torr . This difference in operating temperatures and pressures of ESI-IMS and SESI-IMS accounted for the slight deviation in drift times between the two. The faster drift time of TNT in the ^{63}Ni -IMS spectrum was obtained on a different instrument (the ITEMISER®) with a shorter drift region and operated under different conditions. All three ionization sources were well suited for detecting TNT. Thus, the preference in choosing one ionization source over another is determined by detector availability, sample medium, and convenience of use.

For explosive compounds that thermally decompose, it was necessary to introduce a dopant to reduce the extent of fragmentation and to form more stable product ions. RDX, for example, forms stable adduct ions with several anions, including chloride.^{24;31} Methylene chloride is often employed as a dopant in IMS analysis of explosive compounds.^{5;8;16} Figure 3 showed the ^{63}Ni -IMS spectra of 100 ng RDX, NG and PETN obtained with the ITEMISER® at $200 \text{ }^\circ\text{C}$, where the chloride adduct of

RDX and dissociation product of NG and PETN were observed. The absence of chloride adducts of NG and PETN suggested the need to explore the use of other dopants in search of a more sensitive and more thermally stable adducts that remain associate at higher temperatures. The hypothesis of this project is that both volatile and non-volatile dopants could be introduced and ionized by the SESI process, whereas ^{63}Ni -IMS is limited to the use of volatile dopants.

Figure 4 shows the SESI-IMS spectra of RDX, NG, and PETN at 125 °C without a dopant. The major reactant ions produced from electrospraying methanol-water were chloride, nitrite and nitrate.³² Two peaks were observed for RDX and three for both NG and PETN. In the absence of mass identification, peak assignments for individual explosive species in this experiment were achieved as described below. The study was performed at a temperature at which all species of the explosive were thermally stable. The temperatures were 135 °C for RDX, and 100 °C for both NG and PETN.

All three explosives studied in this experiment have been reported to form adducts of chloride, nitrite and nitrate in ion mobility experiments.^{5;24;33-38} Therefore, non-volatile sodium salts of these anions were selected as dopants and were dissolved in the electrospray solvent of methanol-water.

Initially, two product ion peaks (peaks numbered 5 and 6 in Figure 5a) were observed in the ESI-IMS spectrum when RDX was introduced in the absence of a dopant. Peak 5 had a K_0 value of $1.40 \text{ cm}^2 \text{ V}^{-1} \text{ s}^{-1}$ and peak 6 had a K_0 value of 1.35

$\text{cm}^2/\text{V}\cdot\text{s}$. Peaks 2 and 3, in all of the spectra in Figure 5, corresponded to nitrite and nitrate ions respectively. Figure 5b is the resulting spectrum when RDX was electrosprayed in presence of nitrite dopant. Compared with Figure 1a, the signal intensity of peak 5 increased; Similarly, RDX was electrosprayed in the presence of nitrate dopant, the signal intensity of peak 6 increased (Figure 5c); When RDX was electrosprayed in the presence of chloride dopant, a third peak – peak 4, with a K_0 value of $1.44 \text{ cm}^2/\text{V}\cdot\text{s}$ appeared (Figure 5d). The increase in intensity of specific peaks in different dopant environment suggested that the three peaks of RDX were $\text{M}\cdot\text{Cl}^-$ (K_0 1.44), $\text{M}\cdot\text{NO}_2^-$ (K_0 1.40) and $\text{M}\cdot\text{NO}_3^-$ (K_0 1.35).

Peak assignments for NG and PETN were performed in the same manner, with the exception of $(\text{M}\cdot\text{H})^-$ of NG and of PETN, by observing the increased intensity in different analyte peaks in presence of different dopant additives. The $(\text{M}\cdot\text{H})^-$ species of NG and PETN were assigned based on comparison with literature data. Peak assignments for species of the three explosive compounds are tabulated along with their respective literature values in Table 1.

The non-volatile dopant studies were repeated with SESI-IMS. The SESI-IMS spectra of RDX in the absence of any dopant and in the presence of the added dopants (Figure 5e-h) showed that RDX peaks were more intense when ionized by SESI than by ESI. It was interesting to note that while reactant ions were present in the ESI-IMS spectra, no reactant ions of considerable intensity were observed in the SESI-IMS spectra of RDX. The only difference between the ESI-IMS and SESI-IMS experiments was the sample introduction method. In ESI-IMS, the analyte was

introduced through electrospray and the analyte was ionized in ESI process. In SESI-IMS, the analyte was ionized by charge-transfer from electrosprayed solvent ions. The reduction in reactant ions intensity, together with the enhanced intensity of RDX peaks in SESI-IMS indicated that the charges from solvent ions had mostly transferred to RDX. This resulted in more RDX ions being formed in SESI than in ESI.

Non-volatile nitrate dopant was selected to compare with a common volatile dopant in the SESI-IMS analysis of RDX at 135 °C, because at 2 mM concentration level of dopants introduced by electrospray, the nitrate dopant resulted in the most intense RDX peak (Figure 5e-h). Two methanol-water electrospray solvents were prepared, one containing 4 % methylene chloride and the other containing 2 mM sodium nitrate. Calibration data showed that the detection limit of RDX was 116 µg/L in the presence of chloride dopant, with a sensitivity of 60.2 µA per mg/L and a limit of linearity at 5 mg/L. While the detection limit of RDX was 5.30 µg/L in the presence of nitrate dopant, with a sensitivity of 81.4 µA per mg/L and a limit of linearity at 10 mg/L. In addition to a lower detection limit, the nitrate dopant also provided a better sensitivity and a higher limit of linearity than did the chloride dopant.

While nitrate may not be the most suitable dopant for explosive analysis, this study demonstrated the ability of SESI to introduce both volatile and non-volatile dopants; thus widening the selection of possible dopants that can be employed to select ionization chemistry for increased response of analyte through the formation of more stable adduct ions.

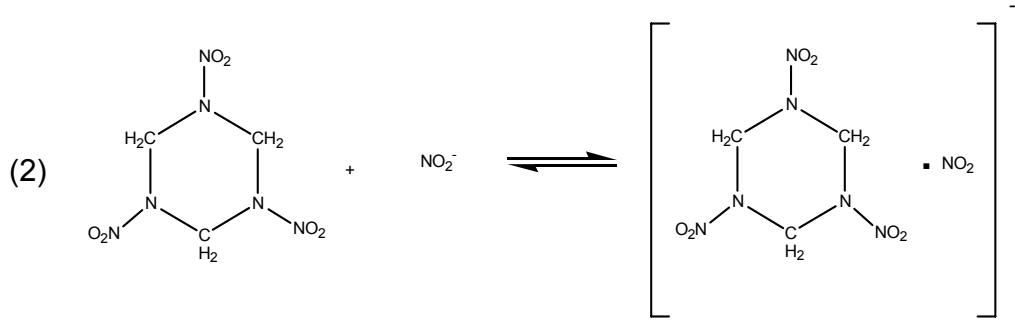
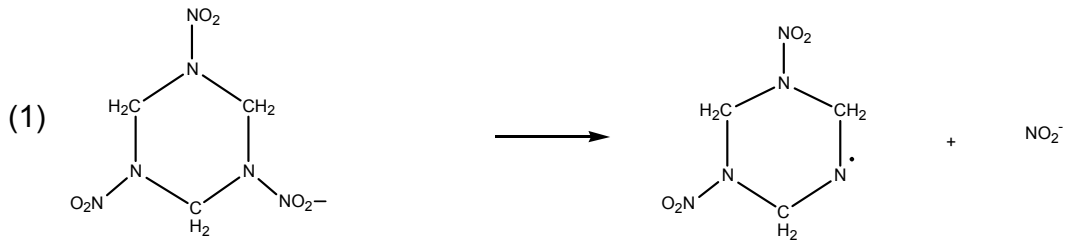
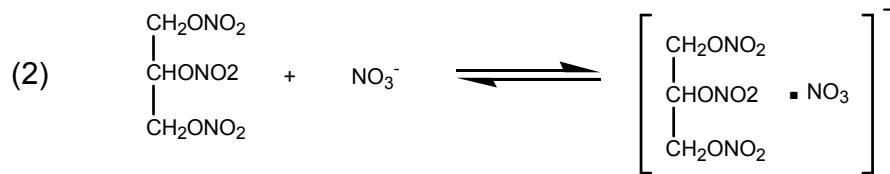
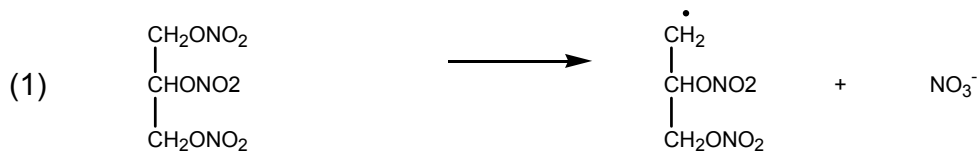
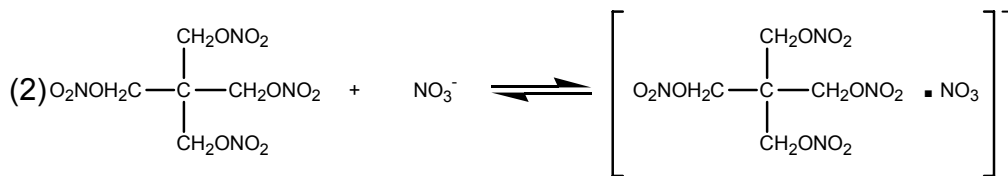
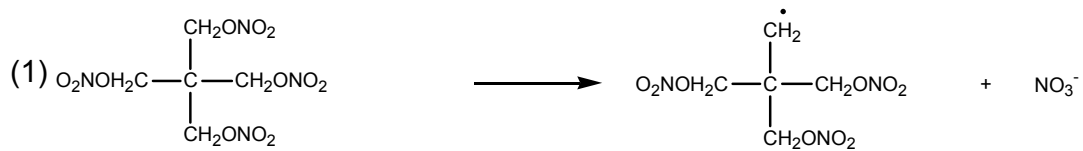
Thermal stability of RDX, NG, and PETN. The thermal stability of the adduct ions of RDX, NG, and PETN created by SESI-IMS were investigated at drift tube temperatures ranging from 75 to 225 °C. A high concentration of 50 mg/L was used to ensure that the absence of the explosive species at high temperatures was due to thermal instability, rather than limitation of detection. The species $\text{RDX}\cdot\text{NO}_2^-$, $\text{NG}\cdot\text{NO}_3^-$ and $\text{PETN}\cdot\text{NO}_3^-$ were chosen as the adduct ions to monitor because they gave the most intense signal for their parent compound at 125 °C (Figure 4).

At drift tube temperatures higher than 150 °C, $(\text{M}-\text{H})^-$, adduct ions of NG and PETN were absent (Figure 6b-c), while NO_3^- , their dissociation product, was prominent. However, at 225 °C, adduct ions of RDX were still detectable, although at a reduced signal intensity than that at a lower drift tube temperature (Figure 6a), together with an increased signal of NO_2^- , the dissociation product of RDX. These data indicated that adduct ions of RDX were more thermally stable than those of NG and PETN, and that the binding energies of the RDX adducts were relatively higher than those of NG and PETN.

Figure 6 also revealed that some adducts, particularly $\text{RDX}\cdot\text{NO}_2^-$, $\text{NG}\cdot\text{NO}_3^-$ and $\text{PETN}\cdot\text{NO}_3^-$, were more sensitive to temperature changes than others were. These three adducts were the same species that gave the most intense signal for their parent compound. $\text{RDX}\cdot\text{NO}_2^-$, $\text{NG}\cdot\text{NO}_3^-$ and $\text{PETN}\cdot\text{NO}_3^-$ had maximum signal intensity at 137, 100 and 125 °C respectively.

From 75 °C up to their optimum temperature, the signal intensity of $\text{RDX}\cdot\text{NO}_2^-$, $\text{NG}\cdot\text{NO}_3^-$ and $\text{PETN}\cdot\text{NO}_3^-$ increased with increasing temperature. This effect of

temperature on response indicated the mechanism of adduct formation. Apparently, $\text{RDX}\cdot\text{NO}_2^-$, $\text{NG}\cdot\text{NO}_3^-$ and $\text{PETN}\cdot\text{NO}_3^-$ were adducts formed between the compound and its decomposition product ion. Since RDX dissociated to NO_2^- , NG and PETN dissociated to NO_3^- , the nitrite and nitrate adduct ions originated from the dissociation products of their respective compound. This involved two steps: (1) the molecular ion dissociated to form nitrite or nitrate and (2) the molecule reacted with the dissociated nitrite or nitrate thus forming an autoionization product.

RDX:**NG:****PETN:**

Above their optimum temperatures, the signal intensity of $\text{RDX}\cdot\text{NO}_2^-$, $\text{NG}\cdot\text{NO}_3^-$ and $\text{PETN}\cdot\text{NO}_3^-$ decreased with increasing temperature. This decrease in signal intensity can be attributed to the thermal decomposition of the autoionization products and/or the advance decomposition of the compound itself into NO_2^- or NO_3^- , as evidenced by the presence of NO_2^- for RDX and NO_3^- for NG and PETN at high temperatures.

Temperature effect on K_0 . The reduced mobility values of the molecular ions and the various adduct ions of RDX, NG and PETN were plotted versus the drift tube temperature used in this study, from 75 to 225 °C (Figure 7). Error bars were omitted from the plot because they were smaller in size than the K_0 markers. The average standard deviation for the K_0 values was 0.001 $\text{cm}^2/\text{V}\cdot\text{s}$, with a maximum standard deviation of 0.002 $\text{cm}^2/\text{V}\cdot\text{s}$. The K_0 values of the various explosive species showed a slight negative dependence on temperature, with the K_0 value decreasing by 2% at most over the temperature range. In conclusion, the K_0 values of the explosive species appeared to be constant ($< \pm 2\%$) over a 150 °C temperature range where SESI-IMS is used.

Signal to Noise Ratio. With 50 $\text{ng}/\mu\text{L}$ of liquid sample entering the sample introduction unit at 10 $\mu\text{L}/\text{min}$, being volatilized at a temperature of 210 °C and carried by nitrogen gas flowing at 940 mL/min , a 50 $\text{ng}/\mu\text{L}$ liquid sample was, therefore, equivalent to 0.53 mg m^{-3} or 102 ppb_v of RDX, 101 ppb_v of NG and 72 ppb_v of PETN in nitrogen.

In the SESI-IMS experiments, in the absence of added dopant, the signal-to-noise ratios for 50 mg/L or 0.53 mg/m³ of RDX (137 °C), NG (100 °C) and PETN (125 °C) were 340, 270 and 170, respectively with a nominal noise of 8 ± 2 pA. At this level of signal-to-noise ratio measured, the sensitivity of the SESI-IMS system was sufficient to detect explosives in workplace air samples, where the maximum airborne concentration of explosives recommended by the American Conference of Governmental Industrial Hygienists (1986) to be 0.5 mg m⁻³ for NG and 1.5 mg/m³ for RDX.

Conclusions

SESI is a non-radioactive ionization source, which can be used to detect both vapor phase and aqueous phase explosives. Non-volatile dopants can be used with SESI to enhance both sensitivity and selectivity. Data showed that SESI-IMS analysis of RDX, in the presence of a non-volatile nitrate dopant, produced not only a lower detection limit, but also a greater response sensitivity and a higher limit of linearity, than in the presence of a common volatile chloride dopant.

Acknowledgement

The authors thank GE Ion Track (Wilmington, MA) for providing the ITEMISER® instrument and partial support for the investigation.

References

- (1) Karasek, K. W.; Denney, D. W. *Journal of Chromatography* **1974**, *93*, 141-147.
- (2) Karasek, K. W. *Research/Development* **1974**, *25*, 32-36.
- (3) Spangler, G. E.; Lawless, P. A. *Analytical Chemistry* **1978**, *50*, 884-92.
- (4) Spangler, G. E.; Carrico, J. P.; Campbell, D. N. *Journal of Testing and Evaluation* **1985**, *13*, 234-40.
- (5) Lawrence, A. H.; Neudorfl, P. *Analytical Chemistry* **1988**, *60*, 104-09.
- (6) Fetterolf, D. D.; Clark, T. D. *Journal of Forensic Sciences* **1993**, *38*, 28-39.
- (7) Ewing, R. G.; Miller, C. J. *Field Analytical Chemistry and Technology* **2001**, *5*, 215-21.
- (8) Lawrence, A. H.; Neudorfl, P.; Stone, J. A. *International Journal of Mass Spectrometry* **2001**, *209*, 185-95.
- (9) Proctor, C. J.; Todd, J. F. J. *Analytical Chemistry* **1984**, *56*, 1794-97.
- (10) Davies, J. P.; Blackwood, L. G.; Davis, S. G.; Goodrich, L. D.; Larson, R. A. *Analytical Chemistry* **1993**, *65*, 3004-09.
- (11) Brittain, A. H.; Brokenshire, J. L. *Proceeding of the Fifth International Workshop on Ion Mobility Spectrometry*, Jackson, Wyoming, **1996**.
- (12) Atkinson, D. A.; Crockett, A. B.; Jenkins, T. F. *Proceeding of the Fifth International Workshop on Ion Mobility Spectrometry*, Jackson, Wyoming, **1996**.
- (13) Eiceman, G. A.; Preston, D.; Tiano, G.; Rodriguez, J.; Parmeter, J. E. *Talanta* **1997**, *45*, 57-74.
- (14) Munro, W. A. ; Thomas, C. L. P.; Langford, M. L. *Analytica Chimica Acta* **1998**, *375*, 49-63.
- (15) Daum, K. A.; Atkinson, D. A.; Ewing, R. G. *Talanta* **2001**, *55*, 491-500.
- (16) Daum, K. A.; Atkinson, D. A.; Ewing, R. G.; Knighton, W. B.; Grimsrud, E. P. *Talanta* **2001**, *54*, 299-306.
- (17) Wu, Z.; Hendrickson, C. L.; Rodgers, R. P.; Marshall, A. G. *Analytical Chemistry* **2002**, *74*, 1879-1883.

- (18) Schreiber, A.; Efer, J.; Engewald, W. *Journal of Chromatography A* **2000**, *869*, 411-25.
- (19) Casetta, B.; Garofolo, F. *Organic Mass Spectrometry* **1994**, *29*, 517-25.
- (20) Cassada, D. A.; Monson, S. J.; Snow, D. D.; Spalding, R. F. *Journal of Chromatography A* **1999**, *844*, 87-95.
- (21) Gapeev, A.; Sigman, M.; Yinon, J. *Rapid Communications in Mass Spectrometry* **2003**, *17*, 943-48.
- (22) Evans, C. S. ; Sleeman, R.; Luke, J.; Keely, B. J. *Rapid Communications in Mass Spectrometry* **2002**, *16*, 1883-91.
- (23) Zhao, X.; Yinon, J. *Journal of Chromatography A* **2002**, *977*, 59-68.
- (24) Asbury, G. R.; Klasmeier, J.; Hill, H. H. Jr. *Talanta* **2000**, *50*, 1291-98.
- (25) Tabrizchi, M.; Abedi, A. *International Journal of Mass Spectrometry* **2002**, *218*, 75-85.
- (26) Khayamian, T.; Tabrizchi, M.; Jafari, M. T. *Talanta* **2003**, *59*, 327-33.
- (27) Chen, Y. H.; Hill, H. H. Jr. *Journal of Microcolumn Separations* **1994**, *6*, 515-24.
- (28) Wu, C.; Siems, W. F.; Hill, H. H. Jr. *Analytical Chemistry* **2000**, *72*, 396-403.
- (29) Clowers, B. H.; Steiner, W. S.; Dion, H. M.; Matz, L. M.; Tam, M.; Tarver, E. E.; Hill, H. H. Jr. *Field Analytical Chemistry and Technology* **2001**, *5*, 302-12.
- (30) Bradbury, N. E.; Nielson, R. A. *Phys. Rev.* **1936**, *49*, 388-393.
- (31) Rodriguez, J. E. *Atmospheric Pressure Chemical Ionization of Nitro-Containing Organic Explosives and Other Nitro-Organic Compounds in Mass Spectrometry and Ion Mobility Spectrometry*, Masters Thesis, New Mexico State University: Las Cruces, NM, **1996**.
- (32) Asbury, G. R.; Hill, H. H. Jr. *International Journal for Ion Mobility Spectrometry* **1999**, *2*, 1-8.
- (33) Ritchie, R. K.; Kuja, F. J.; Jackson, R. A.; Loveless, A. J.; Danylewych-May, L. L. *Proceedings of the Substance Detection Systems*, Bellingham, WA, **1994**.
- (34) Fetterolf, D. D. In *Advances in Analysis and Detection of Explosives*; edited by J. Yinon; Kluwer Academic Publishers: Dordrecht, **1993**; pp. 117-131.
- (35) Huang, S. D.; Kolaitis, L.; Lubman, D. M. *Applied Spectroscopy* **1987**, *41*, 1371-76.
- (36) Spangler, G. E.; Carrico, J. P.; Kim, S. H. *Proceedings of the International Symposium on Analysis and Detection of Explosive*, Quantico, VA, **1983**.

- (37) Wernlund, R. F.; Cohen, M. J.; Kindel, R. C. *Proceedings of the New Concept Symposium and Workshop on Detection and Identification of Explosives*, Reston, VA, **1978**.
- (38) Danylewych-May, L. L. *Proceedings of the First International Symposium on Explosive Detection Technology*, Atlantic City, NJ, **1991**.

Table 1. The experimental and literature reduced mobility values of explosive species

Compound	Species	Experimental K_D cm ² /V·s	Literature K_D cm ² /V·s
RDX ^a	M·Cl ⁻	1.44	1.39 ³³ 1.40 ^{24;34}
	M·NO ₂ ⁻	1.40	1.43 ³⁵ ; 1.45 ³⁶
	M·NO ₃ ⁻	1.35	—
NG ^b	(M-H) ⁻	1.45	1.45 ³³
	M·Cl ⁻	1.40	1.47 ⁵
	M·NO ₃ ⁻	1.31	1.32 ³⁷ ; 1.37 ³⁶ ; 1.40 ⁵
PETN ^b	M-H ⁻	1.25	1.22 ^{c 38}
	M·Cl ⁻	1.20	1.15 ^{c 38}
	Unidentified	1.17	—
	M·NO ₃ ⁻	1.14	1.10 ^{c 38}

^a Reduced mobility values observed at ion mobility drift tube temperature of 135 °C.

^b Reduced mobility values observed at ion mobility drift tube temperature of 100 °C.

^c Reduced mobility values calculated on assumption of (TNT-H)⁻ being 1.450 cm²/V·s.

FIGURE CAPTIONS

Figure 1. Schematic of secondary electrospray ionization-ion mobility spectrometer.

Figure 2. (a) ESI-IMS spectrum of 10 mg L⁻¹ TNT; (b) SESI-IMS spectrum of 10 mg L⁻¹ TNT; (c) ⁶³Ni-IMS spectrum of 100ng TNT with methylene chloride as dopant.

Figure 3. ⁶³Ni-IMS spectra of 100ng of (a) RDX (b) NG and (c) PETN. Spectra were obtained at 200 °C with methylene chloride as dopant.

Figure 4. SESI-IMS spectra of 50 mg L⁻¹ (a) RDX (b) NG and (c) PETN in methanol-water. All spectra were run at 125 °C.

Figure 5. Effect of non-volatile dopants: ESI-IMS spectra of 50 mg L⁻¹ RDX in (a) methanol-water (b) 2 mM NaNO₂ (c) 2 mM NaNO₃ (d) 2 mM NaCl. SESI-IMS spectra of 50 mg L⁻¹ RDX in methanol-water with electro spraying (e) methanol-water (f) 1.45 mM NaNO₂ (g) 2 mM NaNO₃ (h) 2mM NaCl. All spectra were run at 135 °C. Peak assignments: (1) Cl⁻ (2) NO₂⁻ (3) NO₃⁻ (4) RDX·Cl⁻ (5) RDX·NO₂⁻ (6) RDX·NO₃⁻

Figure 6. Thermal stability of RDX, NG and PETN species: Plots of SESI-IMS signal intensity versus drift tube temperature of (a) RDX (b) NG and (c) PETN.

Figure 7. Plot of SESI-IMS reduced mobilities of RDX, NG and PETN species versus drift tube temperature. Average standard deviation for the K_0 values was

0.001 cm² V⁻¹ s⁻¹, with maximum standard deviation at 0.002 cm² V⁻¹ s⁻¹. Error bars were omitted from the plot because they were smaller in size than the data point markers.

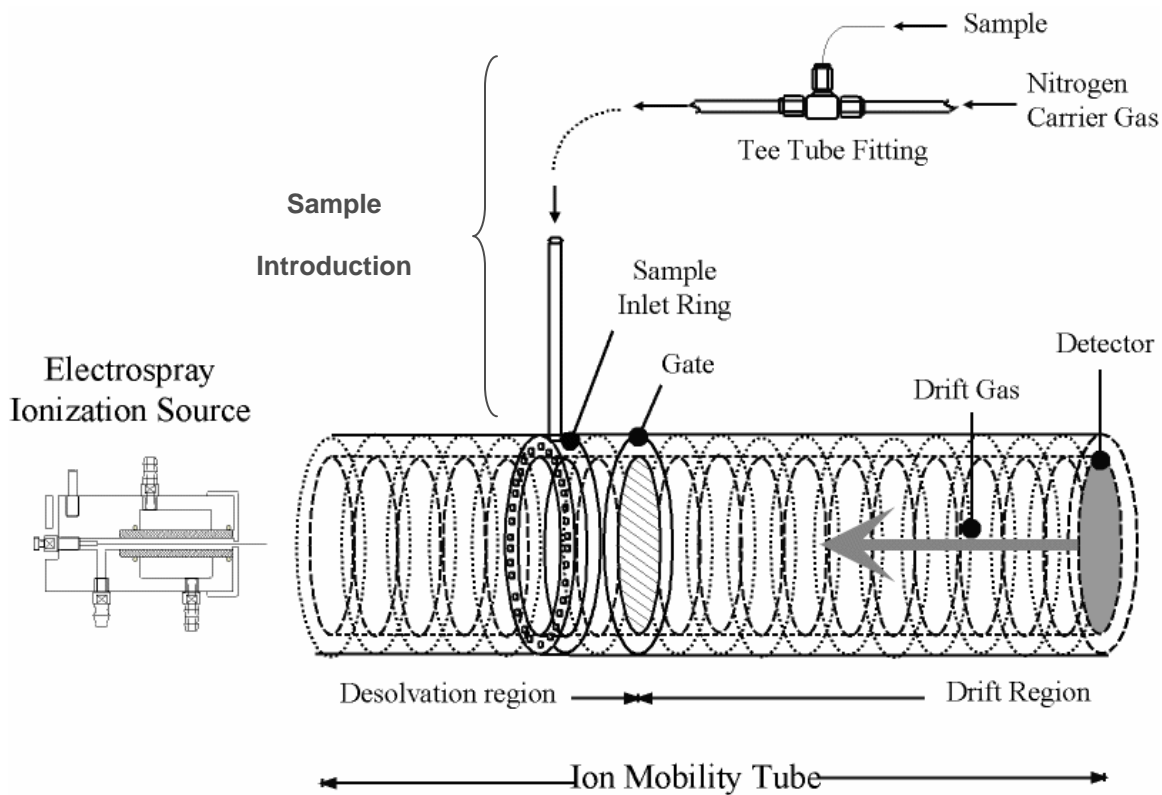


Figure 1: Schematic of secondary electro spray ionization-ion mobility spectrometer.

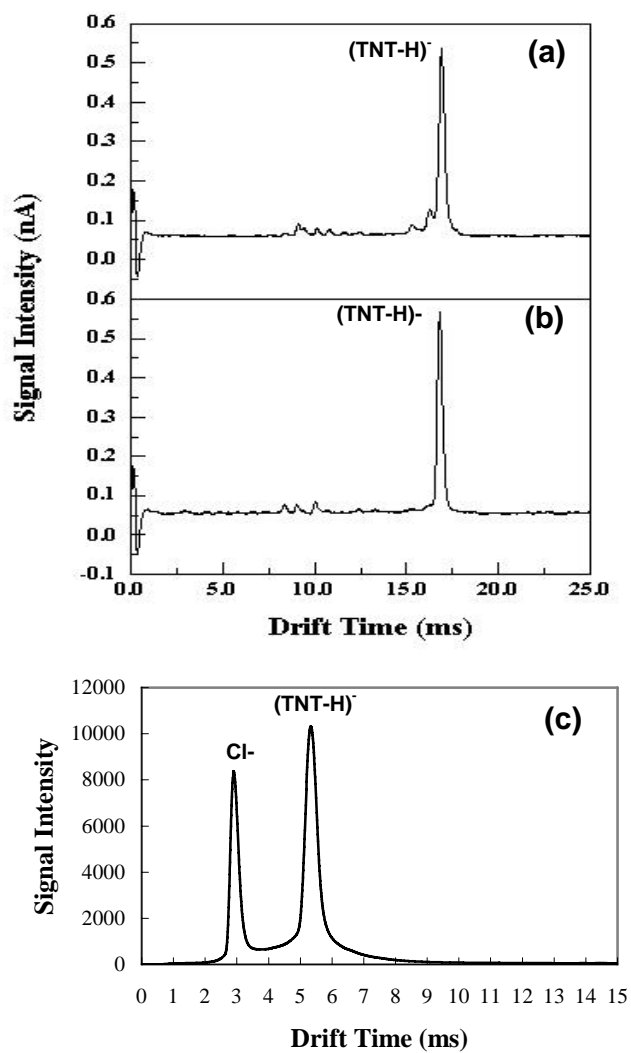


Figure 2: (a) ESI-IMS spectrum of 10 mg L⁻¹ TNT; (b) SESI-IMS spectrum of 10 mg L⁻¹ TNT; (c) ^{63}Ni -IMS spectrum of 100ng TNT with methylene chloride as dopant.

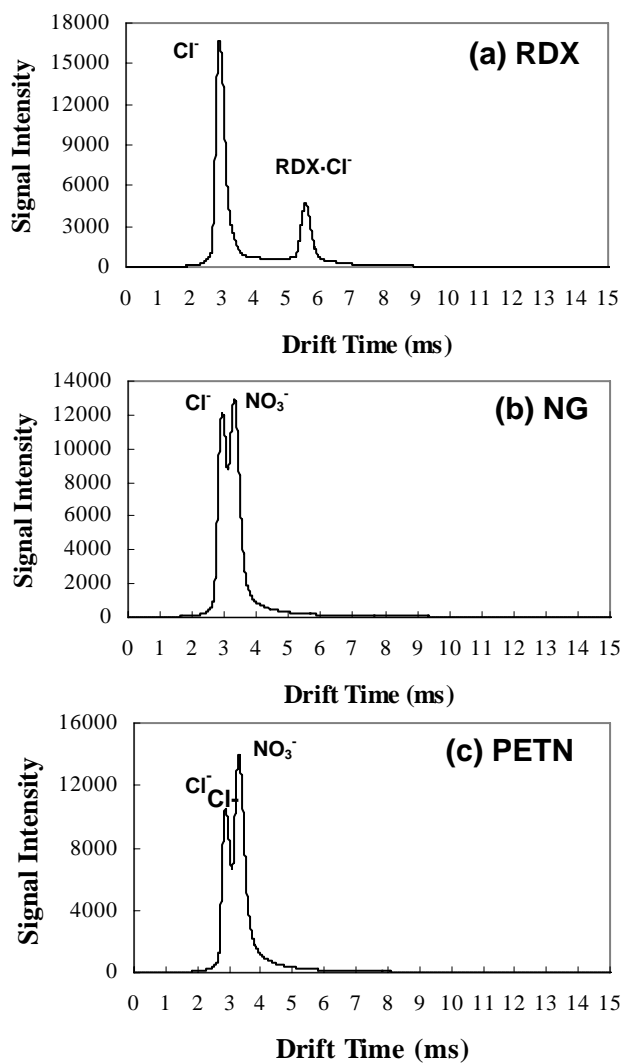


Figure 3: ^{63}Ni -IMS spectra of 100ng of (a) RDX (b) NG and (c) PETN. Spectra were obtained at 200 °C with methylene chloride as dopant.

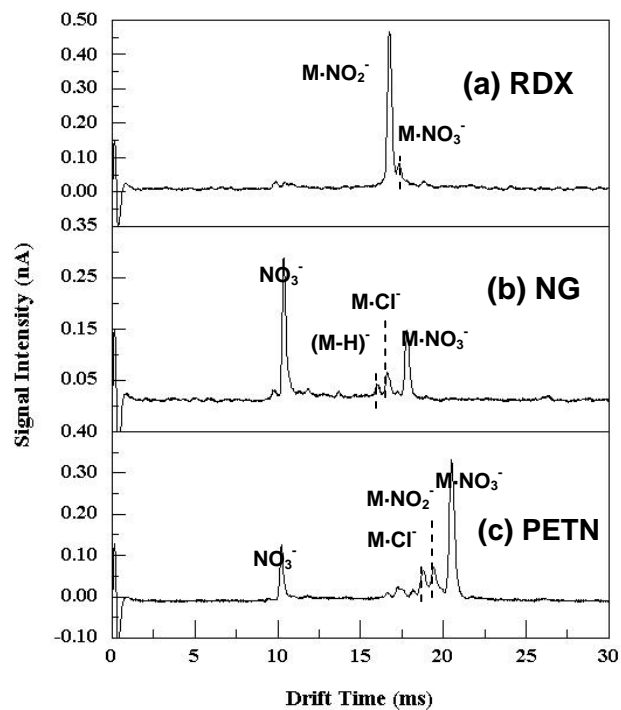


Figure 4: SESI-IMS spectra of 50 mg L⁻¹ (a) RDX (b) NG and (c) PETN in methanol-water. All spectra were run at 125 °C.

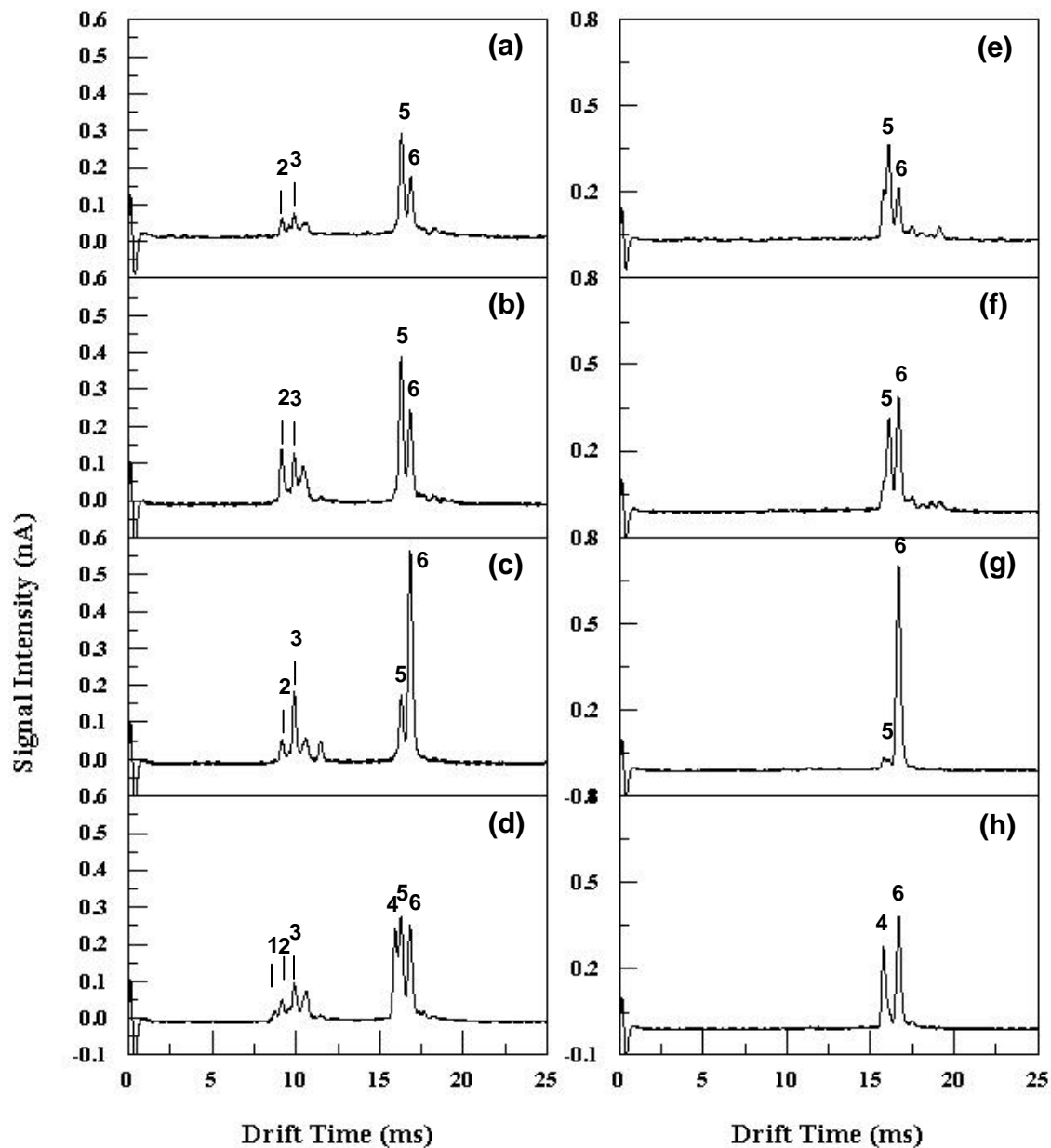


Figure 5: Effect of non-volatile dopants: ESI-IMS spectra of 50 mg L^{-1} RDX in (a) methanol-water (b) 2 mM NaNO_2 (c) 2 mM NaNO_3 (d) 2 mM NaCl . SESI-IMS spectra of 50 mg L^{-1} RDX in methanol-water with electrospraying (e) methanol-water (f) 1.45 mM NaNO_2 (g) 2 mM NaNO_3 (h) 2 mM NaCl . All spectra were run at $135 \text{ }^\circ\text{C}$. Peak assignments: (1) Cl^- (2) NO_2^- (3) NO_3^- (4) $\text{RDX}\cdot\text{Cl}^-$ (5) $\text{RDX}\cdot\text{NO}_2^-$ (6) $\text{RDX}\cdot\text{NO}_3^-$

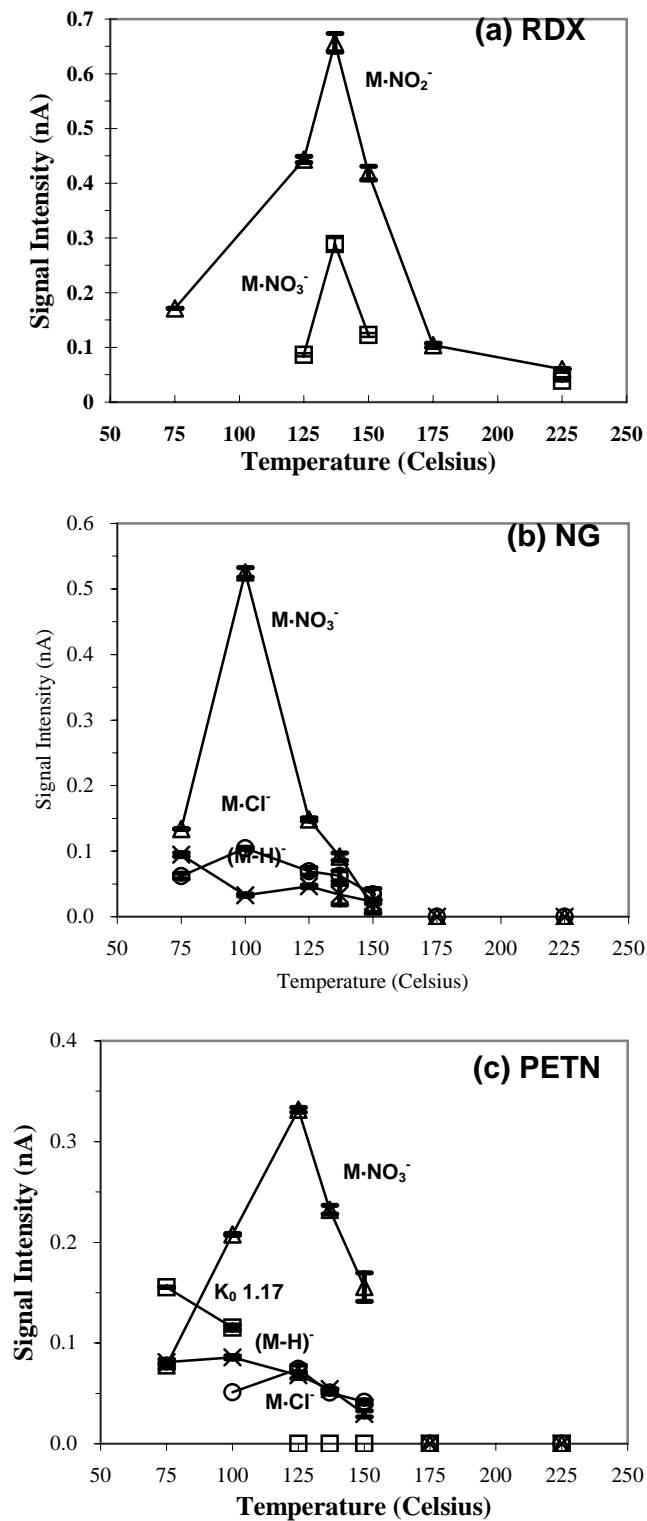


Figure 6: Thermal stability of RDX, NG, and PETN species: Plots of SESI-IMS signal intensity versus drift tube temperature of (a) RDX (b) NG and (c) PETN.

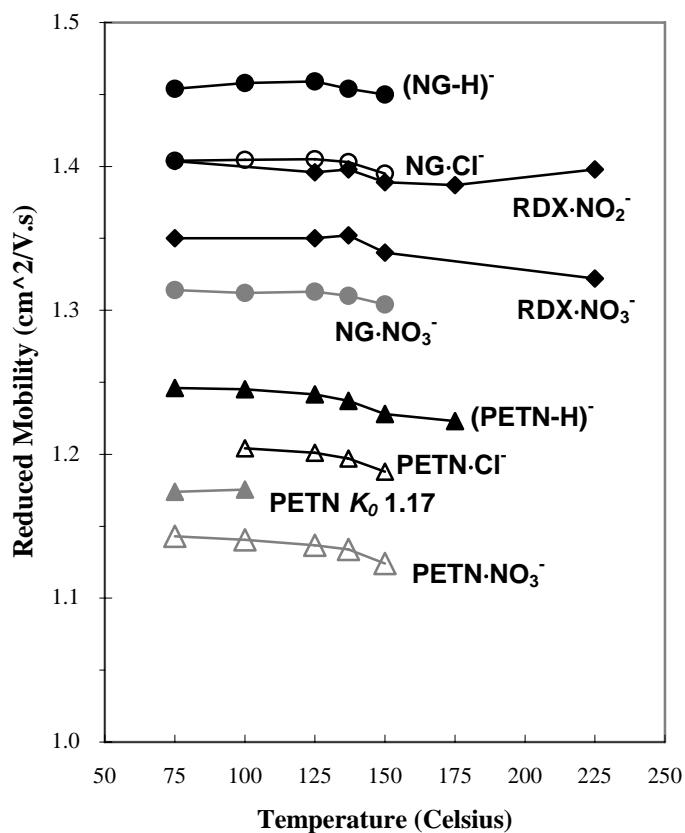


Figure 7: Plot of SESI-IMS reduced mobilities of RDX, NG, and PETN species versus drift tube temperature. Average standard deviation for the K_0 values was $0.001 \text{ cm}^2 \text{ V}^{-1} \text{ s}^{-1}$, with maximum standard deviation at $0.002 \text{ cm}^2 \text{ V}^{-1} \text{ s}^{-1}$. Error bars were omitted from the plot because they were smaller in size than the data point markers.